NONLINEAR OPTICAL STUDIES OF PHTHALOCYANINES AND TRIAZATETRABENZCORROLES IN SOLUTION AND IN THIN FILMS

A thesis submitted in fulfilment of the requirements for the degree of

MASTERS OF SCIENCE

of

RHODES UNIVERSITY

by

Nhlakanipho Colin Mkhize

January 2015

Dedication to

My mentor and spiritual advisor

Rev. Fr Sphiwo Vanqa SAC

My grandmothers

Eunice Yugo Kuzwayo & Thembeni Angeline Mkhize

I thank you for your prayers. Niyizimbokodo!

And

My mother

Khanyisile Beatrice Ndlovu

Thank you, for everything.

ACKNOWLEDGEMENTS

Ngithanda ukuqala la, ngibong' iGama leNkosi! I would like to thank the Source of all wisdom, God the Father the Son and the Holy Spirit, for the blessing of life and the ability to work.

This work would be directionless without the guidance of an amazing supervisor. I thank Distinguished Professor Tebello Nyokong for her outstanding support, insights and encouragement.

I would like to thank Drs Edith Antunes, Jonathan Britton and John Mack for their supporting roles as co-supervisors. Dr Edith Amuhaya, as a post-doctoral fellow, contributed immensely to my development as a synthetic chemist. I thank my fellow lab mates in S22 for making work a joy and play an absolute pleasure. I thank especially Ms Sarah D'Souza for all the things I kept procuring from her desk. The assistance of the technical staff is greatly appreciated, as is the role of the administrative team. I would like to thank Ms Gail Cobus in particular for her role in keeping us all in line.

To my friends, in all shapes and forms, I thank you for keeping me on track and pulling back from the brink of insanity. I thank you for the laughs, the frequent trips to the watering hole after hard lab hours and for the gift of your presence.

Without the gift of my family, I would not be where I am in life. I thank them from the bottom of my heart.

ABSTRACT

This work presents photophysical and nonlinear optical properties of a novel Cd 2,3-[octakis{4-tert-butylphenoxyphthalocyanine}] (**CdOtBPPc**) and compared with those of Pb 2,3-[octakis{4-tert-butylphenoxyphthalocyanine}] (**PbOtBPPc**). For both the **CdOtBPPc** and **PbOtBPPc**, third order imaginary susceptibility and second order hyperpolarizability values were found to be within the limit set for good optical limiters. The Pcs were embedded in poly (methyl methacrylate) (PMMA) and poly(bisphenol A carbonate) (PBC) as thin films. The optical limiting values of the Pcs once embedded in film were found to be greatly improved and the limiting intensity of each film was well below the maximum threshold. Both **PbOtBPPc** and **CdOtBPPc** showed better optical limiting when embedded in PBC compared to PMMA. **CdOtBPPc** shows better nonlinear optical behaviour than **PbOtBPPc** in solution and as thin films, even though the former is aggregated in solution.

Novel phosphorus triazatetrabenzcorroles (TBC) tetrasubstituted at the α- and β- and octa substituted at the β- positions of the peripheral fused benzene rings with *t*-butylphenoxy substituents were prepared and characterized. The effects of the substituents and the missing aza-nitrogen on the electronic structures and optical spectroscopy are investigated with TD-DFT calculations and MCD spectroscopy. The optical limiting properties were investigated to examine whether the lower symmetry that results from the direct pyrrole-pyrrole bond and hence the permanent dipole moment that is introduced result in higher safety thresholds, relative to the values that have been reported for phthalocyanines. The suitability of the compounds for singlet oxygen applications has also been examined.

Novel phosphorus phthalocyanines, analogous to the triazatetrabenzcorroles were also investigated. Due to their high photodegradation quantum yield however, only the fluorescence quantum yields and lifetimes were able to be determined.

TABLE OF CONTENTS

LIST OF SYMBOLS

^1H	-	Proton NMR
C_0	-	Initial concentration
C_t	-	Concentration after time t
I	-	Light intensity
I_{lim}	-	Limiting intensity
$Im[\chi^{(3)}]$	-	Imaginary third order susceptibility
N	-	Avogadro's number
S	-	Irradiated cell area
S_0	-	Singlet ground state
S_1	-	First excited singlet state
S_n	-	n^{th} excited singlet state
T_1	-	First excited singlet state
T_n	-	n^{th} excited triplet state
V_R	-	Solution volume
α	-	Non-peripheral substitution
α	-	linear absorption coefficient
α	-	fraction of light absorbed
β	-	Peripheral substitution
γ	-	Second order hyperpolarizability
ΔA	-	Change in absorbance
ε_T	-	Triplet state extinction coefficient
η	-	Refractive index

τ_F -   Fluorescence lifetime

τ_T -   Triplet lifetime

ϕ_F -   Fluorescence quantum yield

ϕ_{PD} -   Photodegradation quantum yield

ϕ_T -   Triplet quantum yield

ϕ_Δ -   Singlet oxygen quantum yield

$^1O_2$ -   Singlet oxygen

S_Δ -   Singlet oxygen quenching efficiency

LIST OF ABBREVIATIONS

A	-	Absorbance
DBU	-	1,8-diazabicyclo[5.4.0]undec-7-ene
DCM	-	Dichloromethane
DFWM	-	Degenerate four wave mixing
DMF	-	Dimethylformamide
DMSO	-	Dimethyl sulfoxide
ECT	-	Exciton coupling theory
EFISHG	-	Electric field induced second harmonic generation
ESA	-	Excited state absorption
F	-	Fluorescence
FCA	-	Free carrier absorption
H_2Pc	-	Unmetallated phthalocyanine
HF	-	Hartree-Fock
HOMO	-	Highest Occupied Molecular Orbital
IC	-	Internal conversion
IR	-	Infrared
LUMO	-	Lowest Unoccupied Molecular Orbital
MALDI-TOF	-	Matrix assisted laser-desorption/ionization-time of flight
MCD	-	Magnetic circular dichroism
MPc	-	Metallophthalocyanine
NLO	-	Nonlinear optics
NMR	-	Nuclear Magnetic resonance

OKG	-	Optical Kerr gate
OL	-	Optical limiter
P	-	Phosphorescence
PBC	-	Poly(bisphenol A carbonate)
Pcs	-	Phthalocyanines
PMMA	-	Polymethyl methacrylate
PMT	-	photomultiplier tube
RSA	-	Reverse saturable absorption
SEM	-	Scanning electron microscopy
TBC	-	Triazatetrabenzcorrole
TCSPC	-	Time correlated single photon counting
TD-DFT	-	Time dependent density functional theory
TPA	-	Two-photo absorption
UV/Vis	-	Ultraviolet/visible light
VR	-	Vibrational relaxation

LIST OF SCHEMES

LIST OF TABLES

and 4α-POH-TBC calculated with the CAM-B3LYP functional and 6-

31G(d) basis sets.

LIST OF FIGURES

1. INTRODUCTION

This chapter provides a brief overview of the synthesis, characterization and properties of phthalocyanines and triazatetrabenzcorroles and their application as optical limiting materials against intense laser light, both in solution and in polymer thin films.

1.1 Problem statement

The invention of the laser in 1960 by Maiman et al. [1] revolutionized the world. Not only did it push the frontiers of scientific research, but it also opened the door to a new world of communications, data processing, medicine, spectroscopy and many other applications [2]. However, lasers are also used as weapons to incapacitate the enemy by blinding them. There have been many studies carried out on patients who have been lased and all show varying levels of damage depending on the exposure time to the radiation and which wavelength was specifically used [3]. The most dangerous lasers are the 532 nm (green) and 1064 nm (infrared) [4].

The number of laser attacks on both military and civilian aircraft pilots has seen a steady increase over the past several years [5]. This is owing to the fact that lasers are becoming more available and less bulky to carry. The nature of these attacks in most cases is benign, but one must not rule out the possibility of malicious laser attacks on pilots. The danger in shining a laser light is that the beam diverges as it propagates through the air and then forms a very bright swath on the screen of the aircraft, thus dazzling the pilots. This can lead to temporary or permanent visual impairment depending on the duration and intensity of the laser incident. In South Africa, approximately 181 laser incidents were reported from the period January 1 to February 28, 2010 [6]. It is, therefore, very important and highly urgent that methods of preventing this laser damage to human eyes and other sensitive optical sensors be developed. This work seeks to develop an optical limiting thin film to achieve this objective.

Optical limiting is branch of nonlinear optics (NLO). This is the branch of physics which deals with the interaction between matter and intense light. Optical limiters are devices which, when irradiated with strong light, attenuate the intensity to a specific prescribed level. In other words, they act nonlinearly to cut off the transmission of light to a desired maximum value (**Fig 1.1**). Optical limiters have gained significant attention over the last few years. The first made were inorganic limiters, but owing to a lack of structural versatility, research on them tapered off [7,8]. Organic optical limiters have since received more attention. This is because they are easily synthesised and can be modified chemically to obtain the desired properties specifically needed for optical limiting. These properties include: a high excited triplet state population; minimal ground state absorption in the spectral region where limiting is required; high photostability; a fast intersystem crossing rate; and a strong excited state absorption [9]. Different molecules have been investigated including carotene, porphyrins, phthalocyanines and fullerene [9,10]. The optical limiting property arises from the fact that these molecules are highly conjugated and have extended delocalized π-electron density thus allowing for more linear and nonlinear polarizability [11]. This allows for them to exhibit nonlinear absorption in the presence of sudden intense light [12], which is the main phenomena responsible for optical limiting.

Phthalocyanines (Pcs) have gained increased attention for their nonlinear optical properties, owing to their unique structural, chemical and electronic properties. This work makes use of these molecules, and a derivative, triazatetrabenzcorrole, to achieve useful optical limiting materials for the protection of sensitive optical devices and human eyes in aviation, military and other applications.
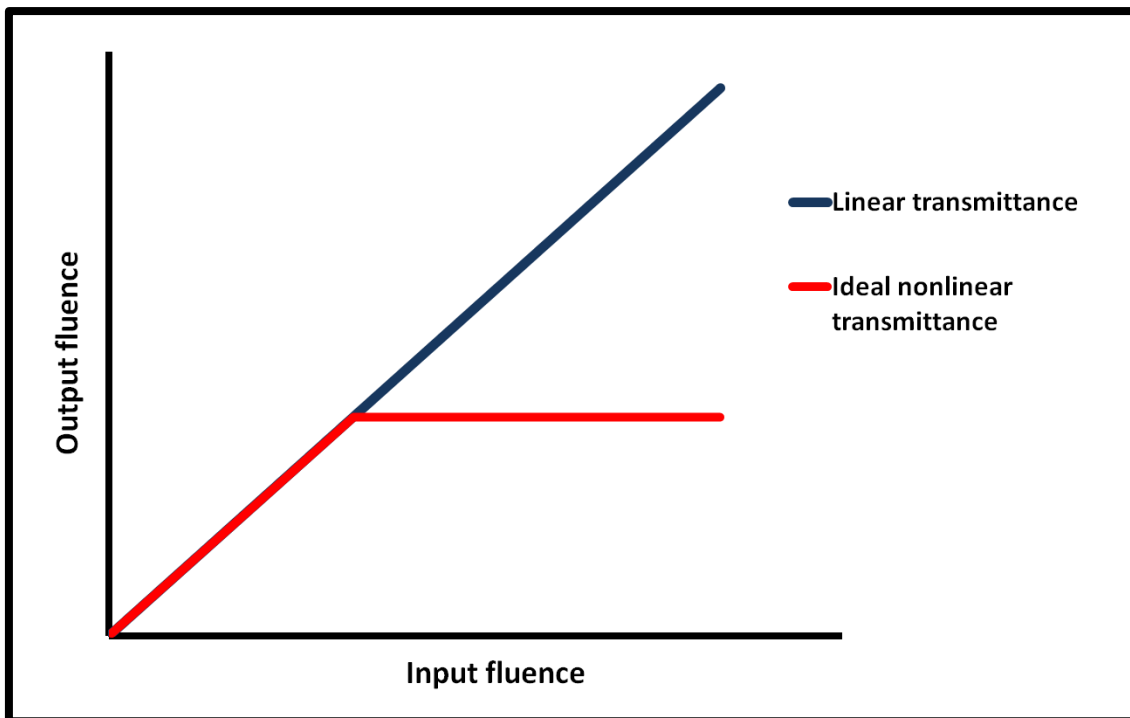
Figure 1.1: The ideal response of an optical limiter to intense light (red) compared to the response to normal light (blue). The point at which the transmittance deviates from linearity is known as the limiting intensity.

1.2 Phthalocyanines

1.2.1   History and applications

Phthalocyanines (Pcs) have been the subject of intense research since their serendipitous discovery in 1907 by Braum and Tcherniac [13,14], who were trying to synthesize o-cyanobenzimide using phthalimide as a starting reagent. In 1927, de Diesbach et al. accidentally synthesised the first copper phthalocyanine [15]. Until Linstead, in 1933 and 1934, elucidated the phthalocyanine structure and explored various properties including its chemical and physical stability [16–18], very little was known about this bluish insoluble compound. Robertson and his co-workers provided crystallographic information on the Pc which confirmed Linstead's structure and showed that the molecule is planar [19].

Phthalocyanines were originally used as stable dyes due to their intense blue or green colour. Copper phthalocyanines were especially utilized owing to their ease of synthesis, modification and purification [20].

Pcs are now been explored for use in medicinal applications; most notably photodynamic therapy [21,22], catalysis [23], opto-electronics [24], sensing, solar cell technologies; and nonlinear optics [11,25,26].

1.2.2   Structure and modification

Pcs are made up of four isoindoline units connected by aza-bridges at the 1,3 positions. The main Pc core is a 16 atom 18-π electron system which results in aromatic planar macromolecules. This arrangement results in the unique electronic and optical properties as well as increased thermal and chemical stability, hence leading to the wide range of applications previously mentioned. The cavity created by the isoindoline units can be filled

with any one of 70 different cations or protonated with two hydrogens [24,27]. Metallated

Pcs are identified by their central metal (MPc) and unmetallated Pcs are denoted as H_2Pc.

The MPcs exhibit D_{4h} symmetry (for central metals which fit into the cavity) and the H_2Pcs

show D_{2h} symmetry (as seen in **Fig 1.2**). Larger central atoms (such as Pb, Cd, and Hg) which

do not fit into the plane of the macrocycle result in the MPc having a reduced C_{4v} symmetry.

D$_{2h}$ symmetry   **D$_{4h}$ symmetry**   **C$_{4v}$ symmetry**
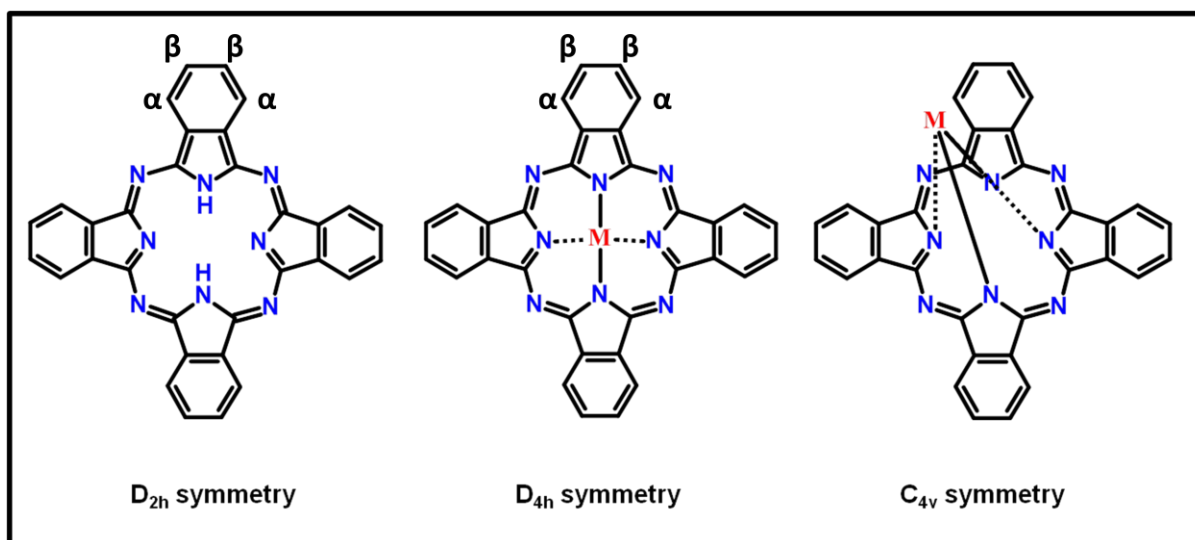
Figure 1.2: Phthalocyanine geometry, showing the positioning of peripheral (β) and non-peripheral (α) binding sites.

Apart from changing the central metal, Pcs can be modified by adding substituents to the

16 available binding sites on their skeletal structure; 8 of which are non-peripheral (α

positions) and the other 8 are peripheral (β) (**Fig 1.2**). It is also possible to obtain axial

substitution, depending on the oxidation state of the central atom (e.g. Al(III), Sn(IV), Ga(III),

In(III)) [12,28,29]. The desired applications and properties of the phthalocyanines will

determine what the overall structure looks like as well as the synthetic route used to obtain

it. For instance, MPcs made using heavy metals have gained more attention recently for use

in optical limiting owing to their increased nonlinear optical response due to a more highly populated excited triplet state [30–33].

1.2.3 Synthesis of phthalocyanines

There are numerous synthetic routes to obtain Pcs. McKeown identifies about 14 different methodologies which have been employed [34]. The most common of these for the synthesis of MPcs is the cyclotetramerization of a phthalonitrile in the presence of urea, a metal salt and a catalyst such as 1,8-diazabicyclo[5.4.0]undec-7-ene (DBU) which also acts as a base - all in a high boiling point solvent such as octanol, pentanol or 1-chloronaphthalene [35,36] (**Scheme 1.1**).
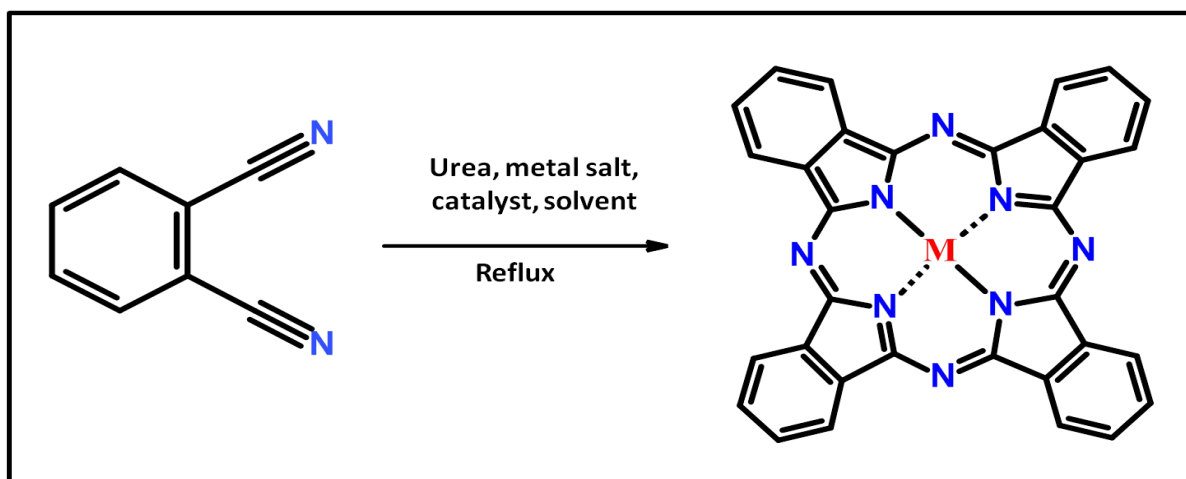
Scheme 1.1: **Cyclotetramerization of phthalonitrile to form MPc**

Other routes to the synthesis of phthalocyanines involve using phthalimide, phthalic acid and phthalic anhydride [37–39]. These are typically used to synthesise low symmetry Pcs or water soluble Pcs such as octacarboxy phthalocyanines [40,41].

1.2.4 Solubility of phthalocyanines

Unsubstituted Pcs tend to be insoluble in most organic media, but are readily dissolved in acidic solutions (as shown by Linstead [18]). Substituted Pcs on the other hand have enhanced solubility and depending on the type of substituent (determined by the proposed use of the Pc), the Pc can be dissolved in aqueous or organic solvents. The number of substituents also has a role in the solubility. Tetrasubstituted MPcs tend to be more soluble than their octasubstituted variants owing to the inherent isomerism of the reaction mixture. These isomers have an unsymmetrical arrangement, thus resulting in high dipole moments and therefore enhanced solubility [42]. It has been shown that peripherally substituted Pcs are more soluble than the non-peripherally substituted Pcs due to the spacing between the macrocycle rings, thus making solvation easier [43]. Even though substituents may increase solubility, aggregation of Pcs is still observed.

1.2.5   Phthalocyanine spectra
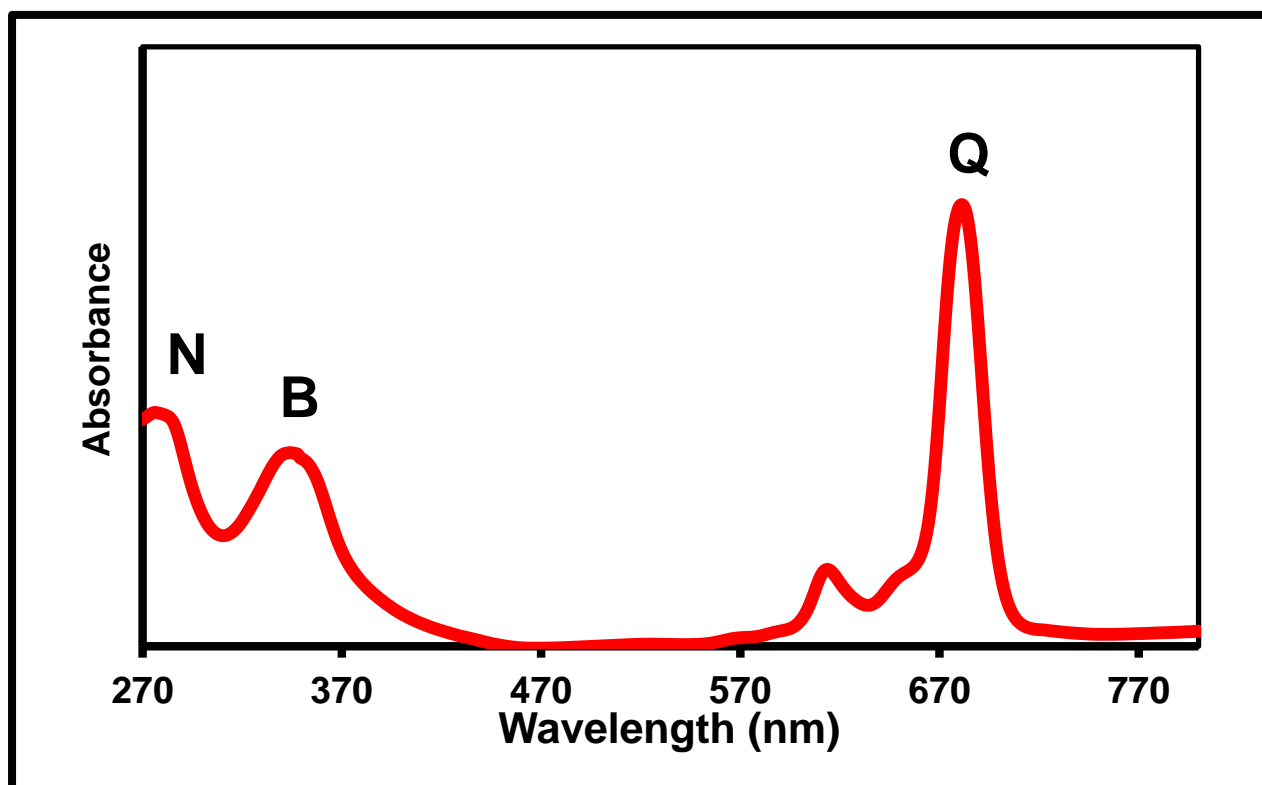
Figure 1.3: Ground state absorption spectrum of metallophthalocyanine

Phthalocyanines are characterized by their unique optical spectra. They have an intense Q band which can be situated between 660 and 1000 nm and a less intense B band around 350 nm (**Fig 1.3**). These peaks are due to the electronic transitions shown in **Fig 1.4**. The Q band position depends on the solvent used to solubilise the Pc, the substituent used, and the central atom present in the MPc [21]. Substituents which increase the conjugation of the Pc also red shift the spectrum. In more transparent solvents, such as chloroform and dichloromethane, more bands are seen in the UV region; namely the N, L and C bands.
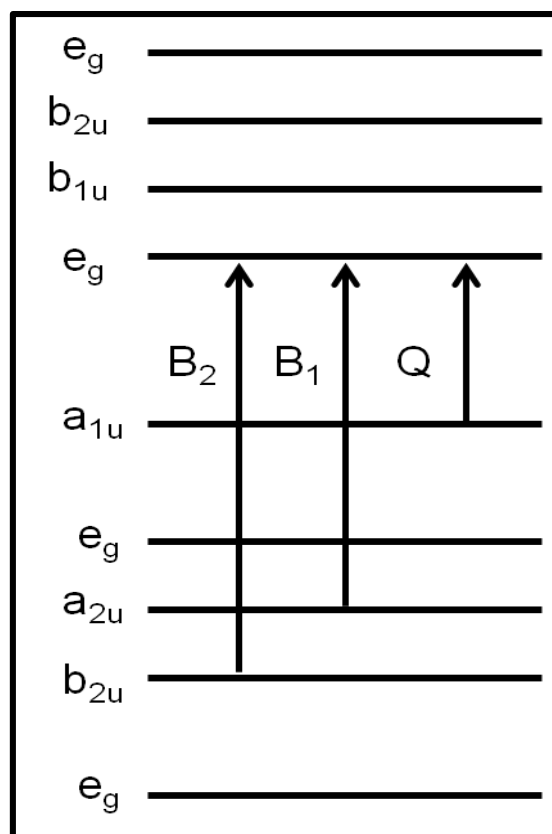
Figure 1.4: Electronic transitions in MPcs

1.2.6   Aggregation

Aggregation in Pcs is a common occurrence due to its extended π system. The attractive Van der Waal's interactions between the Pc rings leads to the coplanar arrangement of the macrocycles which then leads to dimerization or the formation of higher order oligomers. The presence of aggregation is noted by the broadening of the Q-band and the formation of a shoulder on the Q-band. Two types of aggregates can be seen and their properties are explained using exciton coupling theory (ECT); J- aggregates and H-aggregates. J-aggregates form when the Pc rings interact edge to edge [44], whereas H-aggregates result from face to face (or co-facial) interaction [45]. The lowest unoccupied molecular orbital (LUMO), which is degenerate in the monomeric Pc, is split by the overlap of π-electron clouds in dimers (**Fig**

1.5). Transitions then to the higher level (^1E_u) are allowed (H-aggregates) according to ECT whereas the transitions to the lower level (^1E_g) are forbidden (J-aggregates) but can still be observed sometimes.

H-aggregates exhibit a hypsochromic shift when compared to J-aggregates and result in a broad peak being observed next to the Q band. Organic solvents are known to reduce aggregation compared to aqueous solvents, which cause many Pcs to aggregate [43]. Common practises used to avoid observing aggregation in Pcs include the use of bulky substituents, such as t-butylphenol or using axial ligation of the central atom (e.g. P-OH), thus reducing the chance of π-π stacking. Surfactants are also employed in solution to ensure that aggregates dissociate [46]. Such surfactants include Triton X-100 and Cremophor-EL.
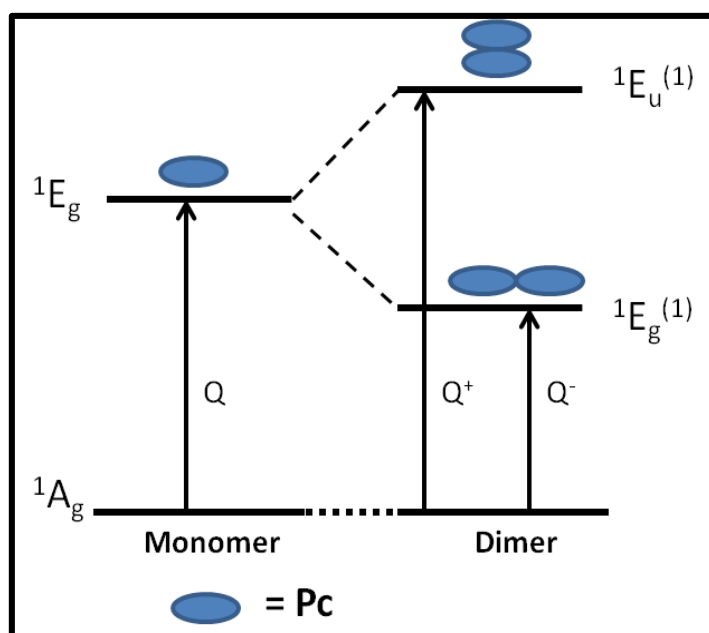
Figure 1.5: Electronic transitions in phthalocyanine aggregates

Dilution studies are usually employed to determine whether a Pc is aggregated. Highly concentrated solutions tend to exhibit aggregation. As more solvent is added, the collapse of the dimer peak and the reappearance of monomer peak, with an isosbestic point being seen, is evidence of the presence of aggregation [32].

1.3 Triazatetrabenzcorroles

1.3.1   History and structure

Triazatetrabenzcorroles (TBCs) are relatively new additions to the macromolecular porphyrinoid family, and are thus very similar to the more well studied porphyrins and Pcs [47]. They differ in structure from Pcs in that they have one meso-nitrogen missing from the core [48] (**Fig 1.6**), resulting in a permanent electric dipole moment and inherent asymmetry. This structure was formally confirmed by Kobayashi et al. using X-ray analysis [49]. The reduced chemical structure makes the central cavity smaller than that of Pcs, therefore restricting the number of atoms which can be incorporated. TBCs, when deprotonated are trianions, compared to the dianionic nature of Pcs. This results in them having very interesting chemical and physical properties [47]. Unmetallated TBC ligands are yet to be synthetically achieved.

TBCs were first synthesised in 1971 but were mistaken for Pcs [50]. As a result of their smaller cavity size due to ring contraction, TBCs have been shown to preferentially incorporate high oxidative state ions such as P(V), Ge (IV) and Si(IV) [48,51] with reports of Sn(III) and Rh(III) TBCs also being made [46,52].
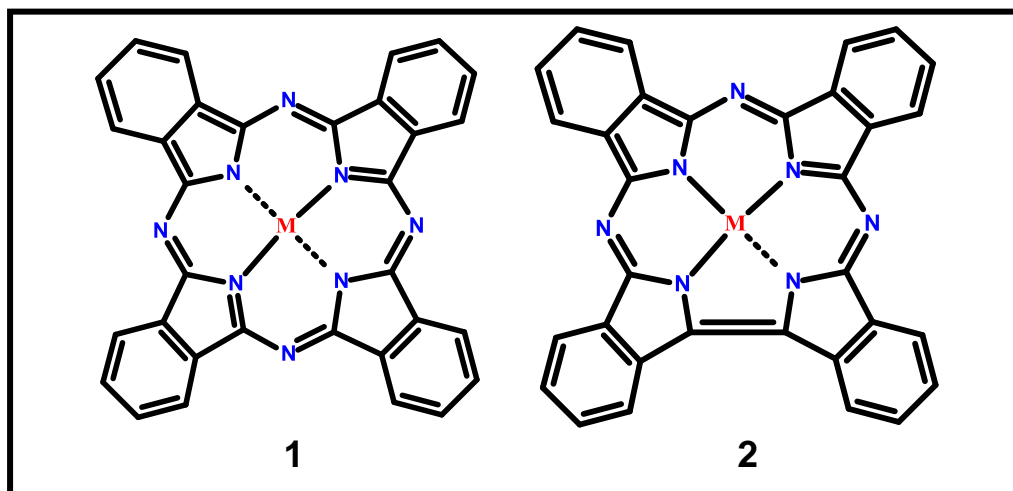
Figure 1.6: Representation of (1) metallophthalocyanine and (2) triazatetrabenzcorrole

1.3.2 Synthesis of triazatetrabenzcorroles

Several synthetic pathways for the formation of TBCs have been reported. They can be grouped into four categories [47].

i)   Pc ring contraction using $NaBH_4$ or H_2Se

Using the mild reducing agent $NaBH_4$ in the presence of a high boiling point alcohol, a meso-nitrogen can be removed from the Pc skeleton, resulting in a TBC. Fujiki et al. used this method to prepare the first purposefully synthesised TBC [53]. This method was limited in the number of central metals which could be used to obtain a TBC.

ii)   Insertion and contraction of H_2Pc using PX_3

The insertion of phosphorus into a parent H_2Pc seems to be the most successful of all the methods. Various groups have synthesised TBCs using this method, starting with Gouterman in 1981 [54]. The reaction has been shown to only proceed in dry pyridine. A

reactive intermediate has been postulated between the pyridine and PX_3 (X=Br, Cl) (see **Fig. 1.7**).

The exact mechanism by which the P(V)TBC forms was postulated by Liu et al. [55]. They made the claim that initially P(V)Pc forms in situ and then the TBC is formed by the excess PBr_3. Li et al. later made the same observation[56]. The result was confirmed by Kasuga et al. when they converted P(V)Pc dissolved in pyridine to P(V)TBC by adding PBr_3 [57].
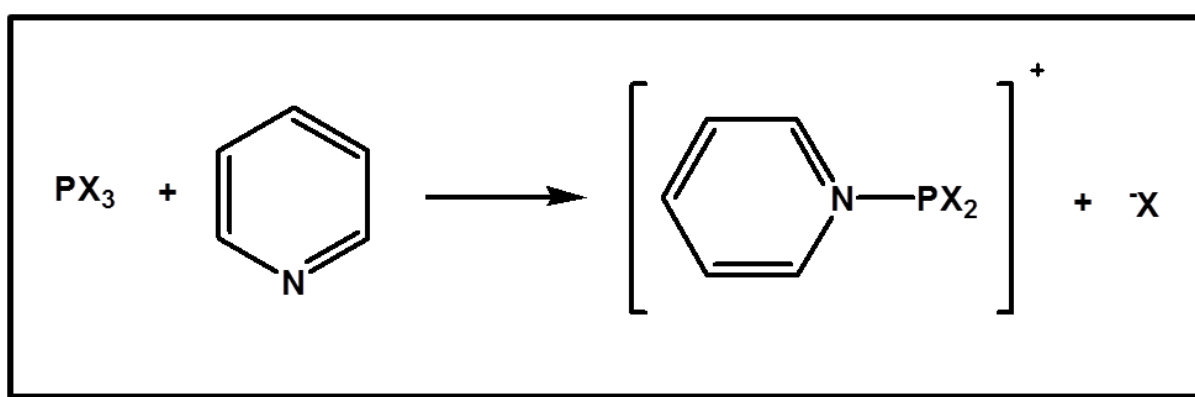
Figure 1.7: Intermediate formed between PX_3 and pyridine (X = Br, Cl)

iii)   Tetracyclization of 1,3-diimine isoindoline with Si_2Cl_6 or $HSiCl_3$

Kobayashi et al. synthesised a Si(IV)TBC by reacting a H_2Pc with $HSiCl_3$ in the presence of benzene and tributylamine. This gave extremely small yields [58]. The only crystal structures were of TBCS produced by the tetracylization of 1,3-diimine isoindoline with Si_2Cl_6. The product obtained was an octa(β-pentyl) Si(IV)TBC [49]. Using polar solvents (tetrahydrofuran, pyridine), Myakov et al. showed that Si(IV)TBCs are also accessible from $(OSiMe_3)_2SiPc$ using $MgMe_3SiCl$ to form $(OSiMe_3)_2Si$-TBC [59].

iv)   Miscellaneous methods

These methods were successful in yielding TBC complexes. They include microwave assisted synthesis where Khene et al. in an attempt to synthesize SnPc, found that if the ratio of urea to phthalic acid added to the reaction was of a specific value, TBC forms [46]; sulfonation of Pc ring [60], and reduction of the parent Si(V) Pc using Mg-MeSiX (X=Cl, Br) [59].

1.3.3   Absorption spectra of triazatetrabenzcorroles
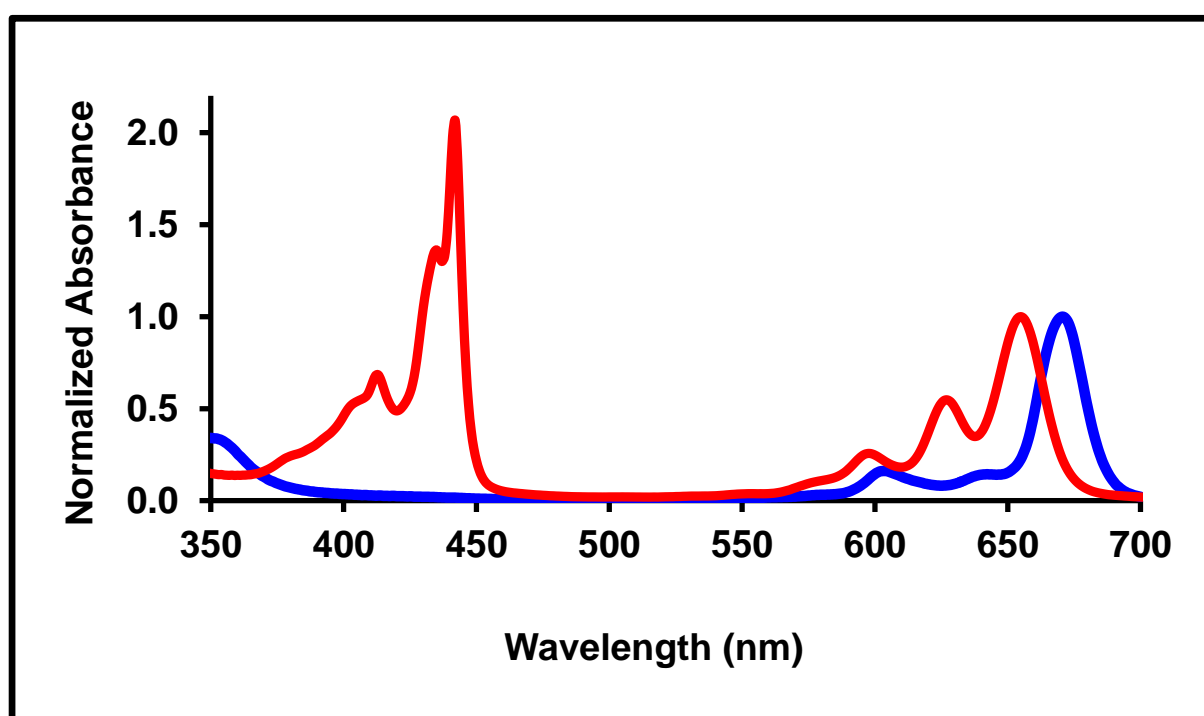
Figure 1.8: Ground state absorption spectrum of phosphorus TBC (red) compared to phosphorus Pc (blue) [unpublished data]

The ground state absorption spectrum of TBCs resembles that of a hybrid between a Pc and a porphyrin (**Fig 1.8**). The B band (390-450 nm) is much sharper and greater in intensity than that of the Q band between 650 and 680 nm. Also, when compared to Pc, the Q band of the TBC is more blue-shifted due to a slight change of the highest occupied molecular orbital

(HOMO) energy level [53,61]. A similar explanation to that of Pc absorption spectra applies to TBCs using Gouterman's frontier π-orbital model. Instead of a 16 atom 18-π electron system as seen in Pcs, TBCs have a 15 atom 18-π electron arrangement. This is why the TBC ligand is a trivalent ion. The alignment of the nodal planes of the frontier π-orbitals of TBCs is similar to that of Pcs and porphyrins, hence we observe similar trends. **Table 1.1** shows a selection of the TBCs which have been reported. A number of phosphorus TBCs with tert-butyl have been reported, but their optical limiting behaviour has not been investigated. This behaviour is reported in this work for the first time, to the best of our knowledge.

Table 1.1: A selection of TBCs that have been reported in literature (adapted from [47]**)**

Compound type	R: Subsituent	L: Axial	Reference
L-P-TBC(β-R)$_4$	H	O	[48,54,62–64]
	Isopropoxy	O	[55,64]
	1-(2-methoxyethyl)piperidine	O	[65]
	Phenoxy	O	[66]
	3-methoxypyridine	O	[60]
	t-Butyl	O	[62,64]
	NO$_2$	O	[64]

	Cl	O	[29]
	Br	O	[29]
	SO$_3$H	O	[63,64,67]
	NH$_2$	O	[64]
	1-(2-methoxyethyl)-1-methyl-piperidin-1-ium;iodide	O	[65]
	3-methoxy-1-methyl-pyridin-1-ium	O	[60]
	1,4-bis(1,1-dimethylbutyl)-2,5-dimethoxy-benzene	OH	[61]
L$_2$-P-TBC(β-R)$_4$	H	n-C$_8$H$_{17}$	[29]
	H	Ph	[29]
	1,4-bis(1,1-dimethylbutyl)-2,5-dimethoxy-benzene	CH$_3$, 4-methylcyclohexyl	[61]
L-P-TBC(α-R)$_4$	Phenoxy	O	[66]
L-P-TBC(β-R)$_8$	Cl	O	[48]
	n-C$_3$H$_7$	O	[62]

	n-C$_5$H$_{11}$	O	[62]
	O-*t*-butyl	O	[51]
L$_2$-P-TBC(β-R)$_8$	O-*t*-butyl	OMe	[68]
	O-*t*-butyl	OH	[68]
L$_2$-P-TBC(β-R)$_{16}$	O-*t*-butyl	OH	[68]
	Cl	OH	[68]
L-Rh-TBC(α-R)$_8$	CF$_3$	Me	[52]
	H	OSiEt$_3$	[49]
	H	Benzyloxy, OH	[53]
L-Si-TBC	H	OCH$_2$Ph	[69]
	H	OSiMe$_3$	[59]
	t-butyl	OH	[58]
L-Si-TBC(β-R)$_4$	n-C$_5$H$_{11}$	OH	[70]
	SO$_3$Na	OH	[60]
L-Sn-TBC(β-R)$_4$	SO$_3$Na	OH	[46]
L-Ge-TBC	H	Benzyloxy, OH, H	[53]

1.3.4   Applications of triazatetrabenzcorroles

TBCs have been investigated as potential photo-sensitizers for photodynamic therapy and water purification [48,63,67], used as novel liquid crystal display colour filters [61], photo-catalysts for the photo-oxidation of pollutant molecules [60], and, to a lesser extent, optical limiting [71].

Due to their structural similarity to Pcs, TBCs are hypothesized to have good optical limiting capabilities. These similarities, coupled with the permanent dipole moment which exists as a result of the inherent asymmetry of the molecule, have sparked interest into TBCs as viable candidates for optical limiting. For the first time, to the best of our knowledge, this work presents TBCs embedded in polymer thin films and reports on the resulting optical limiting parameters.

1.4 Photophysical and photochemical parameters

The Jablonski diagram (**Fig 1.9**) is a useful tool in explaining the optical phenomena which occur in molecules when they are irradiated with light of the appropriate wavelength. Of interest in this work are the fluorescence and triplet state populations.
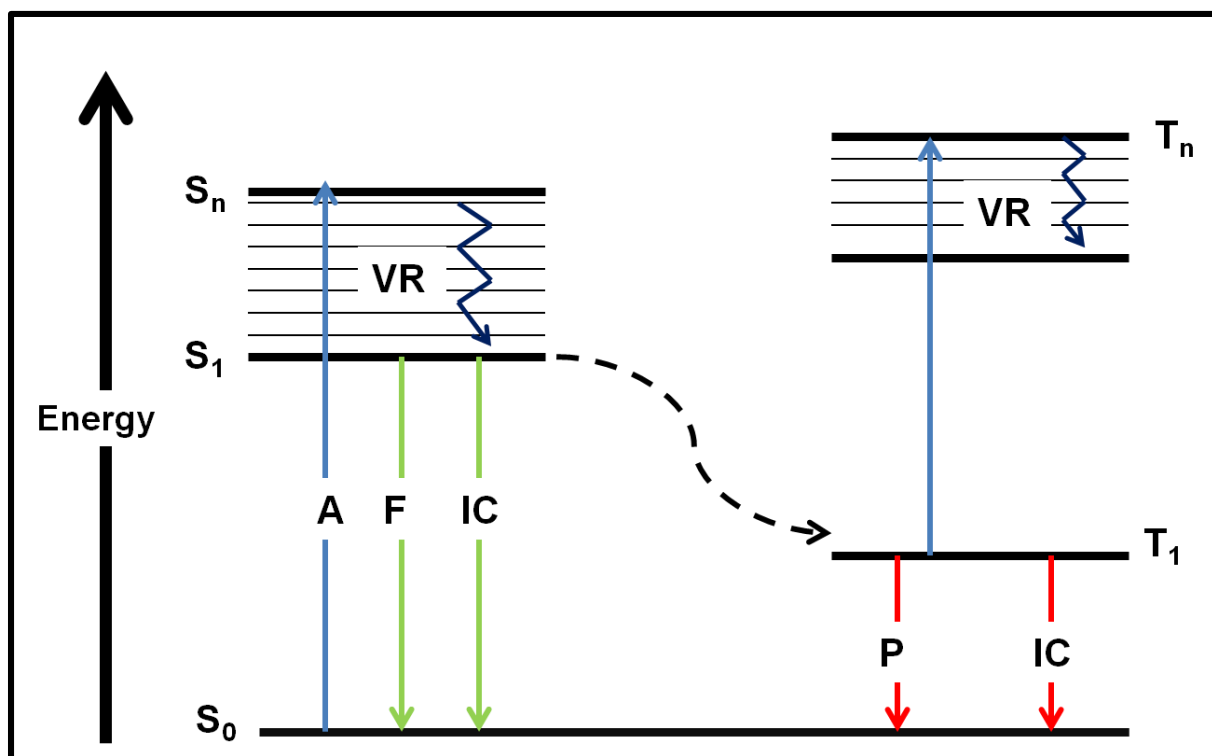
Figure 1.9: A Jablonski diagram showing the electronic transitions between the ground and excited states. A = absorbance, F = fluorescence, IC = internal conversion, VR = vibronic relaxation, P = phosphorescence, S_0 = singlet ground state, S_1 = first excited singlet state, S_n = n^{th} singlet excited state, T_1 = first excited triplet state, T_n = n^{th} excited triplet state.

1.4.1   Fluorescence quantum yields and lifetimes

Fluorescence is a process governed by Kasha's rule, which states that the bulk of photon emission in excited molecules occurs from the lowest excited state (for any given multiplicity). This means that, generally, fluorescence can only occur from the S_1 state (**Fig 1.9**).

The fluorescence quantum yield is a measure of the efficiency of the fluorescence process and is usually determined using the comparative method. This method involves the use of a compound whose fluorescence quantum yield is known as the standard. A variety of standards exist [72]. The most common used for Pcs is the ZnPc standard, with a known quantum yield of 0.20 in DMSO [13]. The fluorescence quantum yield is given by **Equation 1.1**. [73]

$$\Phi_F = \Phi_F^{std} \frac{F.A_{std}.n^2}{F_{std}.A.n_{std}^2} \tag{1.1}$$

where F and F_{std} are the integrals of the fluorescence emission curves of the MPc and the standard respectively. A and A_{std} are the respective absorbances of the sample and the standard at the excitation wavelength and n and n_{std} are the refractive indices of the solvents used for the sample and the standard respectively. Φ_F values are generally small for Pcs containing heavy metals [73,74].

The fluorescence lifetime is a measure of the average amount of time electrons remain in the excited singlet state before returning to the ground state. It can be obtained by the deconvolution of the decay curve (**Fig 1.10**) determined using time correlated single photon counting (TCSPC). The lifetimes for Pcs are generally in the picoseconds to nanosecond regime.
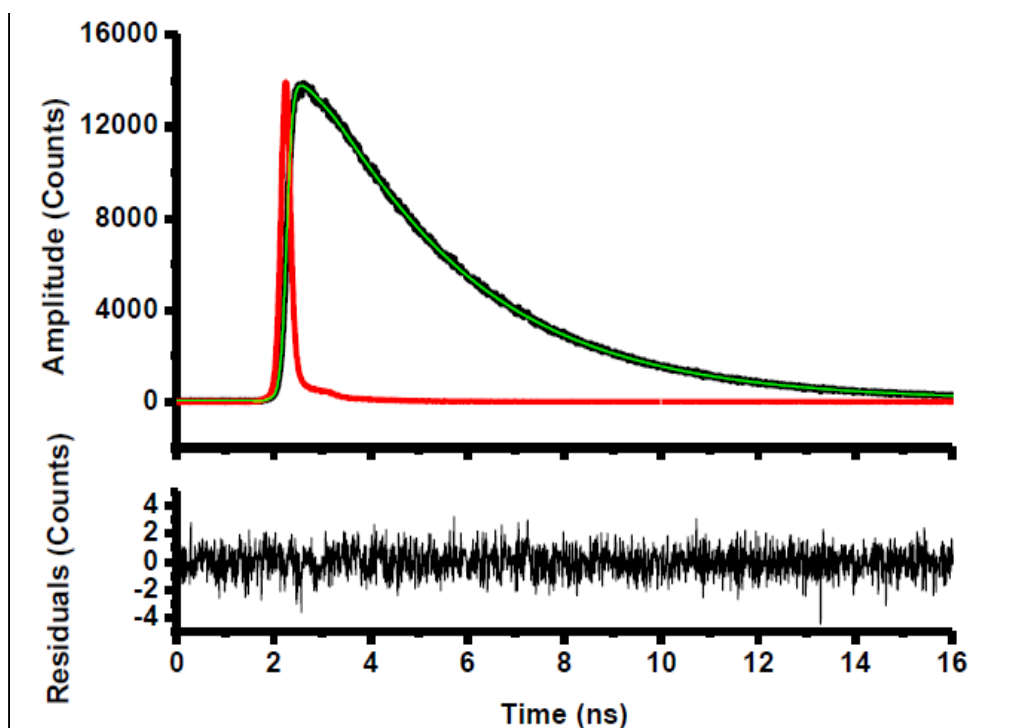
Figure 1.10: Typical fluorescence decay curve found using time-correlated single photon counting and the associated residuals [unpublished data]

1.4.2 Triplet quantum yield and lifetime

The triplet quantum yield is a measure of the number of molecules which undergo the parity forbidden process of intersystem crossing from the first excited singlet state (S_1) state to the first triplet state (T_1) state shown in **Fig 1.9**. The triplet quantum yield of Pcs is enhanced when the symmetry is reduced and when a heavy central atom is included. The latter occurs by the spin-orbit coupling induced by the heavy metal. The technique used to measure the excited state of the molecule is known as laser flash photolysis. It monitors the absorbance between the T_1 and T_n states of the excited molecule. A triplet decay curve (**Fig 1.11**), which is a plot of the change in absorbance (ΔA) against time in seconds, is obtained at each excitation wavelength and can be used to determine the triplet lifetime (τ_T). Pcs

typically exhibit strong triplet-triplet absorption between 490 – 540 nm. This can be observed on a transient spectrum, which plots ΔA against wavelength. The data obtained from the laser flash photolysis experiment is used to determine the triplet quantum yields.
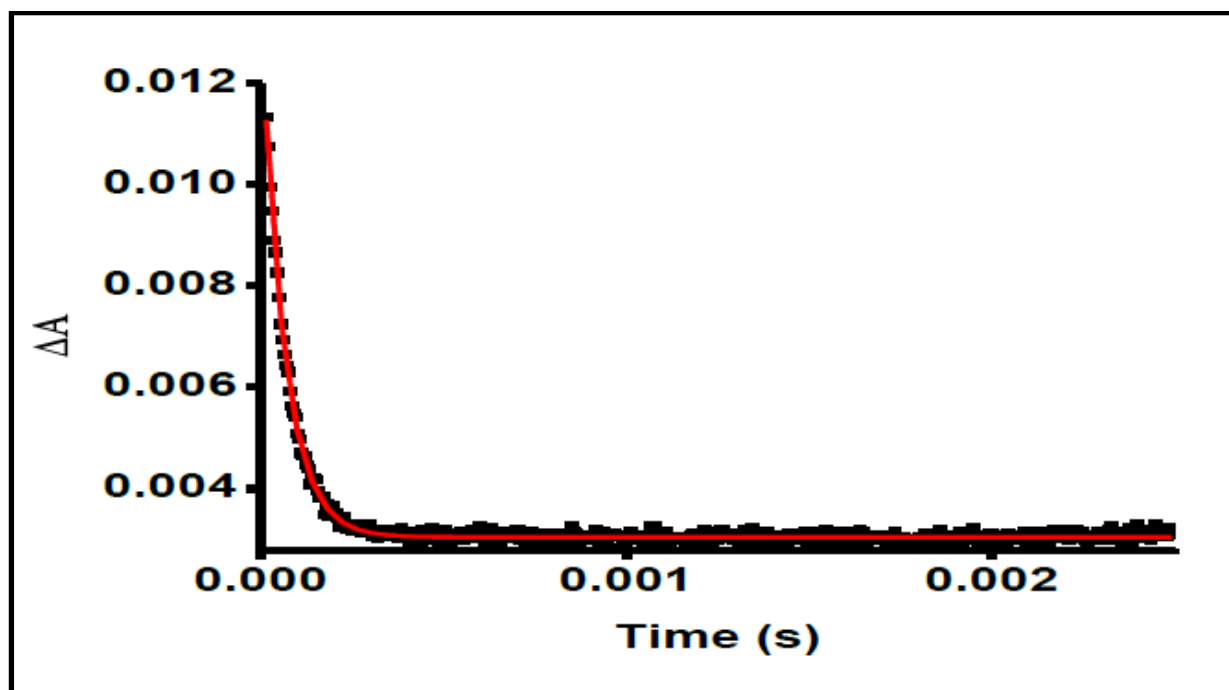
Figure 1.11: Typical triplet decay curve of Pc. The red line is the fit used to determine the triplet lifetime and the black points are the experimental data [unpublished data].

The triplet quantum yield can be determined using the comparative method based on triplet decay, with known Pcs as the standards using **Equation 1.2** [75];

$$\phi_T = \phi_T^{std} \frac{\Delta A_T^{sample} . \varepsilon_T^{std}}{\Delta A_T^{std} . \varepsilon_T^{sample}} \tag{1.2}$$

where ΔA_T^{sample} and ΔA_T^{std} are the changes in the triplet state absorption of the sample and the standard, respectively. ε_T^{sample} and ε_T^{std} are the triplet state extinction coefficients for the sample and the standard, respectively. ϕ_T^{std} is the triplet quantum yield for the standard. For unsubstitued ZnPc in DMSO, this value is 0.65 [75] and this was employed in this study.

1.4.3 Singlet oxygen quantum yield

Singlet oxygen is a cytotoxic moiety formed by the energy transfer from the excited triplet state of a sensitizer molecule such as Pcs to the ground state of molecular oxygen. This reactive species is the key component of photodynamic therapy.

The singlet oxygen quantum yield is a measure of how much singlet oxygen is produced per quanta of light. There are two methods of determining singlet oxygen. The first involves the use of a chemical quencher such as 1,3-diphenylisobenzofuran (DPBF) in organic solvents. When singlet oxygen is produced, the quencher traps it and a reaction occurs. The progress of this reaction is followed by observing the change in the intensity of the absorption peak of the quencher using UV/Vis spectroscopy. The quantum yield of the quencher is given by **Equation 1.3** [76,77]

$$\phi_{quencher} = \frac{(C_0 - C_t)V_R}{I_{abs}.t} \tag{1.3}$$

where C_0 and C_t are the concentrations of the chemical quencher before and after irradiation, respectively. V_R is the solution volume, t is the total irradiation time and I_{abs} is defined by **Equation 1.4**:

$$I_{abs} = \frac{\alpha A I}{N} \tag{1.4}$$

where α is the fraction of light absorbed, I is the light intensity, A and N_A are the irradiated cell area (cm^2) and Avogadro's constant ($mole^{-1}$), respectively.

The singlet oxygen quantum yields ϕ_Δ can then be calculated using **Equation 1.5** [78]

$$\frac{1}{\phi_{quencher}} = \frac{1}{\phi_\Delta} + \frac{1}{\phi_\Delta} \cdot \frac{k_d}{k_a} \cdot \frac{1}{[quencher]} \tag{1.5}$$

where k_d is the decay constant of singlet oxygen in the respective solvent and k_a is the rate constant of the reaction of the quencher with singlet oxygen. The intercept obtained from the plot of $1/\phi_{quencher}$ versus $1/[quencher]$ gives $1/\phi_\Delta$

The second method (employed in this work) involves the use of sensitive germanium detector to generate a time resolved phosphorescence decay curve of singlet oxygen (**Fig 1.12**), which can be was used to determine singlet oxygen quantum yield. The decay curve obeys **Equation 1.6** [79]**:**

$$I(t) = B \frac{\tau_D}{\tau_T - \tau_D} [e^{-t/\tau_T} - e^{-t/\tau_D}] \tag{1.6}$$

where, I(t) is the phosphorescence intensity of $^1O_2$ at time t, τ_D is the lifetime of $^1O_2$ phosphorescence decay, τ_T is the triplet state lifetime of the standard or sample and B is a coefficient related to sensitizer concentration and $^1O_2$ quantum yield. The singlet oxygen quantum yield, ϕ_Δ, of the complex was then determined using a comparative method given by **Equation 1.1,** but with modified symbols

$$\phi_\Delta = \phi_\Delta^{std} \frac{B.A_{std}.n^2}{B_{std}.A.n_{std}^2}$$

where ϕ_Δ^{Std} is the singlet oxygen quantum yields for the ZnPc standard (ϕ_Δ^{Std} = 0.67 in DMSO) [80], B and B^{Std} refer to coefficient involved in sensitizer concentration and $^1O_2$ quantum yield for the sample and standard, respectively.
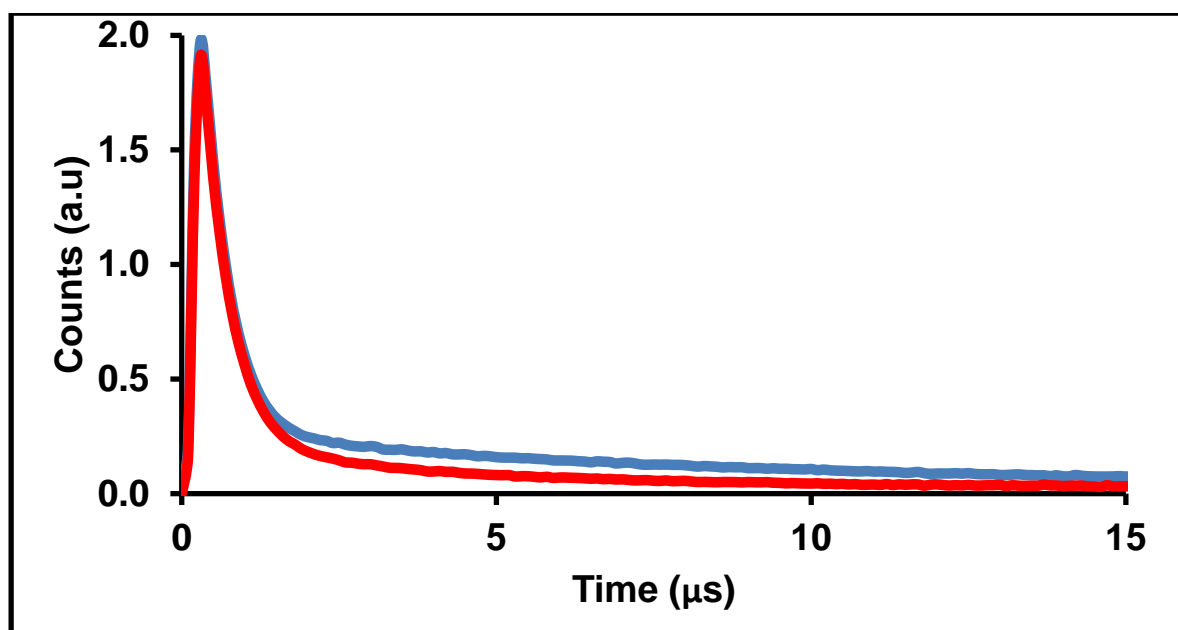
Figure 1.12: Phosphorescence decay curve of singlet oxygen from a ZnPc standard (blue) and in the presence of sodium azide quencher (red) [unpublished data]

1.4.4   Photodegradation quantum yield

Photodegradation is the photochemical reaction which occurs between singlet oxygen and the photosensitizer to produce smaller molecular fragments in the presence of visible light. The singlet oxygen acts as a nucleophile and attacks the conjugated Pc ring system to form phthalimide. Photodegradation can be monitored using UV/Vis spectroscopy by observing the decreasing intensity of the absorption peak and the non-appearance of a new peak.

The photodegradation (or photobleaching) quantum yield (ϕ_{PD}) is the ratio of the number of molecules that degrade per quantum of light absorbed. It is a useful measure of the photostability of molecules.

This value can be calculated using **Equation 1.3,** using ϕ_{PD} instead of $\phi_{quencher}$ [81]

1.5   Nonlinear Optical behaviour of Pcs and TBCs

1.5.1   Reported Pcs and TBCs (NLO)

Due to their large π-electron system, Pcs have received a lot of attention as potential optical limiters [82–85]. Their imaginary third order susceptibility $(Im[\chi^{(3)}]$ and second order hyperpolarizability (γ) values lie in the range that has been seen to be acceptable for good OLs , those being 10^{-9} to 10^{-15} for $Im[\chi^{(3)}]$ and 10^{-29} to 10^{-34} for γ [86]. **Table 1.2** shows a wide variety of Pcs and a few TBCs which have been explored for their optical limiting properties. We observe that a variety of modifications have been done on them, including varying the degree of substitution; varying the substituents and also the central metals.

Table 1.2: A selection of Pcs and TBCs which have been investigated for optical limiting

Compound[a]	Medium	Imaginary third order susceptibility, $Im[\chi^{(3)}]$ (esu)	Reference
$(OSiMePhOH)_2SiPc$	Langmuir-Blodgett film	2.0×10^{-9}	[87]
$Sc(Pc)_2$	-b	1.5×10^{-9}	
PtPc	-b	2×10^{-10}	
ClInPc	-b	1.5×10^{-10}	
FAlPc	Thin film	5×10^{-11}	
$(C_6H_{13}S)_4VOPc$	-b	9.8×10^{-12}	
$(C_4H_9S)_4CuPc$	-b	3.7×10^{-12}	
$[(tBu)_4PcGe(OH)]_2$	Thin film	2.5×10^{-11}	[85]
NiPc	THF	7×10^{-12}	[88]
PdPc		6.5×10^{-12}	
$(C_6H_6O_2)(tBu)_4TiPc$	$CHCl_3$	-b	[89]
$(tBu)_4PcInCl$	Toluene	1.4×10^{-11}	[28]
$(tBu)_4PcIn(p-TMP)$		1.49×10^{-11}	
$(tBu)_4PcIn(p-CPO)$		9.1×10^{-12}	

PbPc(β-cumylphenoxy)$_4$	CHCl$_3$	-b	[90]
Ga(tBuPhO)$_8$Pc	DMSO	8.54×10^{-11}	
β(tBuPhO)$_4$PcInCl		8.97×10^{-11}	
α(t-BuPhO)$_4$PcInCl		4.37×10^{-11}	
Zn(BzyPhO)$_8$Pc		2.88×10^{-11}	
(BzyPhO)$_8$GaClPc		3.95×10^{-11}	[91]
(BzyPhO)$_8$InClPc	DMSO	9.21×10^{-11}	
Zn(β-BzyPhO)$_4$Pc		4.81×10^{-11}	
(β-PhO)InClPc		5.62×10^{-11}	
(PhO)$_8$GaClPc		4.53×10^{-11}	
Zn(β-NH$_2$)$_4$Pc		7.82×10^{-11}	
P(OH)$_2$TBC	DMF	4.40×10^{-14}	
P(OH)$_2$TBCS$_n$		4.27×10^{-14}	[71]
P(OH)$_2$TBC(O^{i}Pr)$_4$		4.91×10^{-14}	

a: Ph = phenyl, p-CPO = para-chlorophenoxy, p-TMP = p-trifluoromethylphenyl, tBu = tert-butyl, Bzy = benzyloxy, O^{i}Pr = isopropoxyl, S$_n$ = SO$_3^-$, THF = tetrahydrofuran, DMSO = dimethyl sulfoxide, DMF = dimethylformamide

b: not reported

It is postulated that Pcs which exhibit a strong dipole moment perform better as optical limiters due to the great polarizability they can exhibit [92]. This has led to research in asymmetric phthalocyanines. This asymmetry can be a result of different substituents being used on the Pc ring, large central metals being used in the cavity, or by making binuclear Pcs and asymmetric Pc analogues such as TBCs (**Table 1.2**). In this work, we explore the use of heavy metals as central atoms in the Pc cavity. The heavy metals promote intersystem crossing from the singlet to the triplet excited state by enhanced spin orbit coupling [83]. We also make use of an inherently asymmetric TBC molecule in this work. The asymmetry affords TBCs a more permanent dipole moment and thus, an increased polarizability. To the best of our knowledge, very little work has been done on the nonlinear optical properties of TBCs. **Table 1.2** shows that indium and gallium Pcs have been extensively studied for NLO. There have been few studies using lead and no studies done using cadmium Pcs. PbPcs have a shuttle-cock arrangement and thus a lower symmetry than other Pcs which means that they have potentially good OL properties, hence why they are employed in this work.

1.5.2   Phthalocyanines and triazatetrabenzcorroles used in this work for NLO

The compounds used in this thesis are listed in the **Table 1.3 – 1.5**. They are divided into

i)   Heavy metal Pcs,

ii)   Phosphorus Pcs and

iii)   Phosphorus triazatetrabenzcorroles.

 They all are synthesised with either tetra or octa substitution with 4-tert-butylphenol.

Table 1.3: Structures of heavy metal phthalocyanines synthesised and employed in this work. PbOtBPPc has been reported before [93]**, whilst CdOtBPPc is reported for the first time**
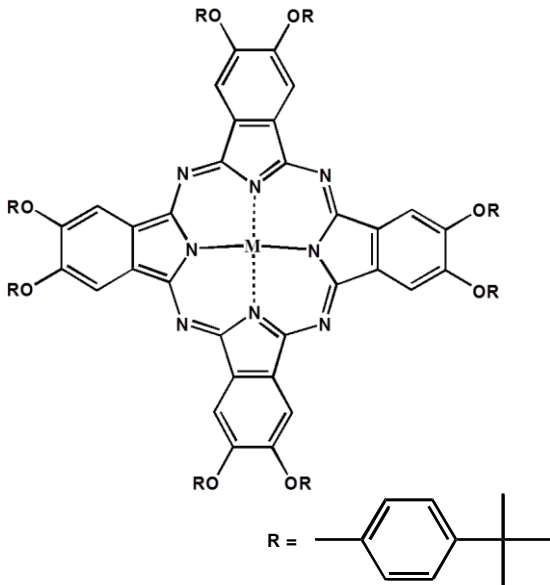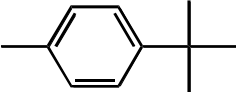
Molecular structure	Metal (M)	Name (abbreviations)
	Pb	**Lead 2,3-[octakis{4-*t*-butylphenoxy}]phthalocyanine** **(PbOtBPPc)**
	Cd	**Cadmium 2,3-[octakis{4-*t*-butylphenoxy}]phthalocyanine** **(CdOtBPPc)**

Table 1.4: Structures of novel phosphorus phthalocyanines employed in this work

R =
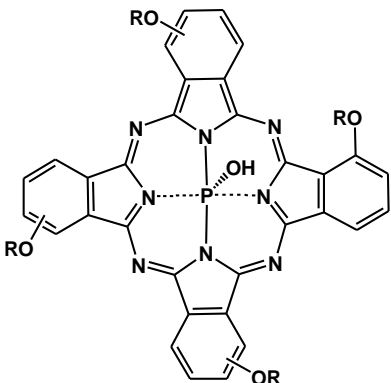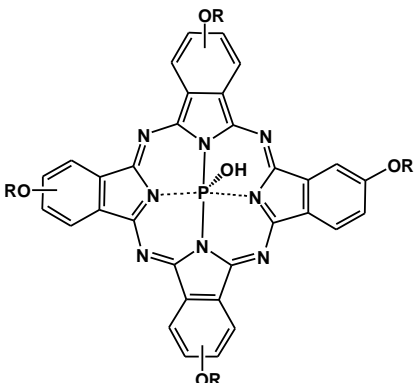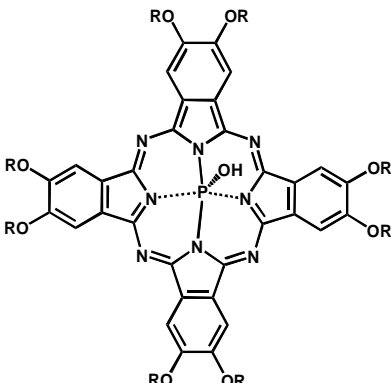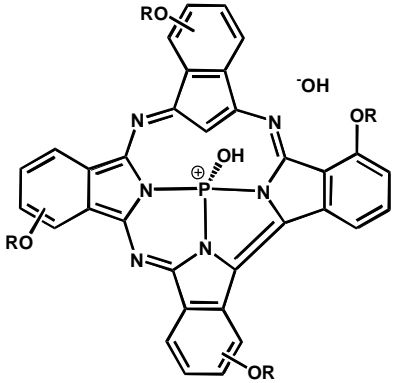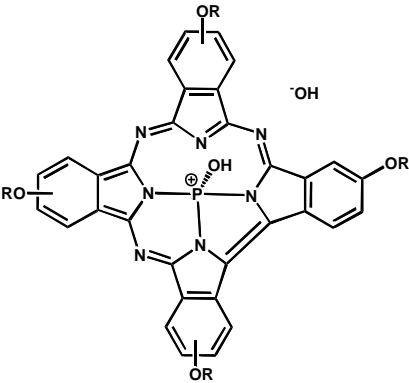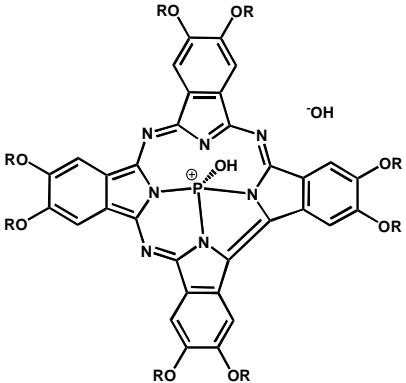
Molecular structure	Name (Abbreviation)
	Hydroxyphosphorus(V) (1(4), 8(11), 15(18), 22(25)-4-*t*-butylphenoxy) phthalocyanine (4α-POH-Pc)
	Hydroxyphosphorus(V) (2(3), 9(10), 16(17), 23(24)-4-*t*-butylphenoxy) phthalocyanine (4β-POH-Pc)
	Hydroxyphosphorus 2,3-{octakis(4-*t*-butylphenoxy)} phthalocyanine (8β-POH-Pc)

Table 1.5: Novel phosphorus triazatetrabenzcorroles synthesised and employed in this work. R =

Molecular structure	Name (Abbreviation)
	Hydroxyphosphorus(V) (1(4), 8(11), 15(18), 22(25)-*t*-butylphenoxy) triazatetrabenzcorrole **(4α-POH-TBC)**
	Hydroxyphosphorus(V) (2(3), 9(10), 16(17), 23(24)-4-*t*-butylphenoxy) triazatetrabenzcorrole **(4β-POH-TBC)**
	Hydroxyphosphorus(V) 2,3-{octakis(4-*t*-butylphenoxy)} triazatetrabenzcorrole **(8β-POH-TBC)**

33

1.5.3   Nonlinear measurements

NLO materials are characterized using a variety of techniques such as the Z-scan technique, degenerate four wave mixing (DFWG), third harmonic generation (THG), electric-field induced second-harmonic generation (EFISHG) and optical Kerr gates (OKG) [10]. The Z-scan technique was employed in this work.

The typical Z-scan measurement of an optical limiter which exhibits reverse saturable absorption (RSA) is shown in **Fig 1.13**. RSA occurs in materials where the excited state absorption cross section is greater than the ground state absorption cross section [33]. This is usually seen in conjugated molecules such as TBCs and Pcs.

A good optical limiter will possess a symmetrical spectrum about the focal point and have a transmittance reduced to 0.5 or less.
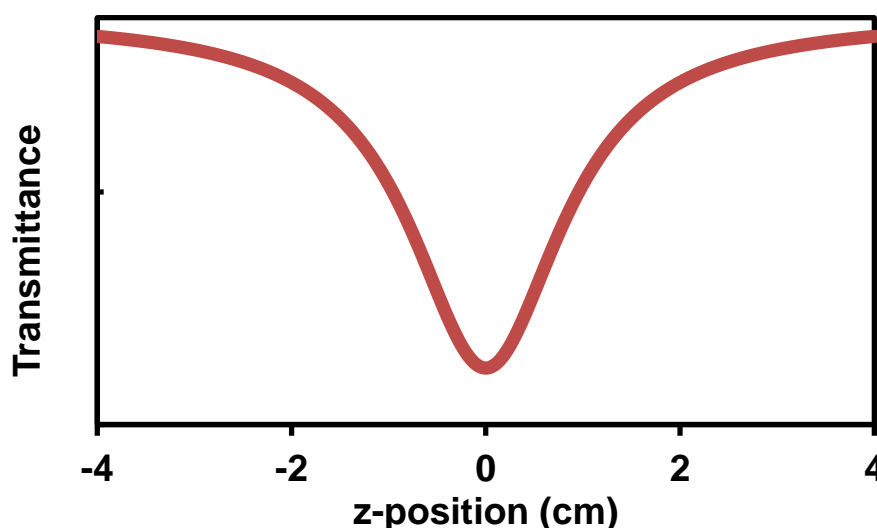
Figure 1.13: RSA behaviour of optical limiters [unpublished data]

1.5.4 Nonlinear optical parameters

The Z-Scan experiment was performed according to the method described by Sheik-Bahae [94–96]. Assuming a Gaussian spatial and temporal pulse, and using the open aperture Z-Scan theory for multi-photon absorption (nPA) by Sutherland et al. [97], the general expression for open aperture normalized transmittance can be written as **Equation 1.8**.

$$T_{OA(2PA)} = \frac{1}{1+\beta_2 L_{eff}(I_{00}/(1+(z/z_0)^2))} \tag{1.8}$$

where I_{00} is the on-focus intensity (peak input intensity), β_2 is the two photon nonlinear absorption coefficient, L_{eff}, z and z_0 are the effective path length in the sample of length L, translation distance of the sample relative to the focus and Rayleigh length respectively. Rayleigh length is defined as $\pi w_o^2/\lambda$ where λ is the wavelength of the laser and w_o is the beam waist at the focus, ($z = 0$). L_{eff} is given by **Equation 1.9**:

$$L_{eff} = \frac{1-e^{-\alpha L}}{\alpha} \tag{1.9}$$

where α is the linear absorption coefficient.

The imaginary component of the third order susceptibility ($I_m[\chi^{(3)}]$) is given by **Equation 1.10** [86]

$$I_m[\chi^{(3)}] = \eta^2 \varepsilon_0 c\lambda\beta_2/2\pi \tag{1.10}$$

where η and c are the linear refractive index and the speed of light respectively, ε_0 is the permittivity of free space, λ and β_2 terms are as described above.

Second order hyperpolarizability (γ) of the material was determined using **Equation 1.11** [86]:

$$\gamma = \frac{I_m[\chi^{(3)}]}{f^4 C_{\mathrm{mol}} N_A} \qquad (1.11)$$

where N_A is the Avogadro constant as defined above, C_{mol} is the concentration of the active species in the triplet state per mole and f is the Lorentz local field factor given as, $f = (\eta^2 + 2)/3$.

1.5.5 Mechanism of optical limiting

It is prudent to make the distinction between active and passive OLs. Active OLs rely on an internal feedback mechanism between its components in order to trigger a response to incoming radiation. These devices are usually slower to respond since different parts of the system perform different roles and thus are not suitable for the protection of sensitive optical devices and eyes. Passive OL devices are more applicable for this purpose as they do not rely on a feedback response between components, but experience a simultaneous response to incoming light due to their physical properties [98]. Organic molecules such as Pcs and TBCs fall into this category.

There are several competing nonlinear processes which lead to passive optical limiting. These include nonlinear refraction, scattering, absorption and phase transitions [89,98,99] (**Fig 1.14**). Each of these processes is a combination of other sub-processes. Nonlinear absorption can be a combination of two-photon absorption (TPA), excited state absorption (ESA), reverse saturable absorption (RSA) and free-carrier absorption (FCA). Nonlinear refraction is a resultant effect of thermal lensing, excitation of free-carriers and other such

processes. Both scattering and phase transitions can be seen to be mainly thermal effects and thus can be reduced or eliminated [98]. OL devices typically exhibit a combination of the above-mentioned processes.
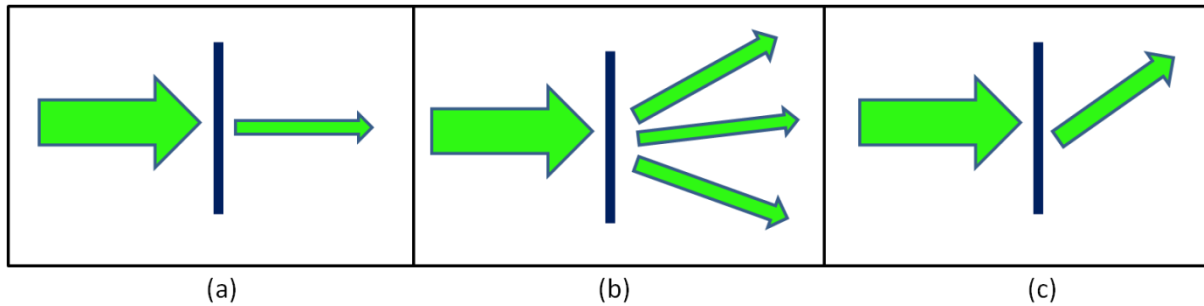
Figure 1.14: The nonlinear processes which result in OL activity (a) nonlinear absorption (b) nonlinear scattering and (c) nonlinear refraction

1.5.6   Enhancement of optical limiting

A major portion of the work done on OL in literature is done in solution. Whilst this is good for understanding trends in the OL behaviour of materials, it is more important to study these properties in the solid state. This is achieved by the formation of OL films. Examples of these include Langmuir-Blodgett films, polymer thin films, fullerene films and doped glass composites [33]. It has been shown that solid state OL devices offer superior properties to solution based products [100].

Polymers which are to be employed as host matrices for OL compounds need to fulfil certain criteria before any composite can be formed. They need to be optically transparent in the visible and infrared range; environmentally and chemically stable; thermally stable; possess a high mechanical strength and also be able to be processed into useful optical materials.

Extensive work has been done using polymethyl methacrylate (PMMA) as a host polymer (**Table 1.6**). In this work, we compare PMMA to poly(bisphenol A carbonate) (PBC). PBC is a common polymer used for the manufacture of optical eyewear, protective sportswear and other safety products [101,102]. It was selected as a comparison to PMMA due to its desirable properties. Although patents showing the use of PBC before [103] exist, this work reports for the first time the embedding of a cadmium Pc and P(V)TBCs into thin films for NLO application.

Table 1.6: Some polymers previously used for embedding phthalocyanines for optical limiting applications

Polymer	Pc	Imaginary third order susceptibility, $Im[\chi^{(3)}]$ (esu)	Limiting threshold ($J.cm^{-2}$)	Ref.
PMMA	(fPhO)$_4$PcSnCl$_2$	1.4×10^{-8}	6.1 ± 1.8	[104]
	(fPhO)$_4$PcGaCl$_2$	2×10^{-8}	11.6 ± 1.1	
	(nPhO)$_2$PcSnCl$_2$	6.7×10^{-8}	3.7 ± 0.3	
	(αNO$_2$)2PcGe(*t*Bu$_2$PhO)$_2$	3.2×10^{-8}	5.3 ± 0.7	
	Cl$_{16}$PcSn(*t*Bu$_2$PhO)$_2$	2.6×10^{-8}	5.6 ± 0.9	
	(*t*Bu)$_4$PcInCl	4.5×10^{-9}	19.7 ± 21.5	
PMMA	(*t*Bu)$_4$PcInCl	-	0.5 ± 0.1	[25]
	(*t*Bu)$_4$PcGaCl	-	1.6 ± 0.1	
	(*t*Bu)$_4$PcZn	-	3.1 ± 0.3	
	(PhS)$_4$PcZn	-	2.5 ± 0.1	
Polysilane	-	1.5×10^{-12}	-	[105]
PMMA	Ga(*t*BuPhO)$_8$Pc	6.21×10^{-4}	-	[106]

	β(tBuPhO)$_4$PcInCl	1.17×10^{-4}	-	
	α(tBuPhO)$_4$PcInCl	1.12×10^{-4}	-	
	Zn(BzyPhO)$_8$Pc	4.7×10^{-4}	-	
	(BzyPhO)$_8$GaClPc	6.22×10^{-5}	-	
	(BzyPhO)$_8$InClPc	4.01×10^{-4}	-	
	Zn(β-BzyPhO)$_4$Pc	3.7×10^{-5}	-	
	(β-PhO)InClPc	8.18×10^{-5}	-	
	(PhO)$_8$GaClPc	1.28×10^{-4}	-	
	Zn(β-NH$_2$)$_4$Pc	8.84×10^{-4}	-	
PMMA	H$_2$(heptyloxy)$_8$Pc	4.86×10^{-11}	0.164	[107]
	Zn(heptyloxy)$_8$Pc	11.3×10^{-11}	0.137	
	Zn(2-(3-butane 1,4-dioic acid) tri-t-butyl Pc	16.2×10^{-11}	0.112	
	Zn(tBu)$_4$Pc	3.71×10^{-11}	0.112	
	H$_2$(tBu)$_4$Pc	2.1×10^{-11}	0.550	
PVC	(fPhO)$_4$PcSnCl$_2$	6.0×10^{-9}	20.2 ± 7.2	[104]
	(fPhO)$_4$PcGaCl$_2$	2.4×10^{-9}	5.9 ± 0.7	

	(nPhO)$_2$PcSnCl$_2$	6.4×10^{-8}	2.9 ± 0.2	
	(αNO$_2$)2PcGe(tBu$_2$P)$_2$	9.1×10^{-8}	4.3 ± 0.5	
	Cl$_{16}$PcSn(tBu$_2$P)$_2$	2.6×10^{-8}	5.6 ± 0.9	
	(tBu)$_4$PcInCl	4.7×10^{-9}	21.8 ± 27.2	
PEI	AlOCPc	5.32×10^{-5}	-	[106]
	ZnOCPc	4.00×10^{-5}	-	

PMMA = polymethyl methacrylate, PVC = polyvinyl chloride, PEI = polyethyleneimine, tBu = tert-butyl, Bzy = benzyloxy, PhO = phenoxy, fPhO = 4-formylphenoxy, nPhO = 4-aminophenoxy, PhS = thiophenoxy

1.6 Summary of aims

1. To synthesize novel cadmium phthalocyanine for comparison with a previously synthesised lead Pc as well as novel phosphorus triazatetrabenzcorroles with their corresponding Pcs.

2. Characterize all synthesised compounds comprehensively using UV/Vis, MALDI-TOF MS, NMR, elemental analysis, MCD (for phosphorus complexes), laser flash photolysis, and IR.

3. Synthesize polymer thin films using poly(bisphenol A carbonate) and fully characterize them.

4. Model P(V)TBCs to understand spectral and NLO properties.

5. Determine the photophysical and photochemical parameters including: fluorescence quantum yield and lifetime, triplet quantum yield and lifetime, singlet oxygen quantum yield (phosphorus complexes only) and photodegradation quantum yield.

6. Determine the nonlinear optical parameters of the complexes in solution and in the solid state thin films; hyperpolarizability, imaginary third order susceptibility, limiting intensity.

2. EXPERIMENTAL

2.1 Equipment

- Ground state electronic absorption spectra were performed on a Shimadzu UV-2550 spectrophotometer between 300 nm and 800 nm.

- Emission and excitation spectra were obtained on a Varian Eclipse spectrofluorimeter. The absorbance of the vibronic bands ranged between 0.04 and 0.05 at the excitation wavelength of 630 nm for emission studies.

- Infra-red spectra were collected on a Perkin-Elmer Universal ATR Sampling accessory spectrum 100 FT-IR spectrometer.

- ^{1}H NMR spectra were obtained using a Bruker AVANCE 600 MHz NMR spectrometer in DMSO-d_6 or chloroform-d$_1$.

- Elemental analyses were done using a Vario-Elementar Microcube ELIII.

- Mass spectra data were collected on a Bruker AutoFLEX III Smart-beam MALDI-TOF mass spectrometer using various matrices and modes of operation depending on the sample.

- A laser flash photolysis system was used for the determination of triplet decay kinetics. The excitation pulses were produced by a Nd:YAG laser (Quanta-Ray, 1.5 J/90 ns) pumped tunable laser (Lambda Physic FL 3002, Pyridin 1 dye in methanol). The analyzing beam source was derived from a Thermo Oriel xenon arc lamp, and a photomultiplier tube (PMT) was used as a detector. Signals were recorded with a Tektronix TDS 360 two-channel digital real-time oscilloscope. Triplet lifetimes were determined by exponential fitting of the kinetic curves using OriginPro 8 software.

- Fluorescence lifetimes were measured with a FluoTime 300 'EasyTau' spectrometer (PicoQuant GmbH) using a time correlated single photon counting (TCSPC)

technique. The samples were excited at 670 nm with a diode laser (LDH-P-670, 20 MHz repetition rate, 44 ps pulse width, PicoQuant GmbH). The detector employed was a Peltier cooled Photomultiplier (PMA-C 192-M, PicoQuant GmbH).

- Time resolved phosphorescence decay of singlet oxygen at 1270 nm was used to determine singlet oxygen quantum yield in DMSO. The dynamic phosphorescence decay of singlet oxygen ($^1O_2$) was demonstrated using time resolved phosphorescence of $^1O_2$ at 1270 nm. For these studies an ultra sensitive germanium detector (Edinburgh Instruments, EI-P) combined with a 1000 nm long pass filter (Omega, RD 1000 CP) and a 1270 nm band-pass filter (Omega, C1275, BP50) was used to detect $^1O_2$ phosphorescence under the excitation using Quanta-Ray Nd:YAG laser providing 400 mJ, 90 ns pulses of laser light at 10 Hz pumping a Lambda-Physik FL3002 dye laser (Pyridin 1 dye in methanol), with a pulse period of 7 ns and repetition rate of 10 Hz. The near-infrared phosphorescence of the samples were focused onto the germanium detector by a lens (Edmund, NT 48-157) with detection direction perpendicular to the excitation laser beam. The detected signals were averaged with a digital oscilloscope (Tektronics, TDS 360) to show the dynamic decay of $^1O_2$.

- All Z-scan experiments described in this study were performed using a frequency-doubled Nd:YAG laser (Quanta-Ray, 1.5 J /10 ns FWHM pulse duration) as the excitation source. The laser was operated in a near Gaussian transverse mode at 532 nm (second harmonic), with a pulse repetition rate of 10 Hz and energy range of 0.1 µJ – 0.1 mJ, limited by the energy detectors (Coherent J5-09). The low repetition rate of the laser prevents cumulative thermal nonlinearities. The beam was spatially filtered to remove the higher order modes and tightly focused

with a 15 cm focal length lens. No damage was detected between runs since the

sample was moved or replaced (**Fig 2.1**).
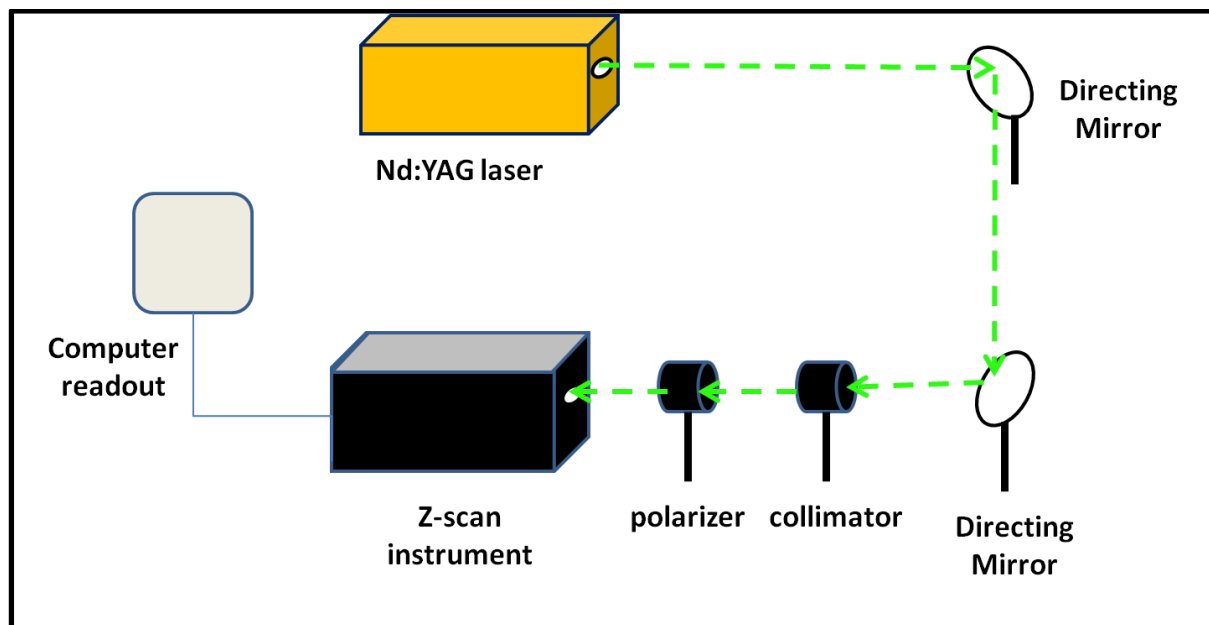
Figure 2.1: Laser setup for Z-scan

- The film thickness and morphology were determined by the TESCAN Vega TS 5136LM scanning electron microscopy (SEM) instrument.

- Irradiations for photodegradation quantum yields of Pcs were performed using a General Electric Quartz lamp (300 W); 600 nm glass (Schott) and water filters were used to filter off ultra-violet and far infrared radiations, respectively. A 700 nm interference filter, with a bandwidth of 40 nm, was placed in the light path just before the cell containing the sample (**Fig 2.2**).
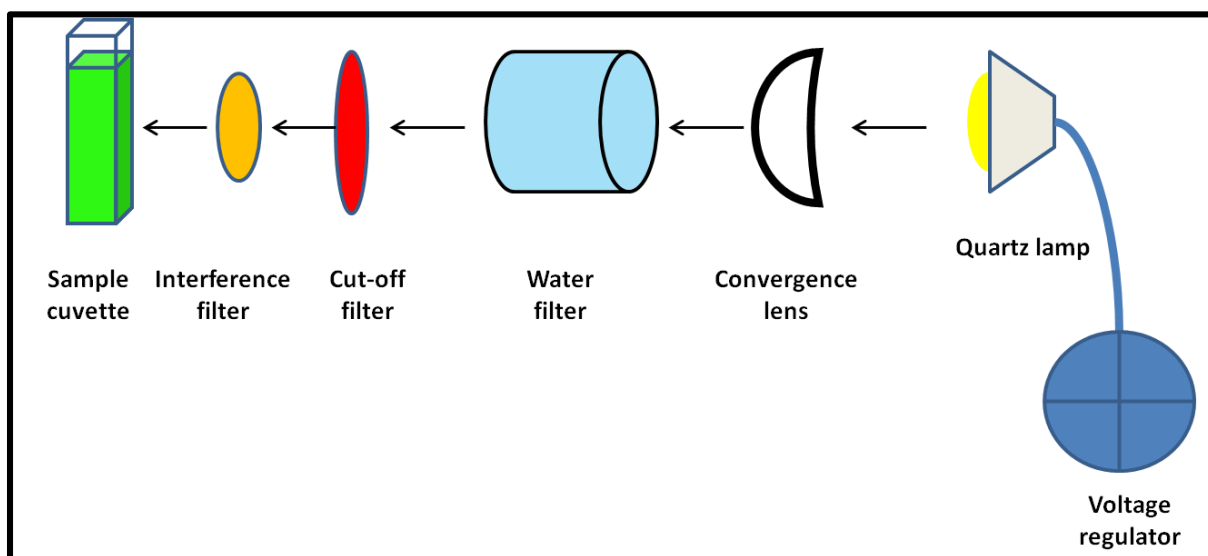
Figure 2.2: Set-up for photodegradation studies

- Magnetic circular dichroism (MCD) spectra were measured with a Chirascan plus spectrodichrometer equipped with a 1 T (tesla) permanent magnet by using both the parallel and antiparallel fields. MCD spectroscopy can be used to elucidate structural information by employing Zeeman splitting of electronic states that cannot be accessed from UV/Vis data [108].

2.2 Materials

N,N-dimethylformamide (DMF), dimethyl sulphoxide (DMSO), dichloromethane (DCM), tetrahydrofuran (THF), methanol, ethanol, 1-octanol and silica gel were purchased from Merck. Reagent grade chloroform was obtained from Minema. Pyridine, phosphorus tribromide (PBr$_3$), phosphorus oxybromide (POBr$_3$), poly(bisphenol A carbonate) (PBC, average molecular weight 28200 g/mol), poly(methyl methacrylate) (PMMA, average molecular weight 120000 g/mol), 4-*t*-butylphenol, cadmium chloride hemi(pentahydrate), 1,8 diazabicyclo[5.4.0]undec-7-ene (DBU), urea and Cremophor-EL were purchased from Sigma Aldrich. Pyridine, DMF, DMSO and DCM were dried using molecular sieves (0.4 nm,

rods). Pb 2,3-[octakis{4-tert butylphenoxyphthalocyanine}] was synthesised according to literature methods [93]. 4,5 Bis(4-*t*-butylphenoxy)phthalonitrile was synthesised according to the method used by Tau and Nyokong [109]. 3-(4-*t*-butylphenoxy)phthalonitrile and 4-(4-*t*-butylphenoxy)phthalonitrile were synthesised according to the method reported in [110]. The unmetallated phthalocyanines used to form the TBCs and phosphorus Pcs, namely 2,3-[octakis{4-*t*-butylphenoxy}]phthalocyanine, tetrakis{1(4), 8(11), 15(18), 22(25)-(4-*t*-butylphenoxy)} phthalocyanine and tetrakis{2(3), 9(10), 16(17), 23(24)-(4-*t*-butylphenoxy)} phthalocyanine were synthesised according to literature methods [29].

2.3 Synthesis of phthalocyanines

2.3.1 Synthesis of cadmium 2,3-{octakis(4-*t*-butylphenoxy)} phthalocyanine - (CdOtBPPc) – Scheme 3.1

Under a blanket of argon, 4,5-bis(4-*t*-butylphenoxy) phthalonitrile (0.30 g, 0.71 mmol) was dissolved in 1-octanol (7 ml) and a few drops of DBU were added. Cadmium chloride hemi(pentahydrate) (0.046 g, 0.19 mmol) was then added to the solution along with urea (0.043 g, 0.7 mmol) and the reaction mixture refluxed at 180 °C overnight. After cooling, the product was refluxed in ethanol for an additional 2 h. The final product was sequentially washed with methanol and water using a centrifuge. A silica column was employed to further purify using THF as the eluent.

Yield: 0.18 g (56 %). UV/Vis (DMSO): λ_{max} nm (log ε) 684 (4.84), 624 (4.09), 345 (4.40), IR [ν_{max}/cm^{-1}]: 2958 (C-H), 1599 (C=C), 1391, 1363 (-C-H), 1307 (C-N), 1244(C–O–C), 1013, 991, 890, 865, 826, 740, 722 (Pc skeletal). ^{1}H NMR (DMSO-d^6): δ, ppm 7.26- 8.02 (16H, m, Pc–H, phenyl-H), 7.01-7.22 (12H, m, Pc-H), 6.46 – 6.98 (12H, m, Pc-H), 0.97-1.08 (72H, m, methyl-

H). Calc for $C_{112}H_{112}N_8O_8Cd\cdot8H_2O$: C 68.82, H 6.60, N 5.73. Found: C 68.50, H 7.41 N 5.56. MS (MALDI-TOF) m/z: Calcd. 1814.7; Found: 1811.7 [M-3H]$^+$

2.3.2 Hydroxyphosphorus 2,3-{octakis(4-*t*-butylphenoxy)} phthalocyanine – (8β-POH-Pc) – Scheme 3.2

To a 20 mL suspension of unmetallated 2,3-{octakis-(4-*t*-butylphenoxy)}Pc (50 mg, 0.029 mmol) in pyridine, phosphorus oxybromide (1 g, 3.5 mmol) was added and heated to 90°C for 1.5 hrs under argon. The reaction, after completion, was cooled and poured into water. The precipitate was filtered off and dried *in vacuo*. Unreacted H_2Pc was extracted using chloroform and the product of interest was eluted using 7:3 CHCl$_3$/MeOH.

Yield: 0.32 mg (62.3 %). UV/Vis (DMSO): λ_{max} nm (log ε) 682 (4.81), 613 (4.14), 348 (4.41), IR [v_{max}/cm^{-1}]: 2957, 2867 (alkyl C-H),1722, 1601 (Aryl C-N), 1506, 1429 (C=C), 1361 (-C-H), 1272, 1235, 1171, 1088 (C–O–C), 1013, 894, 828, 747, 724 (Pc skeletal). ^{1}H NMR (CDCl$_3$): δ, ppm 6.55-7.26 (32H, m, Phenyl–H), 7.29 – 7.43 (8H, m, Pc-H), 1.11 – 1.40 (72H, m, methyl-H), 2.24 – 2.38 (1H, m, O-H). Calc for $C_{112}H_{115}N_8O_9P\cdot10H_2O$: C 69.76, H 7.06, N 5.81. Found: C 69.23, H 6.24 N 5.84. MS (MALDI-TOF) m/z: Calcd. 1746.12; Found: 1745.2 [M-H]$^+$

2.3.3   Synthesis of tetra-substituted phosphorus phthalocyanines

The synthesis was as outlined above for **8β-POH-Pc**, except tetrakis{1(4), 8(11), 15(18), 22(25)-(4-*t*-butylphenoxy)} Pc was used for making **4α-POH-Pc** and tetrakis{2(3), 9(10), 16(17), 23(24)-(4-*t*-butylphenoxy)} Pc was used to make **4β-POH-Pc**. The amount of H_2Pc used (α or β) was 50 mg (0.045 mmol). The amount of POBr$_3$ and experimental conditions were as outlined for **8β-POH-Pc**.

2.3.3.1 Hydroxyphosphorus(V) (1(4), 8(11), 15(18), 22(25)-*t*-butylphenoxy)

phthalocyanine – (4α-POH-Pc) – Scheme 3.3

A light green solvate was obtained. Yield: 0.17 mg (32.6 %). UV/Vis (DMSO): λ_{max} nm (log ε) 706 (4.45), 635 (3.83), 330 (4.16), IR [v_{max}/cm^{-1}]: 3039 (aromatic C-H), 2957, 2867 (*t*-Bu C-H), 1720, 1664 (C-N), 1598 (aromatic C=C), 1391, 1363 (-C-H), 1268, 1171, 1088, 1052(C–O–C), 1013, 972, 895, 827, 747, 724, 682 (Pc skeletal). ^{1}H NMR (CDCl$_3$): δ, ppm 7.31- 7.62 (16H, m, Phenyl–H), 6.93-7.14 (12H, m, Pc-H), 2.58 – 2.60 (1H, m, O-H), 1.29-1.35 (36H, m, methyl-H). Calc for C$_{72}$H$_{65}$N$_8$O$_8$P·6H$_2$O: C 68.64, H 6.39, N 8.77. Found: C 68.85, H 8.25 N 4.88. MS (MALDI-TOF) m/z: Calcd. 1153.3; Found: 1151.8[M-2H]$^+$

2.3.3.2 Hydroxyphosphorus(V) (2(3), 9(10), 16(17), 23(24)-*t*-butylphenoxy)

phthalocyanine – (4β-POH-Pc) – Scheme 3.4

A dark green product was obtained. Yield: 0.24 mg (46.1 %). UV/Vis (DMSO): λ_{max} nm (log ε) 683 (5.27), 613 (4.45), 330 (4.94), IR [v_{max}/cm^{-1}]: 3053 (C-H), 2958, 2860 (alkyl C-H), 1723, 1596 (aromatic C-N), 1505 (C=C), 1361 (O-H), 1267, 1235, 1171, 1082 (C–O–C), 1013, 957, 890, 827, 745 (Pc skeletal). ^{1}H NMR (CDCl$_3$): δ, ppm 7.28 – 7.76 (16H, m, Phenyl–H), 6.83 – 7.23 (12H, m, Pc-H), 2.56 (1H, s, O-H), 1.35 – 1.50 (36H, m, methyl-H). Calc for C$_{72}$H$_{73}$N$_8$O$_9$P·5H$_2$O: C 70.57, H 6.00, N 9.14. Found: C 70.82, H 6.84 N 7.41. MS (MALDI-TOF) m/z: Calcd. 1153.3; Found: 1151.8[M-2H]$^+$

2.4 Synthesis of triazatetrabenzcorroles [51]

2.4.1 Synthesis of Hydroxyphosphorus(V) 2,3-{octakis(4-*t*-butylphenoxy)} triazatetrabenzcorrole – (8β-POH-TBC) – Scheme 3.5

A solution of 0.2 ml PBr$_3$ in 2 mL pyridine was added to a suspension of unmetallated 2,3-octakis-[4-*t*-butlyphenoxy]phthalocyanine (57.5 mg, 0.052 mmol) in 15 ml pyridine. This was refluxed at 90°C for 1.5 hrs under an inert atmosphere. The product was cooled to room temperature and was poured into water and then filtered. The precipitate was washed with 3 × 30 ml methanol and then purified further on a silica column, with the product of interest coming out with a 7:3 CHCl$_3$/MeOH solvent system.

Yield: 0.18 mg (35%). UV/Vis (DMSO): λ_{max} nm (log ε) 664 (4.71), 636 (4.44), 603 (4.16), 449 (5.06), 418 (4.59), IR [ν_{max}/cm^{-1}]: 1246, (C–O–C); 1207, 1169, 1104, 1042 (C-O); 1339 (C-N); 1012 (-C-H), 1602, 1505, 1446, 1405 (C=C), 1363 (O-H), 2958 (alkyl C-H); 886, 826, 746, 723, 682 (TBC Skeletal). ^{1}H NMR (400 MHz; CDCl$_3$-*d*): δH, ppm 9.11 (8H, s, ArH), 7.43 (16H, q, ArH), 7.16 (16H, q, ArH), 1.35 (72H, s, tBu) MS (MALDI-TOF): m/z Calcd. 1730.8, Found: 1730.1 [M-OH]$^+$

2.4.2 Synthesis of tetra-substituted triazatetrabenzocorroles

This synthesis was accomplished using the same method as for **8β-POH-TBC**, using α or β unmetallated tetrakis-(4-*t*-butylphenoxy)phthalocyanine (50 mg, 0.029 mmol), instead of octakis-(4-*t*-butylphenoxy) Pc. Purification conditions and amounts of reagents are as outlined above.

2.4.2.1 Hydroxyphosphorus(V) (1(4), 8,(11), 15,(18), 22,(25)-*t*-butylphenoxy)

triazatetrabenzcorrole – (4α-POH-TBC) – Scheme 3.6

The final product was a very dark green solid. Yield: 27.8 mg (47 %). UV/Vis (DMSO): λ_{max} nm

(log ε) 676 (4.98), 632 (4.55), 602 (4.31), 448 (5.09), 419 (4.68) IR [ν_{max}/cm^{-1}]: 3027

(aromatic C–H), 2958 (alkyl C-H), 1610, 1574, 1506, 1483 (aromatic C–C stretch), 1249, 1214,

1174, 1129 (C–O–C), 1342 (C–N), 1054 (C–H bend), 886, 826, 746, 723, 682 (TBC skeletal). ^{1}H

NMR (CDCl$_3$): δ, ppm 7.38-7.54 (16H, m, Phenyl-H), 6.72–7.12 (12H, m, TBC-H), 2.1 (2H,4s,

OH) 0.81–1.49 (36H, m, methyl-H). Calc for $C_{72}H_{66}N_7O_6P \bullet 4H_2O$: C 69.27, H 6.30, N 7.85.

Found: C 69.75, H 6.15 N 7.30. MS (MALDI-TOF) m/z: Calcd. 1140.3; Found: 1137.6 [M-3H]$^+$.

2.4.2.2 Hydroxyphosphorus(V) (2(3), 9,(10), 16,(17), 23,(24)-*t*-butylphenoxy)

triazatetrabenzcorrole – (4β-POH-TBC) – Scheme 3.7

A dark green product was obtained. Yield: 40.3 mg (68 %). UV/Vis (DMSO): λ_{max} nm (log ε)

660 (4.82), 632 (4.55), 602 (4.31), 448 (5.09), 419 (4.68), IR [ν_{max}/cm^{-1}]: 3306 (O–H); 3071

(aromatic C–H); 2957, 2924 (aromatic C–H), 1596, 1504 (C–C); 1274, 1239, 1171, 1106 (C–

O–C); 1359, 1014 (C–N); 958, 876, 825, 747, 680 (TBC skeletal). ^{1}H NMR (CDCl$_3$): δ, ppm

7.36–7.48 (12H, m, TBC-H), 6.83–7.19 (16H, m, Phenyl-H), 2.21 (2H, s, O-H), 1.22-1.40 (36H,

m, methyl-H). Calc for $C_{72}H_{66}N_7O_6P \bullet 12H_2O$: C 62.91, H 6.75, N 7.13. Found: C 62.25, H 5.89 N

7.33. MS (MALDI-TOF) m/z: Calcd. 1140.3; Found: 1141.8 [M+H]$^+$.

2.5   Preparation of polymer thin films

Solutions of Pcs and TBCs were prepared using DCM. To 5 mL of each of these solutions, PBC

or PMMA were added to form PBC/Pc, and PMMA/Pc and PBC/TBC solutions. The P(V)Pcs

and P(V)TBCs were only prepared in PBC. The final concentrations of the Pcs and TBCs and polymer mass used are shown in **Table 2.1**. The films was prepared by placing 1 ml of solution in a small glass petri dish (diameter = 5 cm), and placing it under vacuum ($\sim 10^{-3}$ Torr) until the solvent was completely removed. Three films were produced from each of the above mentioned solutions and characterization was done on each in order to obtain an average result. Following synthesis, the films were stored in a dessicator in the dark to minimise interaction with light and a chemical environment.

Table 2.1: Concentrations of compounds embedded in thin films

Compound	Concentration (M)	Polymer	Polymer mass (g)
CdOtBPPc	5.6×10^{-4}	PBC	0.3
		PMMA	0.6
PbOtBPPc	6.6×10^{-4}	PBC	0.3
		PMMA	0.6
8β-POH-Pc	2.3×10^{-5}	PBC	0.5
4α-POH-Pc	5.3×10^{-5}	PBC	0.5
4β-POH-Pc	8.1×10^{-6}	PBC	0.5
8β-POH-TBC	2.9×10^{-5}	PBC	0.5
4α-POH-TBC	1.6×10^{-5}	PBC	0.5
4β-POH-TBC	2.3×10^{-5}	PBC	0.5

The differing masses used for the PBC and PMMA (0.3 and 0.6 g) were for the reason of obtaining a similar solution viscosity. The use of 0.5 g for the P(V)Pcs and P(V)TBCs is of little significance. The concentration of PBC used did not alter the result of the optical limiting.

2.6 Molecular modelling

All molecular models were drawn using the ArgusLAB software. Geometry optimization calculations were carried out using the B3LYP functional of the Gaussian09 software packages [31] with 6-31G(d) basis sets. The B3LYP optimized geometries were then used to carry out TD-DFT calculations using the Coulomb-attenuated B3LYP functional (CAM-B3LYP) functional with 6-31G(d) basis sets. The CAM-B3LYP functional was used to calculate the electronic absorption properties based on the time-dependent (TD-DFT) method, since it includes a long-range correction of the exchange potential, which incorporates an increasing fraction of Hartree-Fock (HF) exchange as the interelectronic separation increases. This has been demonstrated to make it more suitable for studying porphyrinoid compounds where there is significant charge transfer in the electronic excited states [111,112] as is likely to be the case with TBC and Pc complexes.

3. Synthesis, Photophysical & Photochemical Characterization

This section presents the photophysical and photochemical properties of

the compounds synthesized in this work; both in solution and in thin films.

Publications

The results that are presented in this thesis have been published in the following journals. These journal articles shall not be referenced in this text.

1) "Enhanced nonlinear optical properties of octa-substituted lead and Cadmium phthalocyanines when embedded in poly(bisphenol A carbonate) as thin films", **Colin Mkhize**, Jonathan Britton and Tebello Nyokong, Polyhedron 81 (2014) 607-613

2) " Synthesis, characterization and photodynamic therapy properties of an octa-4-*tert*-butylphenoxy-substituted phosphorus(V) triazatetrabenzcorrole", Maohu Shi, Jiangwei Tian, **Colin Mkhize**, Gugu Kubheka, Jinfeng Zhou, John Mack, Tebello Nyokong, Zhen Shen, Journal of Porphyrins and Phthalocyanines 18 (2014) 698-717

3) "Optical limiting and singlet oxygen generation properties of phosphorus triazatetrabenzcorroles", **Colin Mkhize**, Jonathan Britton, John Mack, Tebello Nyokong, Journal of Porphyrins and Phthalocyanines, *in press.*

3. Synthesis and characterization

3.1 Phthalocyanines

CdOtBPPc was synthesised for the purpose of comparing its NLO properties with the previously reported **PbOtBPPc** [93,113]. The characterization of **CdOtBPPc** is described in this work for the first time. Novel phosphorus Pcs were synthesised for comparison with P(V)TBCs, to evaluate the effect of the loss of an aza-nitrogen on the photophysical and NLO properties. The P(V)Pcs were also compared with the **CdOtBPPc** and **PbOtBPPc** for NLO behaviour.

3.1.1 Cadmium 2,3-[octakis{4-*t*-butylphenoxy}]phthalocyanine (Scheme 3.1)
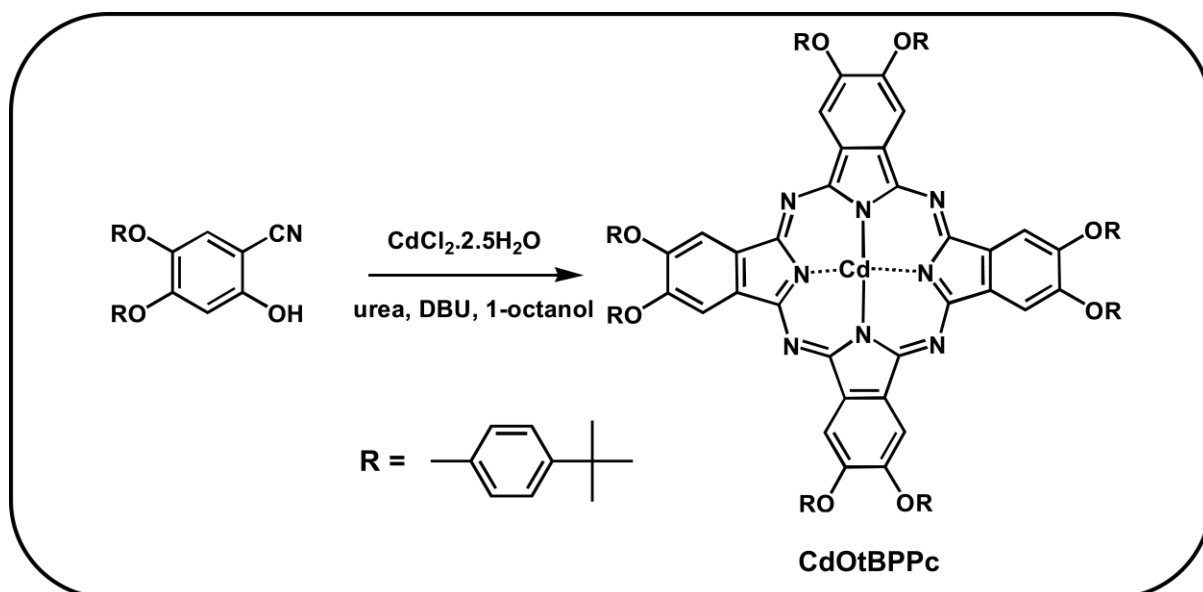
Scheme 3.1: Synthetic route for CdOtBPPc

Scheme 3.1 gives the synthetic pathway for the octa-substituted cadmium Pc used in this work. The **CdOtBPPc** was obtained by the cyclotetramerization of 4,5-bis(4-*t*-butylphenoxy)phthalonitrile in the presence of DBU as a base and cadmium chloride hemi-

pentahydrate using 1-octanol as a high boiling point solvent. The reaction was performed overnight at 180 °C under an argon atmosphere. The reaction mixture was cooled then further refluxed in ethanol for 2 hrs to dissolve any unreacted phthalonitrile. The precipitate was washed with methanol and water successively and then dried at 70°C. The product was the purified on a silica column with tetrahydrofuran (THF) used as an eluent.

The IR spectrum showed peaks between 700 and 1013 cm^{-1}, which correspond to the vibrations of the Pc skeletal structure. The band at 2958 cm^{-1} is assigned to the aromatic C-H bond stretch, whilst 1363 cm^{-1} and 1391 cm^{-1} are assigned to the C–C bond on the terminal methyl groups.

The ^{1}H-NMR results showed three multiplets between 7.26 – 8.02, 7.01 – 7.22 and 6.46 – 6.98 ppm. The peaks integrated to 40 protons in total, which are all aromatic. The broad signal from 0.97 -1.08 ppm corresponds to the 72 methyl protons on the substituents. The CHNS elemental analysis showed values lower than expected due to the presence of water. It is known that Pcs and their analogs are often isolated as solvates [114].

Fig 3.1 shows the ground state electronic absorption spectra of **CdOtBPPc** and **PbOtBPPc** in DMSO. The use of bulky substituents such as 4-*t*-butylphenoxy is known to reduce aggregation [21] and increase solubility [41], but we see in **Fig 3.1** a broad Q band with a band due to aggregation (for **CdOtBPPc**). The Q band became more resolved on the addition of a surfactant, Cremophor-EL (**figure not shown**).

The spectrum of the **PbOtBPPc** is more typical of a monomeric Pc in solution. The better solubility of the **PbOtBPPc** is due to the fact that it has a lower symmetry compared to the **CdOtBPPc**. The lower symmetry affords for better dispersion due to the dipole-dipole interactions of the molecule and solvent. There is a significant red-shift (ca. 25 nm) in the Q band of the **PbOtBPPc** (**Table 3.1**) compared to **CdOtBPPc**. This is due the fact that lead is

heavier than cadmium. Heavy metals typically cause the Q band to be red-shifted [115].

Asymmetry (shuttle cock arrangement of Pb) also results in red shifting [116].
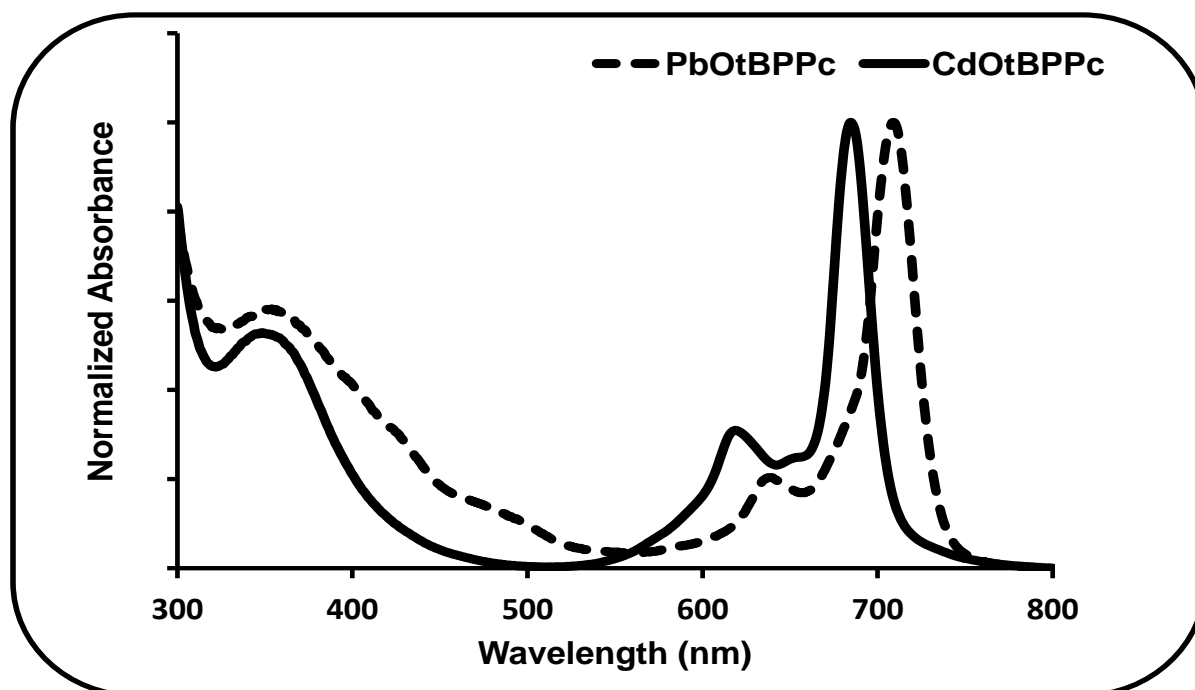
Figure 3.1 Ground state absorption spectra of CdOtBPPc and PbOtBBPc in DMSO (concentration: ~9 x 10⁻⁵ M)

Table 3.1: Q band maxima of all synthesised compounds in solution

Compound	$\lambda_{Q,abs}$	log ε	solvent
CdOtBPPc	684	4.84	DMSO
PbOtBPPc[a]	709	4.94	DMSO
8β-POH-Pc	682	4.81	DMSO
4α-POH-Pc	706	4.45	DMSO
4β-POH-Pc	683	5.27	DMSO
8β-POH-TBC	664	4.71	DMSO
4α-POH-TBC	676	4.98	DMSO
4β-POH-TBC	660	4.82	DMSO

a- values taken from [93]

59

3.1.2 Phosphorus phthalocyanines

Schemes 3.2 – 3.4 show the synthetic pathways for the new phosphorus Pcs reported in this work. The synthesis is very similar to that of the phosphorus TBCs discussed below, the only difference being the source of the phosphorus. POBr$_3$ is not as reactive as PBr$_3$, which affords for the milder conditions of these reactions. Pyridine was determined to be the only solvent in which this methodology works [54]. **8β-POH-Pc**, **4β-POH-Pc** and **4α-POH-Pc** were all formed using previously synthesised H$_2$Pc.

3.1.2.1 Hydroxyphosphorus(V) 2,3-[octakis{4-*t*-butylphenoxy}]phthalocyanine (Scheme 3.2)
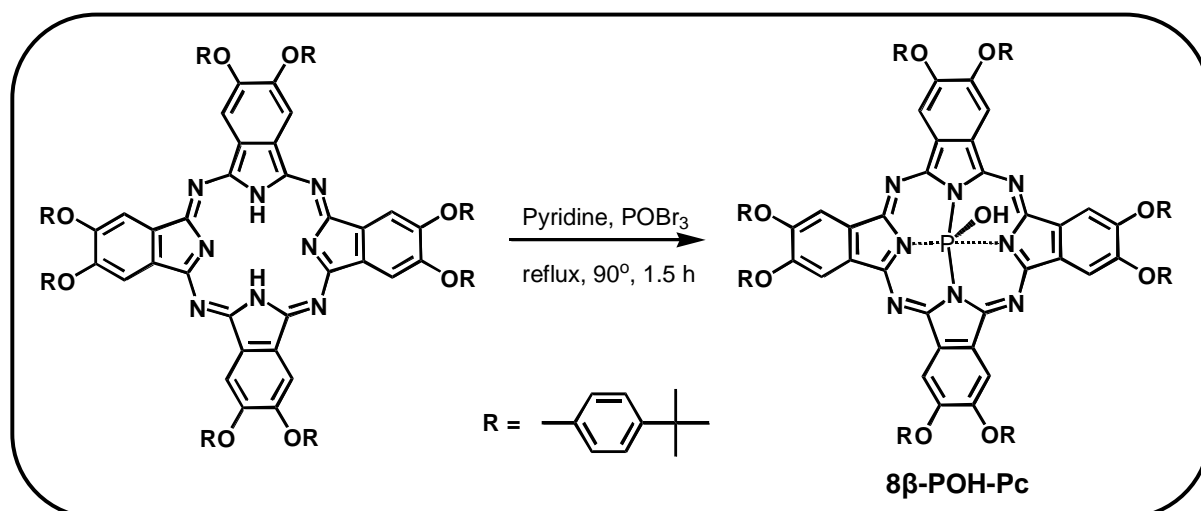
Scheme 3.2: Synthetic pathway for 8β-POH-Pc

The IR spectrum of **8β-POH-Pc** showed the typical peaks expected for a Pc. The Pc skeletal vibrations appeared in the range 720 – 1015 cm^{-1}. The C-O stretch vibrations were seen at 1088, 1171, 1235 and 1272 cm^{-1}. Aromatic C=C stretch vibrations had peaks at 1429 and 1506 cm^{-1}. The ^{1}H NMR spectrum (in CDCl$_3$), showed a total of 113 protons. A broad multiplet between 6.55 and 7.26 ppm integrated to 32 aryl protons. 8 protons were found in the broad singlets between 7.29 and 7.43 ppm for the Pc ring. 72 alkyl protons were

accounted for between 1.11 and 1.40 ppm. Lastly, a sharp singlet (2.24-2.38 ppm) showed the presence of the hydroxyl group.

Fig 3.2 shows the ground state absorption spectrum of **8β-POH-Pc** in DMSO. Substituted Pcs are known to have very high extinction coefficients ($\sim10^5$) in the 600 – 750 nm region owing to their good solubility in organic solvents [117]. The Q band shown is very sharp, which is indicative of a pure monomeric species in solution, as is observed for the **PbOtBPPc** Q band (**Table 3.1**). The Q band was observed at 682 nm, close to that of **CdOtBPPc**. It is easy to see what kind of influence the central atom size has on the Q band position; with lighter atoms resulting in more blue shifted peaks and heavier atoms giving more red shifted peaks.
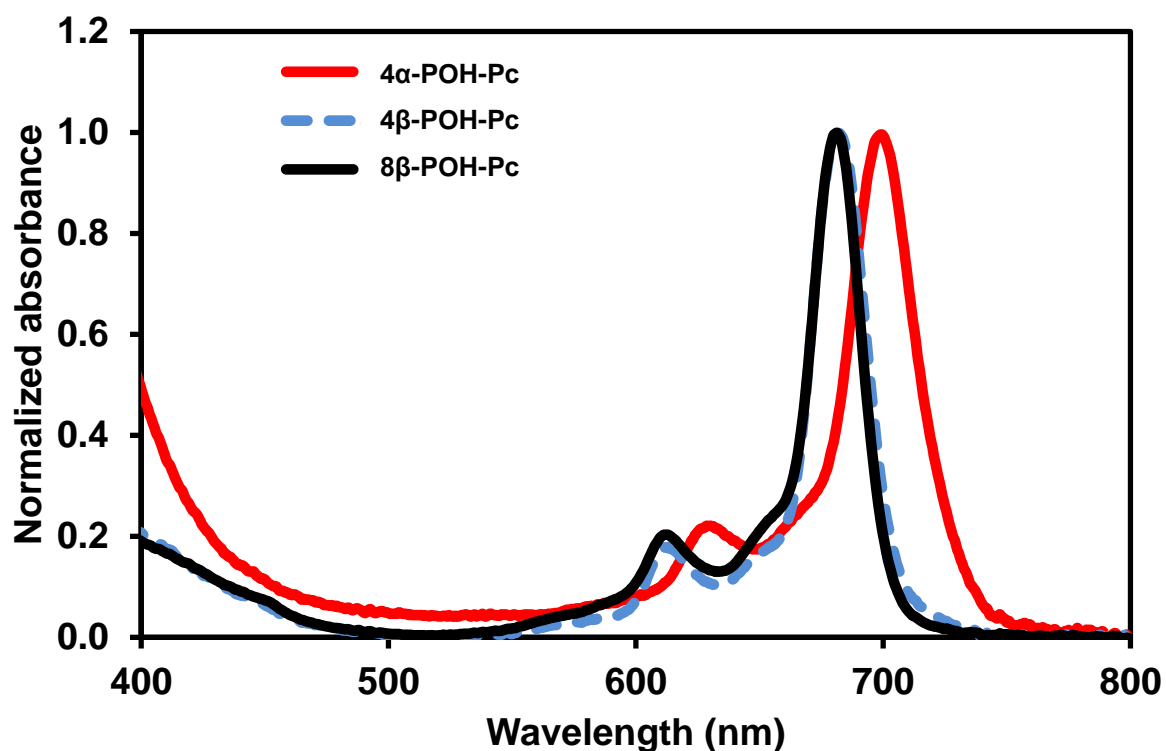
Figure 3.2: Ground state absorption spectrum of i) 8β-POH-Pc, ii) 4α-POH-Pc and iii) 4β-POH-Pc in DMSO. Conc i) 3.1 x 10^{-5} M, ii) 2.7 x 10^{-5} M and iii) 4.9 x 10^{-6} M.

3.1.2.2 Hydroxyphosphorus(V) (1(4), 8(11), 15(18), 22(25)-*t*-butylphenoxy) phthalocyanine (Scheme 3.3)
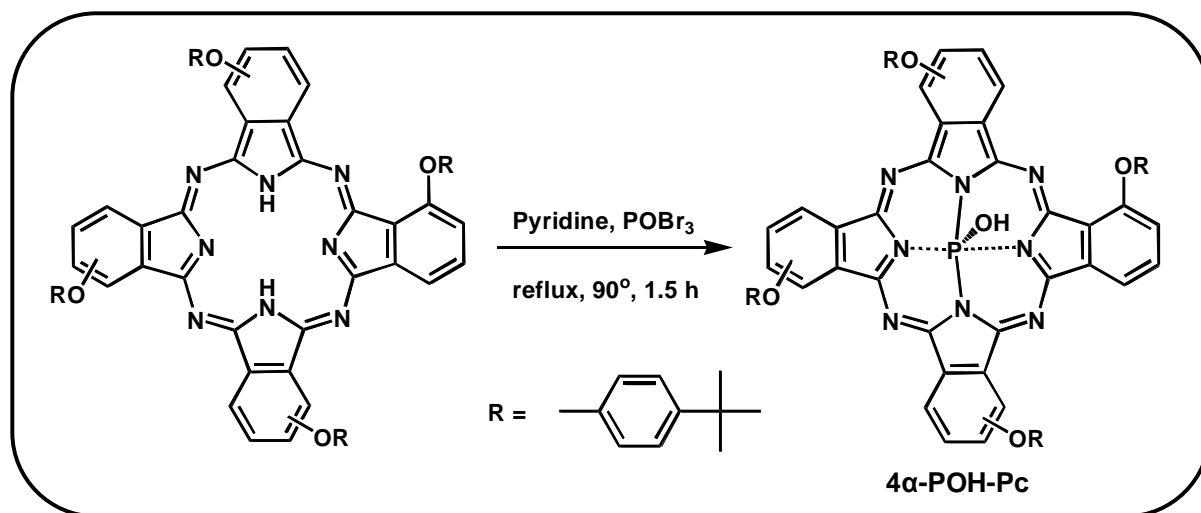
Scheme 3.3: Synthetic pathway for 4α-POH-Pc

4α-POH-Pc was formed with a relatively low yield (32.6%). It was quite difficult to isolate the product from solution, but once precipitated, a light green compound (which remained quite hydrated) was obtained. Li et al. discuss that P(V)Pcs can become water soluble if the reaction proceeds for too long [62] (most likely due to quaternization of the substituents), but the conditions used in this reaction leave doubt that this was the case here. In any event, the compound was isolated after further purification. The IR results showed Pc skeletal vibrations between 680 and 1015 cm^{-1}. The bands at 1720 and 1664 cm^{-1} were identified as being C-N stretch vibrations. A distinct peak at 3039 cm^{-1} was attributed to the presence of aromatic C-H stretches, whilst the peaks at 2957 and 2867 cm^{-1} were a result of the C-H vibrations on the terminal t-butyl groups. Proton NMR showed the presence of 73 protons (which was confirmed by elemental analysis and MALDI-TOF mass spectroscopy).

The ground state absorption spectrum of **4α-POH-Pc** (**Fig 3.2**) shows the characteristic Q and B bands associated with Pcs. The Q band is red shifted (706 nm) when compared to the

Q bands of **8β-POH-Pc** and **4β-POH-Pc**. This is typical of non-peripherally substituted Pcs. The Q band of **4α-POH-Pc** is almost as red shifted as that of **PbOtBPPc**. This could result in similar trends being observed in terms of NLO activity.

3.1.2.3 Hydroxyphosphorus(V) (2(3), 9(10), 16(17), 23(24)-*t*-butylphenoxy) phthalocyanine (Scheme 3.4)
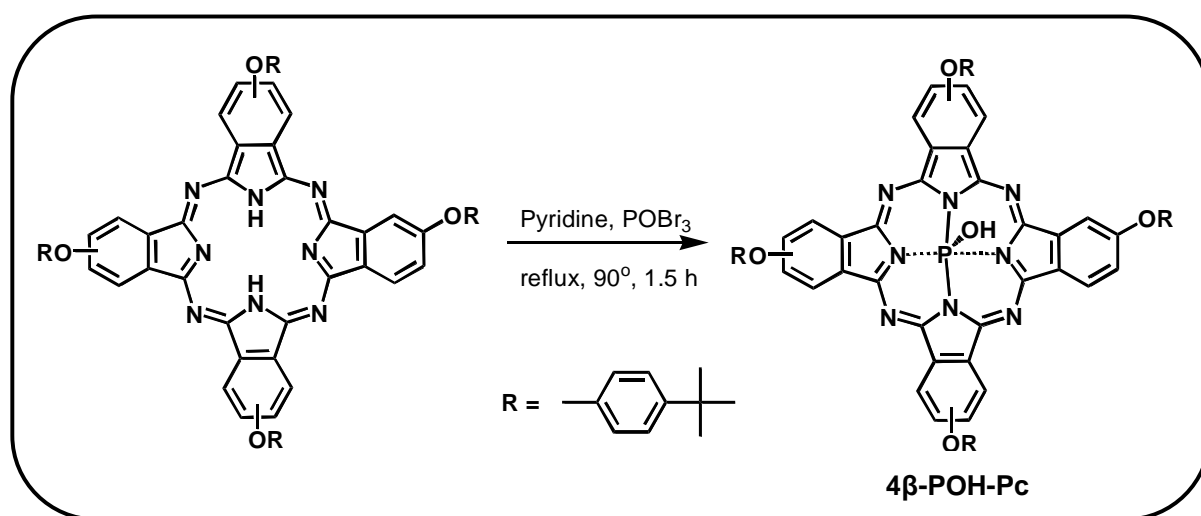
Scheme 3.3: Synthetic pathway for 4β-POH-Pc

The yield obtained for this product was better than for the non-peripherally substituted analogue at 46.1%. This is most likely due to the fact that the substituents are less likely to interact sterically during cyclotetramerization, thus allowing a greater fraction of the starting material to fully form into the product.

IR spectral peaks were identified for Pc skeletal vibrations (740 – 1015 cm^{-1}), C-O-C bond stretch vibrations (1080 – 1270 cm^{-1}), aromatic C-H stretch vibration (3053 cm^{-1}), and aromatic C=C vibrations at 1505 cm^{-1}. A peak at 1361 cm^{-1} was found to be due to the presence of the hydroxyl ligand. The ^{1}H NMR spectrum showed the presence of 73 protons; 16 aromatic protons between 7.28 and 7.76 ppm; a further 12 aromatic Pc protons in the range 6.83-7.23 ppm; 1 hydroxyl proton in a sharp singlet at 2.56 ppm and 36 methyl

protons from 1.35 to 1.50 ppm. Mass spectral data confirmed the molecular mass of the compound.

Fig 3.2 shows the ground state absorption spectrum of **4β-POH-Pc** in DMSO. The compound showed superb solubility, and this is confirmed by the large extinction efficient (~186 000) (**Table 3.1**). The spectrum for **4β-POH-Pc** is very similar to that of **8β-POH-Pc** in terms of Q band position and shape due to the similarity of the substitution. **4β-POH-Pc** is blue shifted compared to **4α-POH-Pc** due to the non-peripheral substitution in the latter. Compared to **PbOtBPPc**, **4β-POH-Pc** is blue shifted by a significant 26 nm. Again, this is due to the difference in central atom size. Compared to **CdOtBPPc**, however, **4β-POH-Pc** (like **8β-POH-Pc**) is very similarly positioned.

3.2 Synthesis of phosphorus triazatetrabenzcorroles

The synthesis of the TBC complexes is reported in this work for the first time. They all followed the same synthetic method (as shown in **Schemes 3.5 – 3.7**). The relevant H_2Pc was used in each case, and the insertion and contraction method reported in [48,51] was used to achieve the desired product. Each TBC molecule was modelled theoretically using TD-DFT calculations and compared to its parent H_2Pc. This was done to investigate the effect of the removal of a meso-nitrogen atom on the photophysical and NLO properties of the compounds. The NLO results will be discussed in chapter 5.

3.2.1 Hydroxyphosphorus(V) 2,3-[octakis{4-*t*-butylphenoxy}]triazatetrabenzcorrole

(Scheme 3.5)
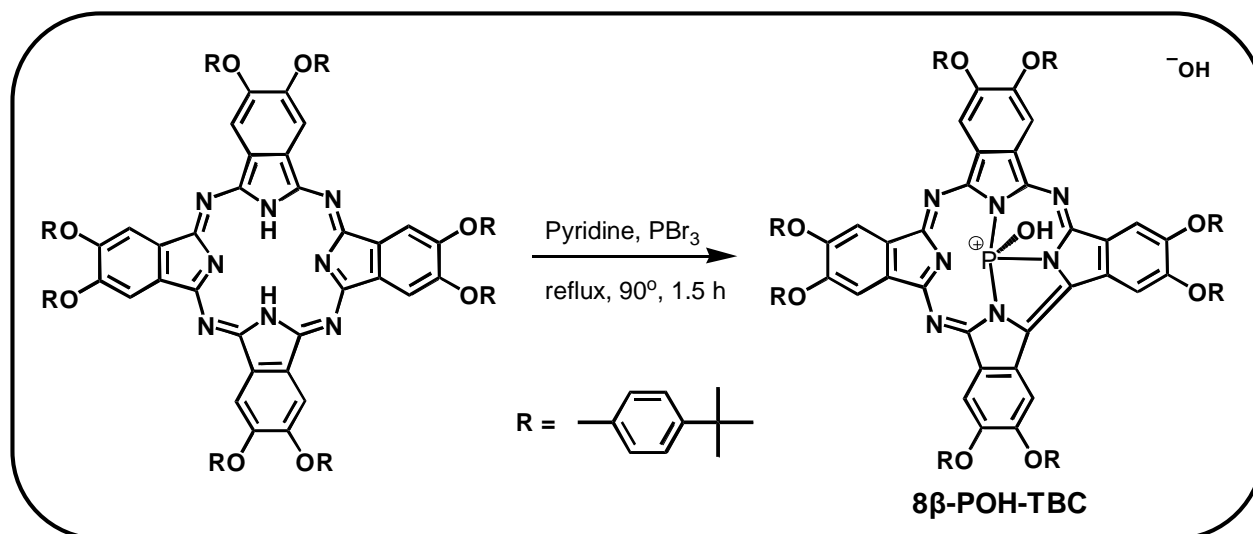
Scheme 3.5: Synthetic pathway for 8β-POH-TBC

A relatively low yield of 35% was achieved for this compound. The IR spectrum showed peaks in similar positions as those seen in Pcs. Peaks between 680 and 890 cm^{-1} are from the TBC skeletal vibrations. C – O stretch vibrations were found between 1040 and 1210 cm^{-1}. The methyl C-H stretch vibrations were visualised by quite a strong peak at 2958 cm^{-1}. The axial ligand (O-H) vibration was also detected at 1363 cm^{-1}.

The ^{1}H-NMR spectrum showed a singlet at 9.11 ppm integrating to 8 protons the TBC, a singlet at 1.35 ppm for 72 alkyl protons and two multiplets which both integrated to a total of 32 aryl protons found on the substituents. A total of 112 protons were accounted for.

Fig 3.3 shows the ground state absorption spectrum of **8β-POH-TBC**. We notice the sharp B band and weaker Q band compared to the P(V)Pcs. The Q band is red shifted significantly and is of lesser intensity than the P(V)Pcs. This too shall be explained in chapter 5.
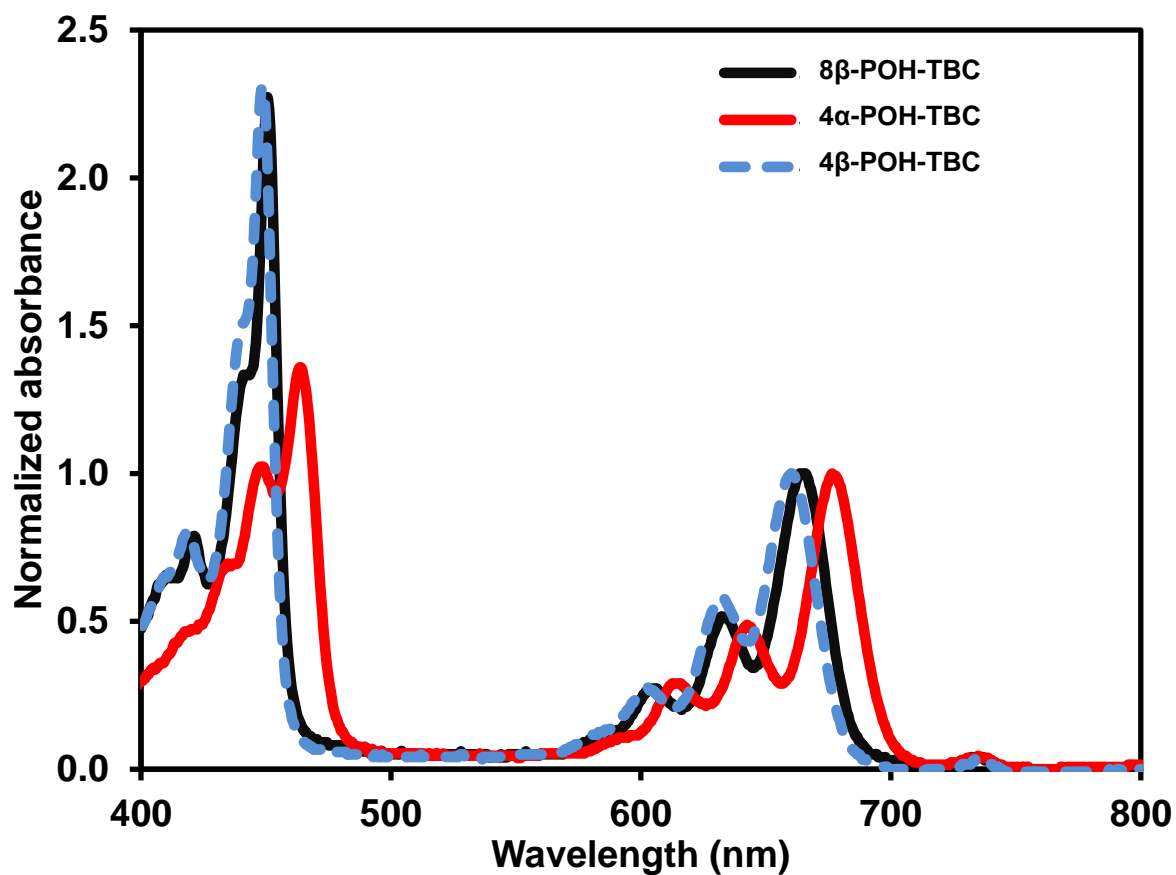
Figure 3.3: Ground state absorption spectrum of 8β-POH-TBC, 4α-POH-TBC and 4β-POH-TBC in DMSO. Concentration ~1 – 2 x 10⁻⁵ M.

The spectrum also shows that the Q band of the TBC is split. This is explained using Gouterman's frontier π molecular orbital model. This effect is better explained in chapter 5, with magnetic circular dichroism results used to distinguish between vibronic and electronic transition bands.

3.2.2 Hydroxyphosphorus(V) (1(4), 8(11), 15(18), 22(25)-*t*-butylphenoxy)

triazatetrabenzcorrole (Scheme 3.6)
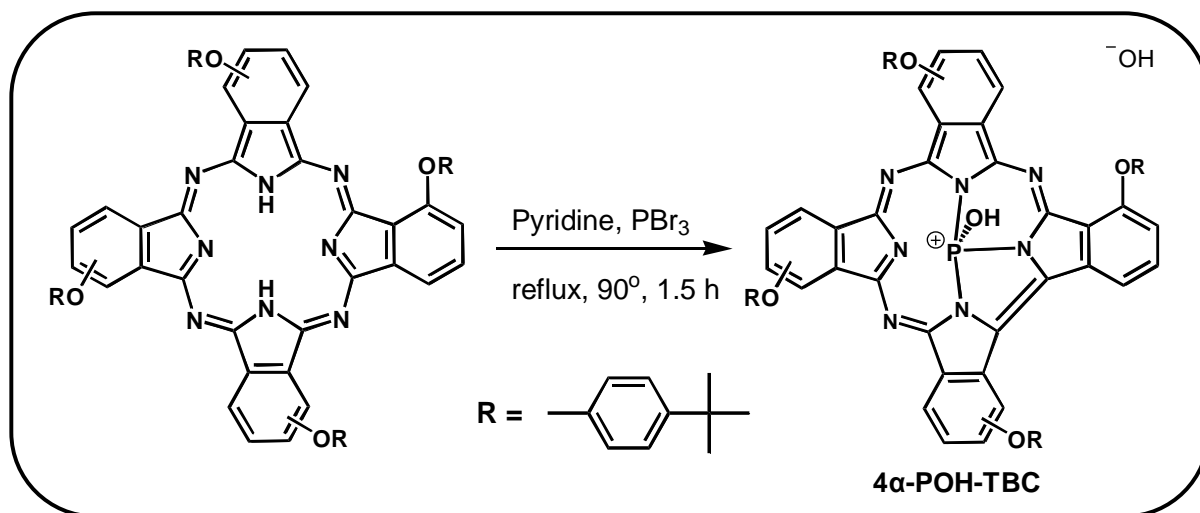
Scheme 3.6: Synthetic pathway for 4α-POH-TBC

The IR spectrum showed TBC skeletal vibrations between 680 and 890 cm^{-1}. This is consistent with the skeletal vibrations observed in Pcs. Aromatic C–C stretches were observed at 1610, 1574 and 1506 cm^{-1}, where we also expect to observe the direct bond between two isoindoline units. A typical aromatic C-N bond stretch at 1342 cm^{-1} was detected. The proton NMR spectrum integrated to a total of 68 (including two protons from the hydroxyl substituents). A multiplet from 7.38 to 7.54 ppm integrated for 16 protons (originating from the aryl region of the substituents). Between 6.72 – 7.12 ppm, 12 protons were found correlating to the skeletal aryl protons. 36 alkyl protons gave a strong signal between 0.81 – 1.49 ppm. Lastly, two protons from the free and coordinated hydroxyl groups were detected at 2.1 ppm as a sharp singlet.

The compound showed good solubility in DMSO as well as in CHCl$_3$ (**Table 3.1**). The Q band is red shifted compared to **8β-POH-TBC** and **4β-POH-TBC** due to the compound being non-peripherally substituted (**Fig 3.3**), which results in the Q band being very close to the

peripherally substituted P(V)Pcs (**8β-POH-Pc** and **4β-POH-Pc**). This could manifest itself in similar properties for all three compounds.

3.2.3 Hydroxyphosphorus(V) (2(3), 9(10), 16(17), 23(24)-*t*-butylphenoxy) triazatetranbenzcorrole (Scheme 3.7)
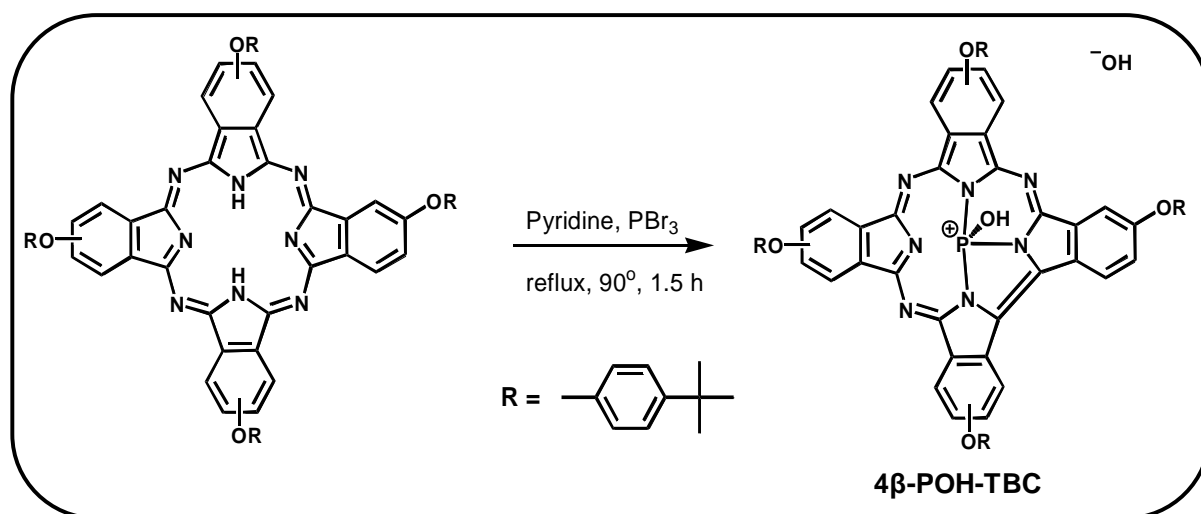
Scheme 3.7: Synthetic pathway for 4β-POH-TBC

The IR spectrum of **4β-POH-TBC** is very similar to those of **4α-POH-TBC** and **8β-POH-TBC**. We observed the TBC skeletal vibrations between 680 and 960 cm^{-1}. A strong O-H stretch vibration was seen at 3306 cm^{-1}. C-C stretch vibrations were seen at 1504 and 1596 cm^{-1}. C-O vibrations (from the ether bonds) were identified by peaks between 1100 and 1280 cm^{-1}.

The ^{1}H NMR showed great similarity with that of **4α-POH-TBC**, with a total proton count of 68 (including the 2 hydroxyl protons). **Fig 3.3** shows the ground state absorption spectrum **4β-POH-TBC** in DMSO. The compound showed good solubility in DMSO as well as in CHCl$_3$. This spectrum is very similar to that of **8β-POH-TBC** except for the slight blue shift (ca. 4 nm) due to the lesser number of substituents present. **Table 3.1** lists all the Q band data.

3.3 Photophysical and photochemical properties

3.3.1 Phthalocyanines

3.3.1.1 Fluorescence spectra and quantum yields
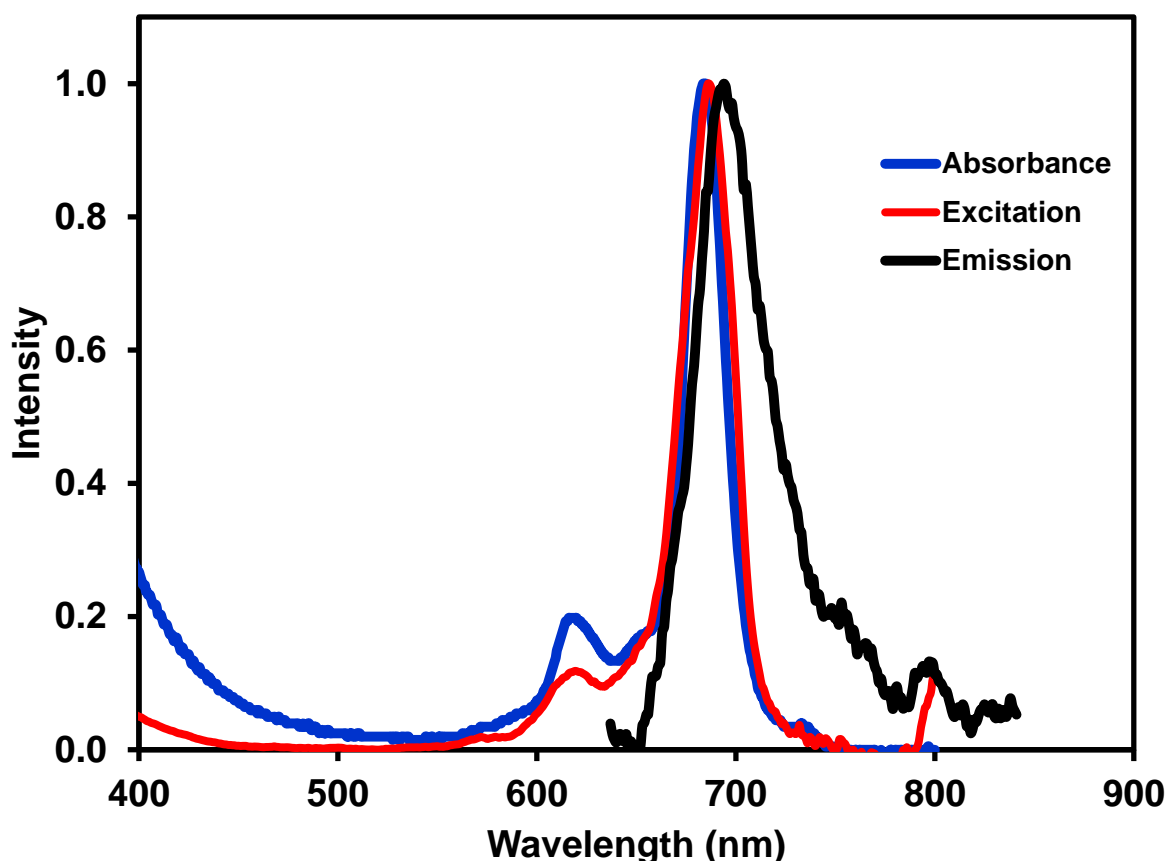
Figure 3.4: Absorption, excitation and emission spectra of CdOtBPPc in dimethyl sulfoxide. Excitation wavelength = 630 nm.

The excitation and emission spectra of **CdOtBPPc** were obtained in DMSO (**Fig. 3.4**). The absorption and excitation spectra are very similar, implying that the molecule retains the same nuclear configuration even upon excitation. The emission spectrum is Stokes shifted as expected, but we see that it is quite weak, which indicated poor fluorescence. The fluorescence quantum yields of both **CdOtBPPc** and **PbOtBPPc** (**Table 3.2**) are low owing to the heavy atom effect which encourages intersystem crossing to the excited triplet state

[118]. The fluorescence lifetime of **CdOtBPPc** was very short (2.68 ns). This was obtained by fitting a mono-exponential curve on the decay curve obtained by TCSPC (**Fig 3.5**). The fluorescence signal was too weak to obtain a decay curve for **PbOtBPPc**. This is consistent with the fact that its ϕ_F is less than 0.01.
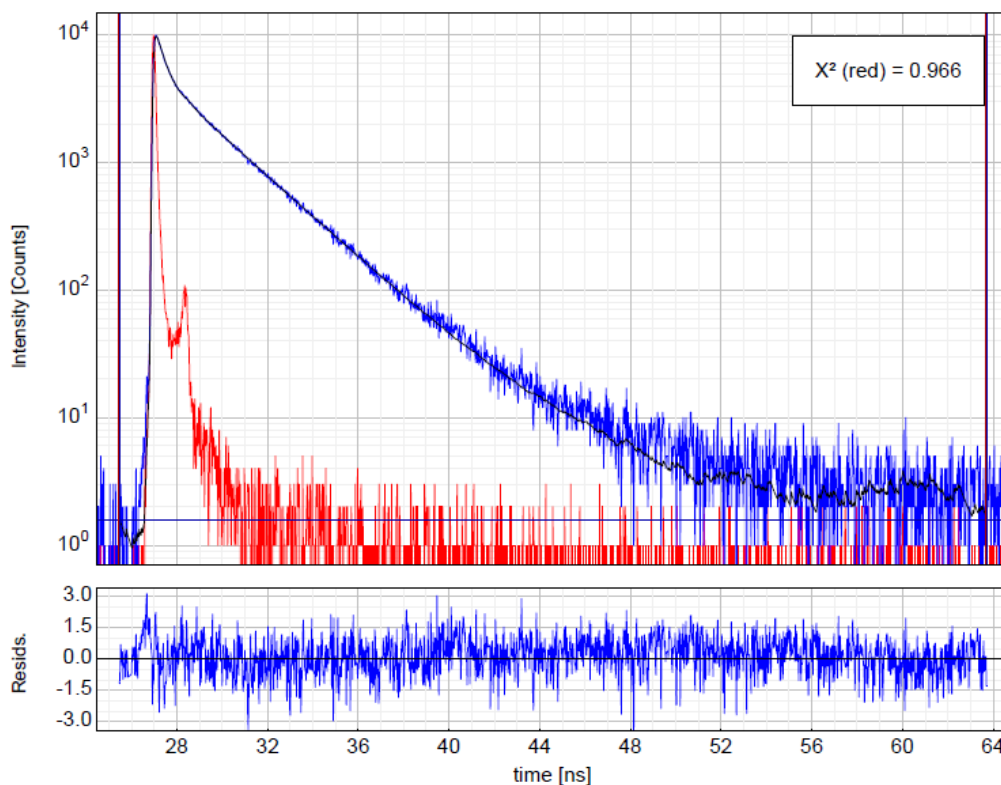
Figure 3.5: Fluorescence decay curve of CdOtBPPc in DMSO with residuals. Excitation wavelength = 670 nm

Table 3.2: Photophysical data for synthesised products in DMSO

Compound	λ_{abs} (nm)	λ_{em} (nm)	λ_{ex} (nm)	ϕ_F	τ_F(ns)	ϕ_{PD}	ϕ_T	τ_T(µs)
PbOtBPPc	709	678[a]	673[a]	<0.01	b	0.9×10^{-6} [a]	0.88[a]	50
CdOtBPPc	684	694	685	0.02	2.68	1.6×10^{-6}	0.26	61
8β-POH-Pc	681	692	682	0.12	2.27	5.7×10^{-1}	c	c
4α-POH-Pc	704	719	707	0.05	2.76	3.8×10^{-2}	c	c
4β-POH-Pc	681	694	682	0.16	2.23	3.3×10^{-1}	c	c
8β-POH-TBC	664	673	665	0.19	2.28	4.5×10^{-4}	0.81	877
4α-POH-TBC	676	686	678	0.12	2.91	2.4×10^{-3}	0.89	1228
4β-POH-TBC	660	669	660	0.20	2.34	3.7×10^{-2}	0.64	882

a – values obtained from [93]. b – No fluorescence signal detected. c – no data
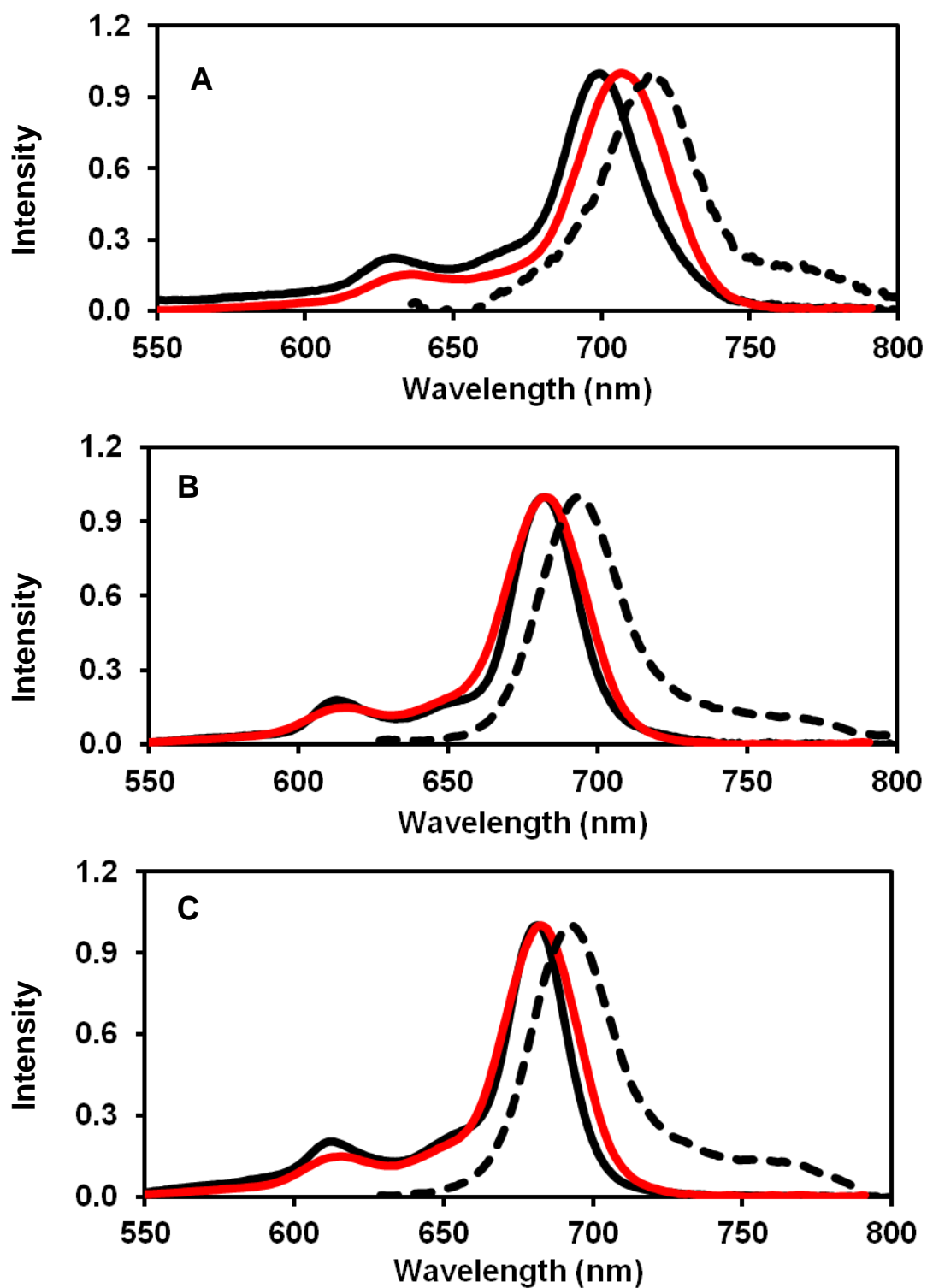
Fig. 3.6: Ground state absorption (solid black), fluorescence emission (dashed black) and excitation (red) spectra of (A) 4α-POH-Pc, (B) 4β-POH-Pc and (C) 8β-POH-Pc in DMSO

Fig. 3.6 shows the ground state absorption, fluorescence emission and excitation spectra of the phosphorous phthalocyanines synthesised in this work. **Fig 3.6B** and **C** show the spectra for **4β-POH-Pc** and **8β-POH-Pc**. The emission spectra are almost mirror images of the absorption and excitation spectra implying good geometric similarity of ground and excited states. This is typical of heteroaromatic π-systems. The Stokes shift values are consistent with those typically reported for MPcs in DMSO [119]. **Fig 3.6A** however is interesting. The fluorescence excitation spectrum is red-shifted compared to the absorption spectrum. This could be the result of the alpha substitution whose symmetry leads to a deformation of the Pc ligand [116]. This deformation then results in interaction between the central atom and the Pc ligand, which presents itself then in a red shift of the fluorescence spectrum.

The ϕ_F values of **4β-POH-Pc** and **8β-POH-Pc**, 0.16 and 0.12 respectively, are quite similar, but are lower than that of the ZnPc (ϕ_F = 0.20) used for comparison. The value for **4α-POH-Pc** is much lower, at 0.05. Non-peripherally substituted Pcs have been shown to have lower ϕ_F values [120]. The P(V)Pc ϕ_F values are higher than those of the **CdOtBPPc** and **PbOtBPPc** due to the smaller size of the phosphorus central atom. Mono-exponential curves were used to fit the fluorescence decay curves of each Pc, indicative of a single fluorescent species. The τ_F values for the P(V)Pcs are comparable to that of **CdOtBPPc**, especially that of **4α-POH-Pc**. A trend noticed with the P(V)Pcs was that as the τ_F decreased, the ϕ_F increased. Magde et al. [121] showed similar results and attribute this to there being a higher radiative probability in a shorter time frame.

3.3.1.2 Triplet quantum yields and lifetimes

Pcs which have heavy central atoms (such as Pb and Cd) are expected to show a high ϕ_T. A high value of 0.88 was observed for **PbOtBPPc**, showing that the intersystem crossing was

very efficient. For **CdOtBPPc** however, a relatively low value of 0.26 was observed (**Table 3.2**). This was due to the tendency of **CdOtBPPc** to aggregate in solution. Aggregation is known to reduce the triplet quantum yield of molecules through the process of exciton coupling which leads to more radiationless energy loss [13]. Looking at **Fig 3.1**, we see that the vibronic band of **CdOtBPPc** is broader than that of **PbOtBPPc**, which alludes to the aggregation behaviour of **CdOtBPPc**. On dilution of the **CdOtBPPc** solution (**Fig 3.7**), the aggregate peak at 630 nm persisted. This is not typical of the so called "H" aggregates. If H aggregation was present, we would expect the aggregate peak to decrease faster than the monomer peak. Strong aggregation behaviour of CdPc complexes has been reported before [122]. The nature of the aggregation peak at 630 nm is thus unclear at present. This behaviour was not seen with the **PbOtBPPc**.
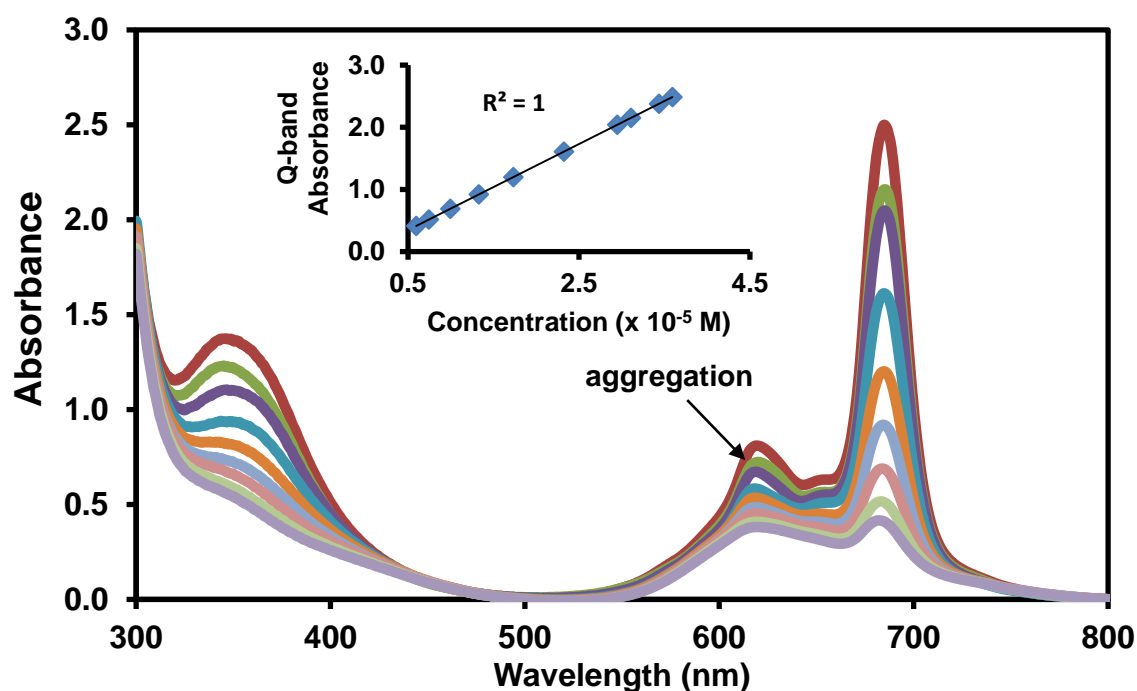
Figure 3.7: UV spectral changes with concentration for CdOtBPPc in DMSO between 5.9 x 10^{-6} and 3.4 x 10^{-5} M. The inset shows how the Q band absorbance decreases with the concentration.

The triplet lifetimes of both **CdOtBPPc** and **PbOtBPPc** were shorter than what is generally seen with Pcs (61 and 50 µs respectively). An increase in the ϕ_T leads to a shortened τ_T. **Fig 3.8** shows the triplet decay curve used to determine τ_T for **CdOtBPPc** using OriginPro 8 software. The data is summarised in **Table 3.2.**
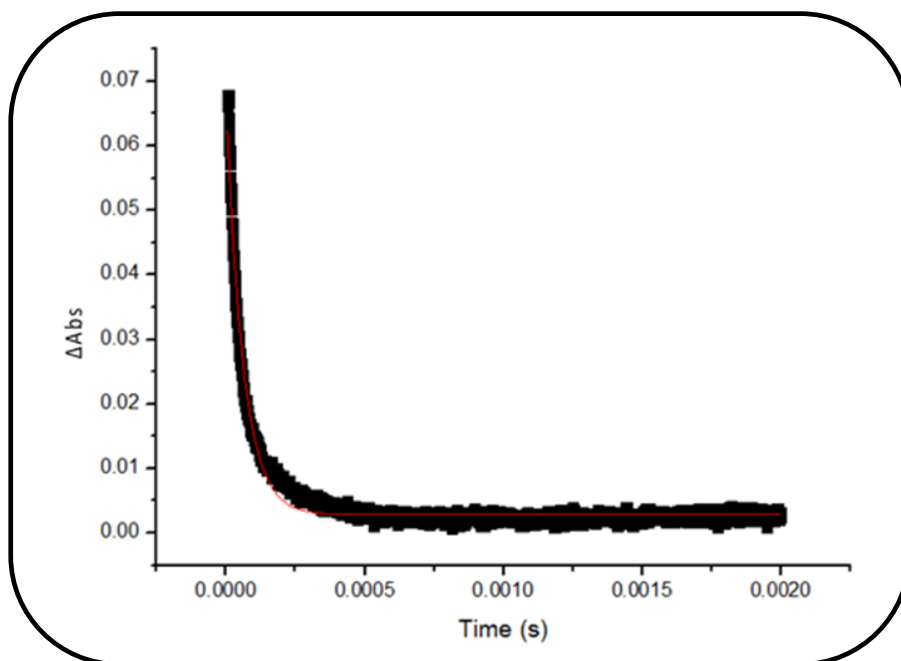
Figure 3.8: Triplet decay curve of CdOtBPPc in DMSO

Owing to the great photo instability of the phosphorus Pcs employed in this work, reliable triplet lifetime and quantum yields were unable to be determined using the set-up described in the experimental section of this thesis. **Fig. 3.9** shows the colorimetric change of the **8β-POH-Pc** after being exposed to ambient light for no more than 10 minutes.
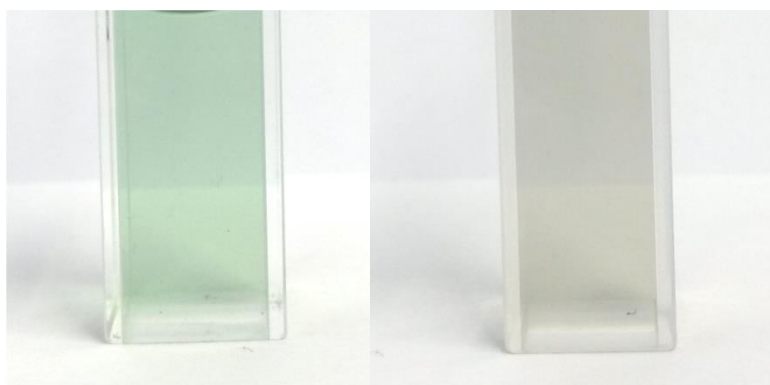
Fig. 3.9: 8β-POH-Pc in DMSO. Original solution (on left) has a stronger green colour than the solution after being exposed to ambient light (right)

3.3.2 Triazatetrabenzcorroles

3.3.2.1 Fluorescence quantum yields and lifetimes
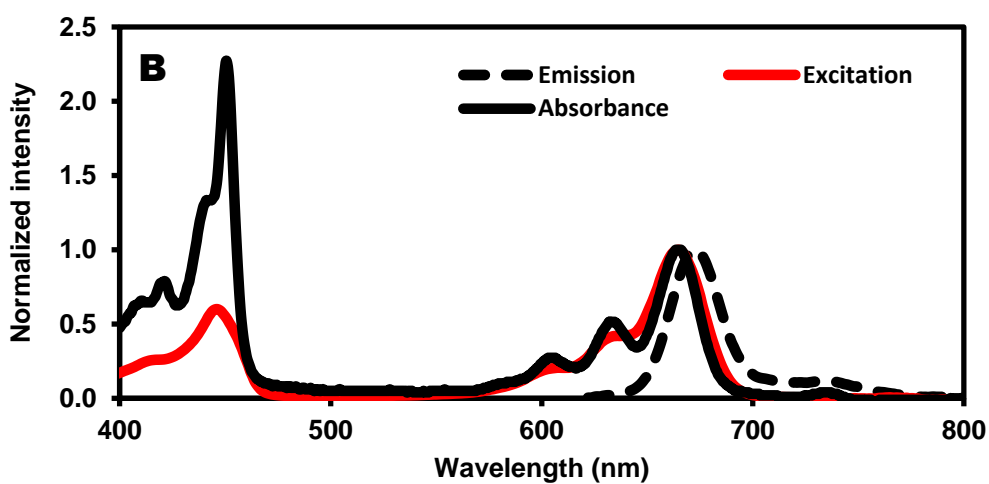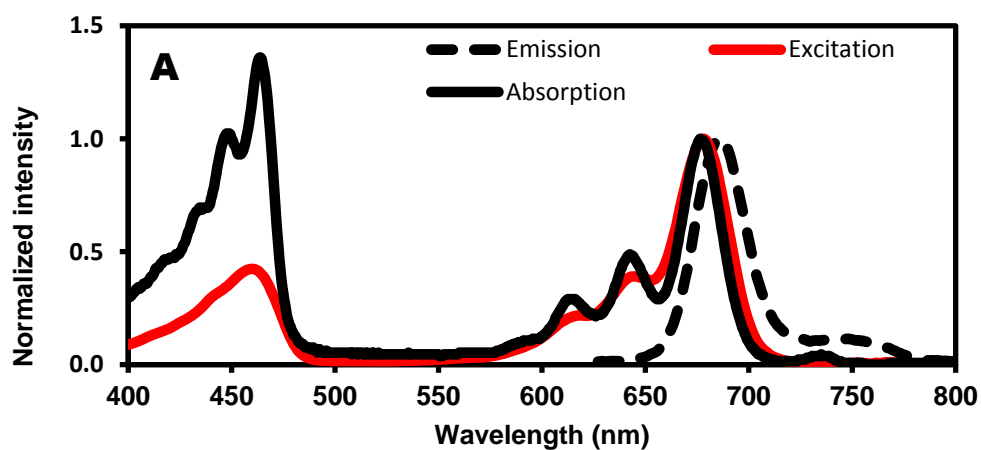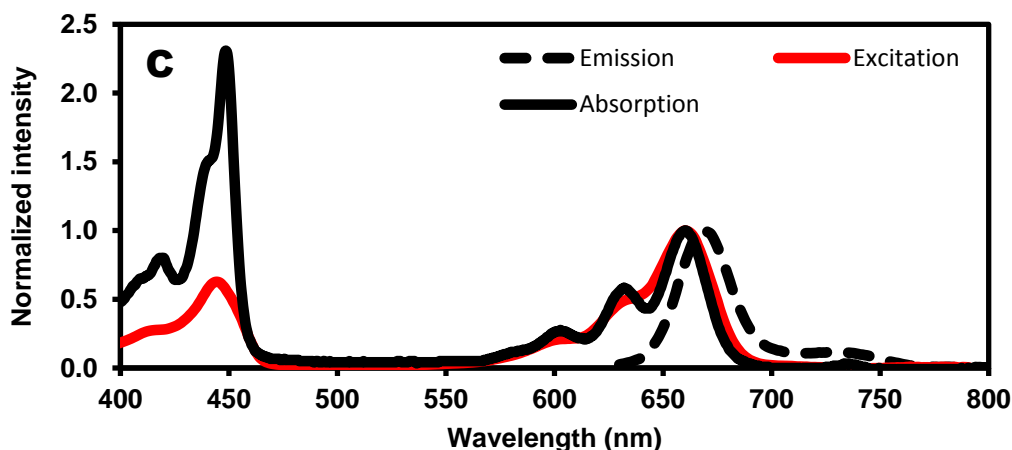
Figure 3.10: Ground state absorption, excitation and fluorescence spectra of (A) 4α-POH-TBC, (B) 4β-POH-TBC and (C) 8β-POH-TBC in DMSO

The absorbance and emission spectra of the phosphorus TBC complexes synthesised in this work are seen in **Fig. 3.10**. All three compounds have well resolved fluorescence emission spectra, which are almost perfect mirror images of the lower energy Q absorption and excitation bands. This means that the nuclear configurations of the ground and excited states are similar. They all show significantly higher ϕ_F values as compared **CdOtBPPc** as well as their corresponding P(V)Pcs, determined by using the comparative method with ZnPc (ϕ_F = 0.20) as a standard. **4β-POH-TBC** and **8β-POH-TBC** have comparable ϕ_F values. **4α-POH-TBC** has the smallest ϕ_F of the TBCs due to the non-peripheral substitution, which is known to show lower ϕ_F values [120] as discussed above.

Mono-exponential curves were used to fit the fluorescence decay curves of each TBC, to obtain ns regime fluorescence lifetimes, indicating that only one fluorescent species was present in solution. The τ_F values mimic the trend observed for the P(V)Pcs, with **4α-POH-TBC** having the longest (2.91 ns) and **4β-POH-TBC** and **8β-POH-TBC** having similar values (2.34 and 2.28 ns respectively). Again, it was observed that the species with the longest τ_F had the lowest ϕ_F and the species with the shortest lifetime had the highest ϕ_F. The

77

similarity in the trends observed in the P(V)Pcs and P(V)TBCs indicate that the loss of an aza-nitrogen does not affect the manner with which light interacts with the different positional isomers, but merely enhances the response observed.

3.3.2.2 Triplet quantum yields and lifetimes

The triplet decay curves were found to obey second order kinetics due to the effect of triplet-triplet recombination [123], and thus are consistent with the data observed previously (in literature) for MPc complexes at high concentrations (> 1 x 10^{-4} M). The ϕ_T values of the TBC complexes are comparable or greater than that of the ZnPc standard ($\phi_{T=}$ 0.65) in DMSO (**Table 3.2**). **4α-POH-TBC** has a greater ϕ_T than **4β-POH-TBC.** This can be explained by symmetry considerations. The non-peripheral arrangement results in more intersystem crossing to the triplet state, hence a larger ϕ_T. Ke et al. [120] found that non-peripherally substituted compounds give a higher ϕ_Δ, which implies a high ϕ_T. The large ϕ_T of **4α-POH-TBC** corresponds to a low ϕ_F. **8β-POH-TBC** has a large $\phi_T,$ which shows the effect of increased substitution. Both **4α-POH-TBC** and **8β-POH-TBC** have ϕ_T values similar to **PbOtBPPc**. Strangely, the triplet lifetimes of the TBCs were found to be much longer than that ordinarily seen in Pcs (τ_T = 350 µs for ZnPc [124]), but this has been reported before [48]. We observed values of 1228, 882 and 877 µs for **4α-POH-TBC**, **4β-POH-TBC** and **8β-POH-TBC**, respectively. The similarity of the values for 4β and 8β is primarily due to the fact that the number of substituents does not change the way that the molecule interacts with light, but the geometry does – hence why such a significant difference with **4α-POH-TBC.** The peripherally substituted compounds are more likely to have some degree of aggregation, therefore a shorter triplet lifetime [13] and a reduced ϕ_T.

3.3.3 Photodegradation quantum yields

The photodegradation quantum yield is an important measure of the photostability of a compound. **Fig 3.11** shows the photodegradation of **4α-POH-TBC** as an example. Typically, a value of the order of 10^{-6} is considered to allude to good stability. When a Pc photodegrades, it undergoes a physical transformation into phthalimide, which is why the reaction can be monitored spectroscopically. The decomposition products of TBC are thought to be similar to those of Pcs. Pcs with values of the order 10^{-3} have been reported and have been shown to be unstable [13]. **Table 3.2** gives the values obtained for the molecules reported in this work. The most photostable compounds are **CdOtBPPc** and **PbOtBPPc** (1.62×10^{-6} and 0.92×10^{-6}, respectively). Such stability makes these compounds suitable for applications where intense light is used, such as optical limiting. The ϕ_{PD} values shown by the P(V)TBCs and P(V)Pcs are indicative of great photo instability. This unfortunately makes them poor candidates for light intensive applications. The instability could be as a result of the solvent in which they were investigated or the substituents used in their synthesis. The bulky electron donating nature of the t-butylphenoxy substituents destabilise the frontier π molecular orbitals, and this may adversely affect the photostability of the compounds. Interesting to note, however, is that even though Pcs are known to be very photostable, the phosphorus Pcs in this work are less stable than the P(V)TBCs, by an order of magnitude at least.
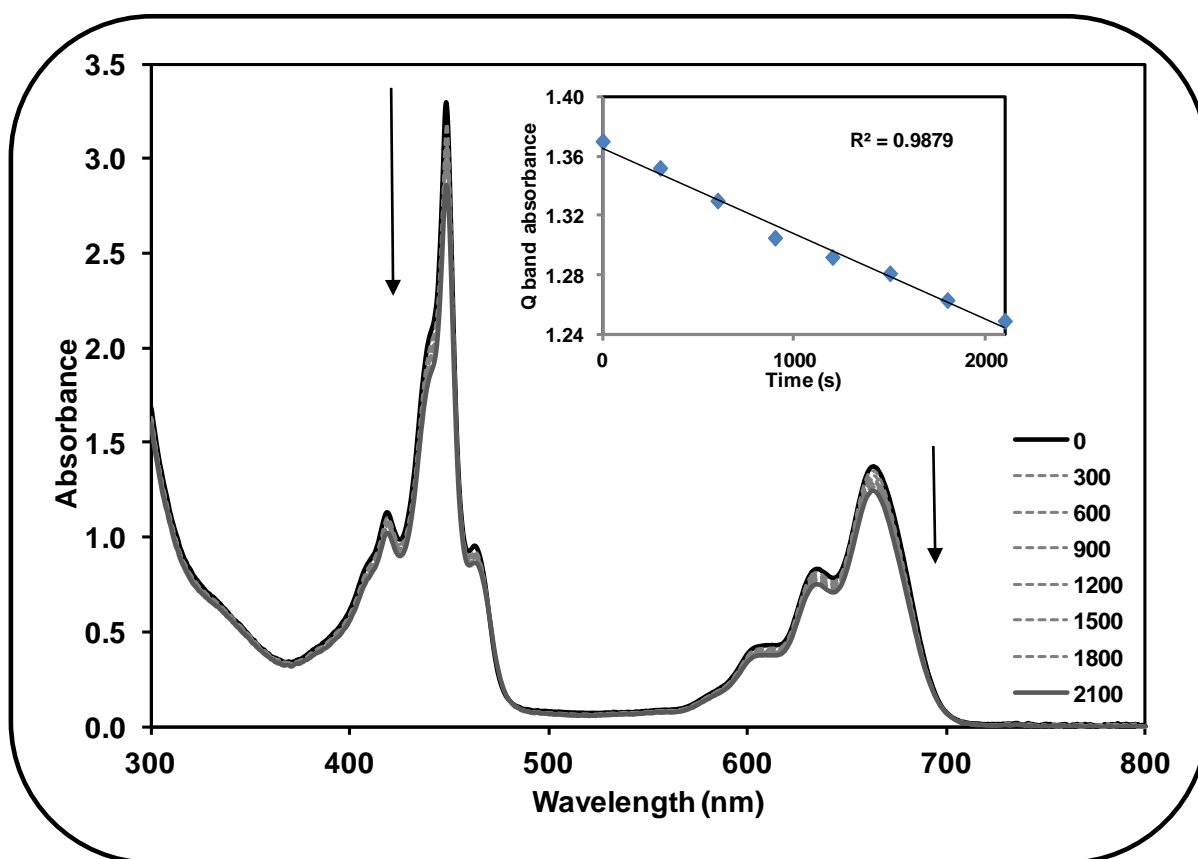
Fig 3.11: Photodegradation of 4α-POH-TBC over 2100 s in DMSO

A possible reason for the increased instability of the P(V)Pcs (which would lead to the poorer photochemical results) is the fact that a pentavalent atom was used as the central atom. P(V)Pc is coordinated to two pyrrole nitrogen atoms and to two axial ligands, leaving the moiety with an overall positive charge. This charge could be contributing to the high instability. DMSO, as a basic solvent, is known to coordinate to Pcs – especially charged moieties. So this could be a contributing factor to the ease with which the P(V)Pc breaks down.

3.3.4 Singlet oxygen quantum yield

The singlet oxygen quantum yield (ϕ_Δ) of Pcs has been well documented in many publications. Very little work, however, has been done in the assessment of the singlet

oxygen generating properties of TBCs. From this work, and from literature [46,48], we see that TBCs have high ϕ_T values, which lead us to believe that they too will possess high ϕ_Δ.

Table 3.3 shows that the singlet oxygen quantum yields of the P(V)TBC complexes are comparable or slightly less than the value of 0.67 for ZnPc in DMSO [125]. The **8β-POH-TBC** and **4β-POH-TBC** have higher ϕ_Δ values than **4α-POH-TBC**, even though the latter has the highest ϕ_T. Durmuş and Nyokong [110] in their study of various In and Ga Pcs found there to be virtually no difference between the ϕ_Δ values found of α and β substituted compounds. The difference observed in this work can be hypothesised to be a result of inefficient quenching of triplet state by energy transfer to singlet oxygen (S_Δ), which is calculated to be 0.58 for **4α-POH-TBC**. The value of ϕ_Δ for **4β-POH-TBC** is higher than the ϕ_T. This is not usually expected, as molecules cannot transfer non-existent energy. We would expect S_Δ, the singlet oxygen quenching efficiency, to be less than 1, meaning that the ϕ_T is higher than the ϕ_Δ. The value 0.66 reported however, is assumed to be correct within the reported error. The high ϕ_Δ values show that the P(V)TBCs could be very good photodynamic therapy photosensitizers, but the high ϕ_{PD} (**Table 3.2**) suggest that these compounds would be unsuitable, as they would decompose readily in the presence of high intensity light. The ϕ_Δ of the **CdOtBPPc** and **PbOtBPPc** used in this work were not determined as these materials would be of little use in biological or physiological environments owing to their very high levels of toxicity. Also, the phosphorus Pcs showed poor photostability, hence were not considered candidates for singlet oxygen applications.

Table 3.3: Singlet oxygen quantum yields in DMSO found using Ge detector

Compound	$\phi_\Delta \pm 0.01$	ϕ_T	$S_\Delta = \dfrac{\phi_\Delta}{\phi_T}$
8β-POH-TBC	0.74	0.81	0.91
4α-POH-TBC	0.52	0.89	0.58
4β-POH-TBC	0.66	0.64	1.03

3.4 Polymer thin films

In order to make good comparisons, two polymers were initially used for this study, polymethyl methacrylate and poly(bisphenol A carbonate), using only the **CdOtBPPc** and **PbOtBPPc**. After confirming that PBC gave better results than the PMMA, the rest of the compounds made were only embedded into the better performing PBC polymer.

Both **PbOtBPPc** and **CdOtBPPc** were prepared in PBC and PMMA films. The most notable physical difference between PBC and PMMA films was the brittleness. The PMMA films tore more easily and were more likely to break when handled. This is a disadvantage as the goal was to achieve a long-lasting, durable thin film. The PBC films were found to be more flexible, robust and easy to handle.

The ground state absorption spectra of the films were obtained in order to assess what happened to the Pc in a solid state support. **Fig. 3.12** shows the absorption spectra for **PbOtBPPc** and **CdOtBPPc** in DMSO, PBC and PMMA. The DMSO spectrum is typical of a Pc in solvent. The Q and B bands are well defined and show no sign of H-aggregation. The PBC spectrum shows that the **PbOtBPPc** maintains its electronic character, but the entire spectrum is red-shifted. This is due to the fact that Pcs tend to aggregate in solid support

media [106]. This aggregation then results in a red shift. This aggregation is much more pronounced in the PMMA spectrum, with the appearance of strong dimer peak. There is no Q band shift seen with the PMMA. For **CdOtBPPc**, the DMSO spectrum is monomeric, but both the PBC and PMMA show pronounced aggregation, with the bands due to aggregation being higher than that of the Q band of the monomer.
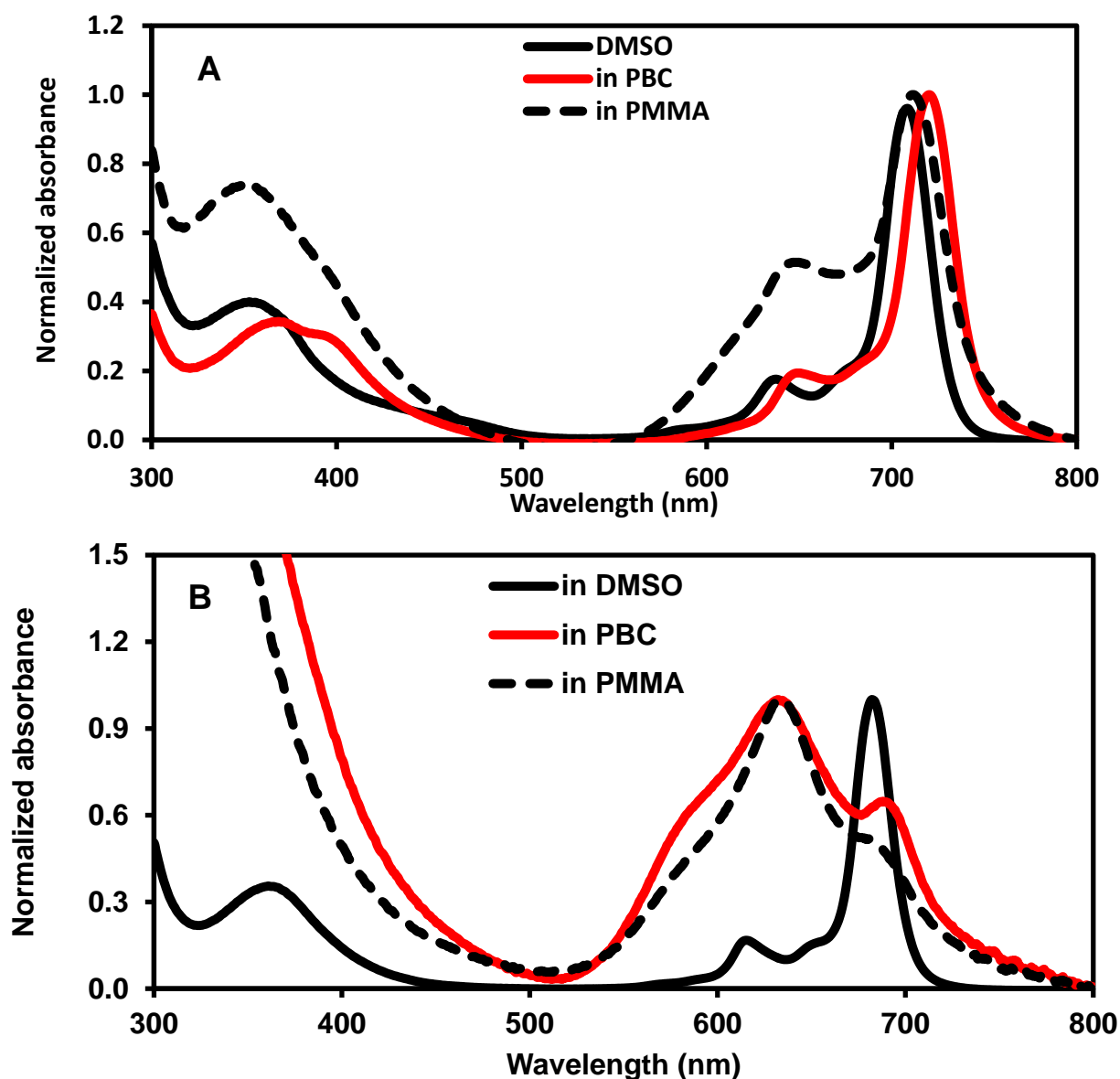
Figure 3.12: Ground state absorption spectra for (A) PbOtBPPc and (B) CdOtBPPc in DMSO, PBC and PMMA
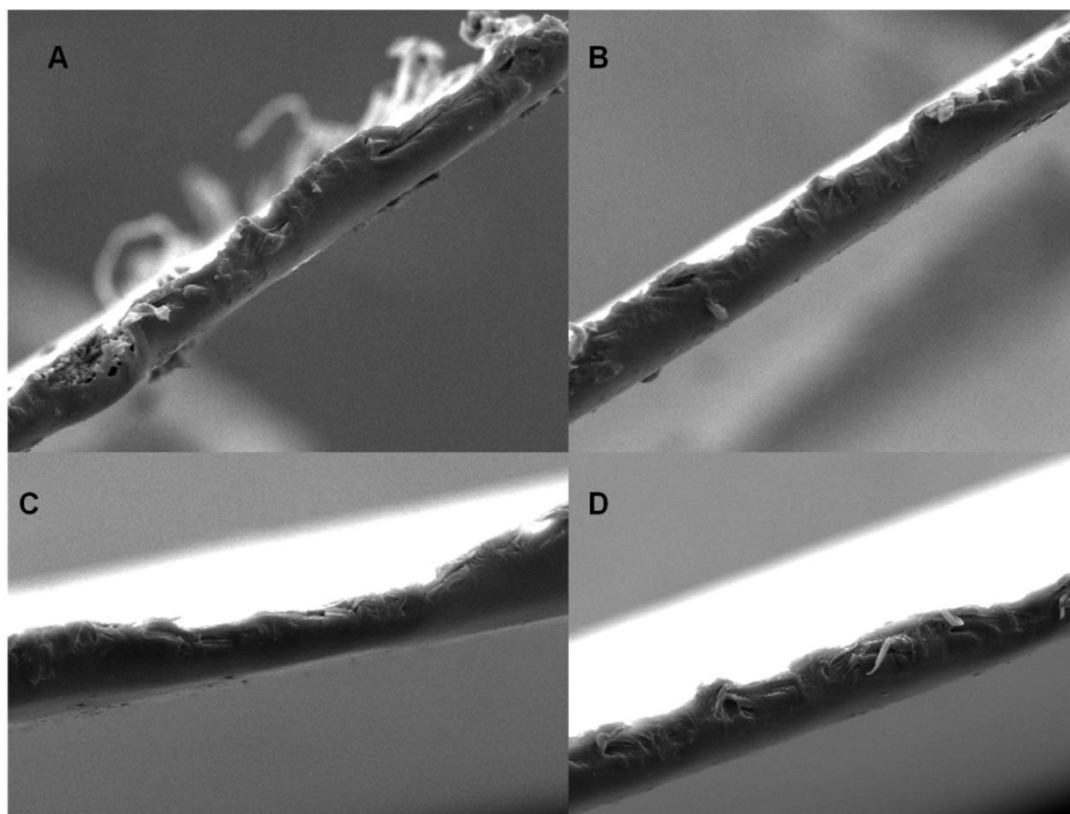
Fig. 3.13: Scanning electron microscopy images of the PBC thin films embedded with 8β-POH-Pc. (A) and (B) show clearly the edge of the thin film, whereas (C) and (D) show the edge and part of the surface. In (C), it can be seen that the film is not of uniform thickness.

Fig 3.13 is a SEM image of the thin films. It was possible to determine the average film thickness using this method with the SEM equipment software. The film thicknesses were found to average 25 μm of the PMMA and 13 μm for the PBC using both **CdOtBPPc** and **PbOtBPPc**. The major factor which controlled the final thickness of the films was the viscosity of the polymer solutions prepared. It was important to determine at what concentration the best films could be prepared in order to prevent film breakage and other defects.

To further assess the interaction between the embedded Pc and the polymer, IR spectra of a blank film, a film with **H₂OtBPPc** and a film with **PbOtBPPc** were obtained and compared (**Fig 3.14**). The purpose of this was to establish whether the embedded MPc remained

metallated or if it demetallated in the film making process. If it had demetallated, the IR spectrum would look like the $H_2OtBPPc$. Due to the very strong vibrations observed with the thin films however, it was very difficult to determine any other peaks in the spectrum. Hence, it is only possible to rely on colorimetric and UV/Vis spectral data to assess the success of Pc embedment. The UV results showed that the Pcs remained metallated in the films.
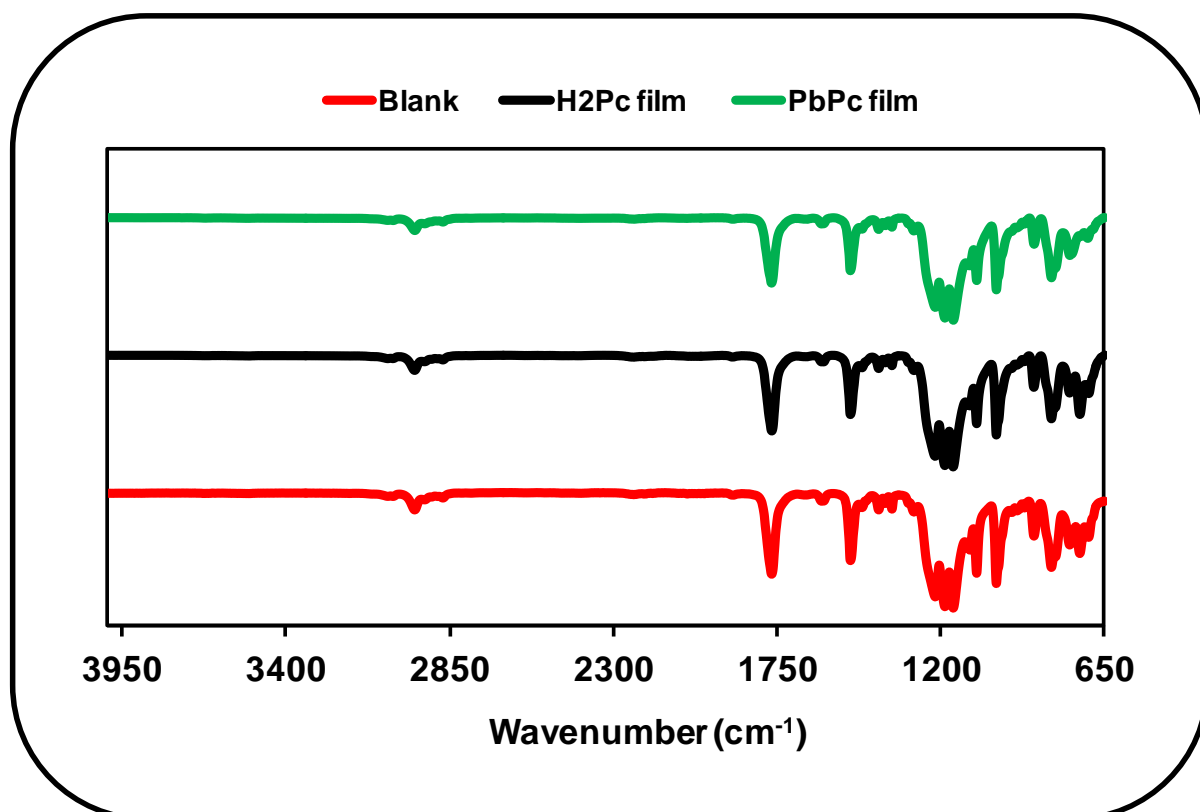
Figure 3.14: IR Spectra of plain PBC, H_2Pc embedded in PBC and PbOtBPPc embedded in PBC films. Embedded Pc peaks are hidden by the strong polymer peaks

Characterization techniques for films were carried out for the P(V)Pc thin films made only using PBC. The ground state absorption spectra obtained for these films showed very weak signals, with a slight Q-band, suggesting that the compound still existed, but most likely had degraded in the solid support. When examined under the fluorescence microscope

however, we found that the species fluoresced quite intensely as can be seen in **Fig 3.15**.

The bright spots again are indicative of probable aggregation in the polymer matrix.
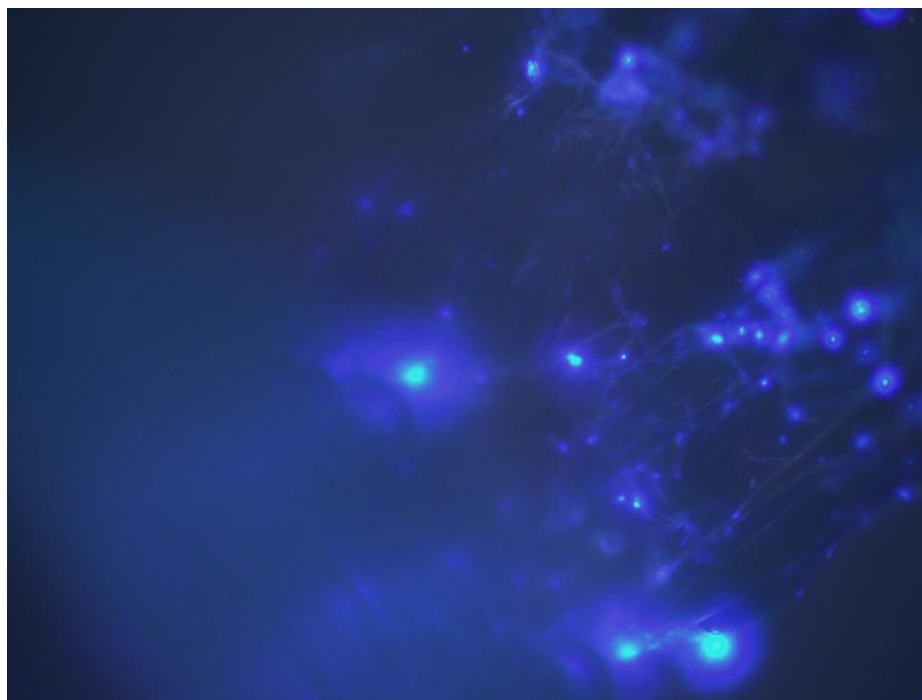
Figure 3.15: Fluorescence microscope image of 4β-POH-Pc in PBC. This image was taken using UV excitation

As PBC was determined to be the better polymer due to better dexterity and showing a lesser degree of Pc aggregation, only PBC-P(V)TBC films were prepared. The ground state absorption spectra were determined in order to assess the electronic nature of the P(V)TBC in solid state. The spectra showed that the compounds were present, but their spectra were much weaker than in solution, as observed for the P(V)Pcs. The colour of the P(V)TBC films was also not as intense as that seen in the **CdOtBPPc** or **PbOtBPPc** films.

Owing to the high fluorescence quantum yield of the P(V)TBCs, their films were investigated under a fluorescence microscope to gauge the distribution of the TBC throughout the film.

Due to the low concentration, the fluorescence observed was not very pronounced, but bright spots were seen at the faults in the films. These bright spots are found in regions of accumulation. This could have occurred during the removal of solvent from the polymer solution under vacuum.

4. Nonlinear optical parameters

The nonlinear optical parameters were determined using the Z-scan methodology and setup described earlier. The studies were initially conducted in solution and in solid state. The parameters were the imaginary third order susceptibility ($Im[\chi^{(3)}]$), the second order hyperpolarizability (γ) and limiting intensity (I_{lim}).

4.1 Solution studies

All Z-scan solution experiments were performed in DMSO. DMSO is a preferred solvent due to its high boiling point (which allows it to resist differential temperature effects due to incoming laser beams), its high photostability and the good solubility it affords the majority of compounds utilized in this study. To further minimise potential temperature effects in the form of thermal lensing, the pulse energy of the laser was kept to 35 μJ. Thermal lensing is the occurrence of an optical lens *in situ* due to the localized heating caused by the laser beam.

Table 4.1: NLO parameters for synthesised compounds in DMSO

Complex	$Im[\chi^{(3)}]/\alpha$ (esu)	γ (esu)	I_{lim} (J/cm^2)	Φ_T
PbOtBPPc	6.76 x 10^{-14}	3.15 x 10^{-32}	0.82	0.82
CdOtBPPc	8.32 x 10^{-14}	1.57 x 10^{-32}	1.65	0.26
8β-POH-Pc[a]	-	-	-	-
4α-POH-Pc	1.21 x 10^{-14}	2.55 x 10^{-35}	-	-
4β-POH-Pc	4.39 x 10^{-15}	4.55 x 10^{-35}	-	-
8β-POH-TBC	2.75 x 10^{-14}	4.26 x 10^{-32}	0.61	0.81
4α-POH-TBC	3.23 x 10^{-14}	1.68 x 10^{-34}	-	0.89
4β-POH-TBC	1.60 x 10^{-14}	8.93 x 10^{-35}	-	0.64

a – unable to fit data

4.1.1 NLO activity in Pcs

Fig 4.1 shows the typical Z-scan of material which is a reverse saturable absorber. The RSA is a result of a two-photon absorption process from the ground state to an excited state. Once excited, the molecule then undergoes excited state absorption which results in there being NLO properties [126].

An RSA profile is observed for both **PbOtBPPc** and **CdOtBPPc**. Cadmium was chosen as a comparison to lead primarily because it is a heavy metal and there have been to date, no NLO studies published with CdPcs to the best of our knowledge. The parameters in **Table 4.1** are the imaginary third order susceptibility and the second order hyperpolarizability. For both **CdOtBPPc** and **PbOtBPPc**, these values fall within the limits which have been found to exist for potential Pc optical limiters. The reported limits for Im[$\chi^{(3)}$] are from 10^{-9} to 10^{-15} and 10^{-29} to 10^{-34} for γ [86]. Similar values are shown in literature [87,91] (**Table 1.2**). Comparing the I_{lim} found for **CdOtBPPc**, 1.65 J/cm^2, we see that the **PbOtBPPc** does almost twice as well at limiting high intensity light (0.82 J/cm^2). The limiting threshold for damage to the human eye is 0.95 J/cm^2. This means that in solution, the **PbOtBPPc** would qualify as a better optical limiter. Sanusi et al. report very good results for a series of pyridyloxy substituted PbPcs, with the best value reported being 0.32 J/cm^2 [127]. Although these results are better, **PbOtBPPc** is a firm contender for OL applications.

(D)
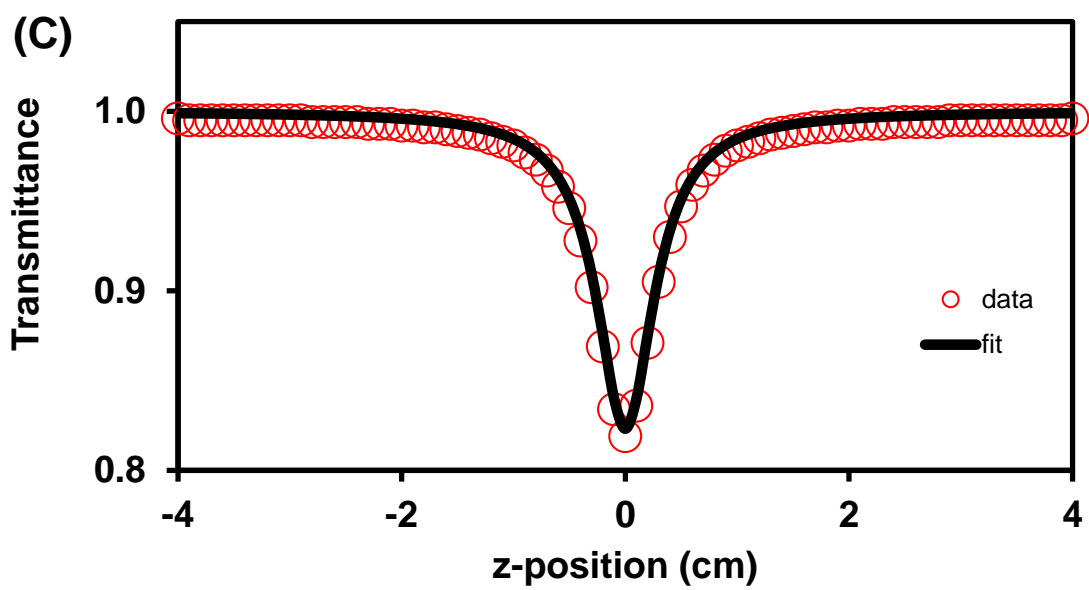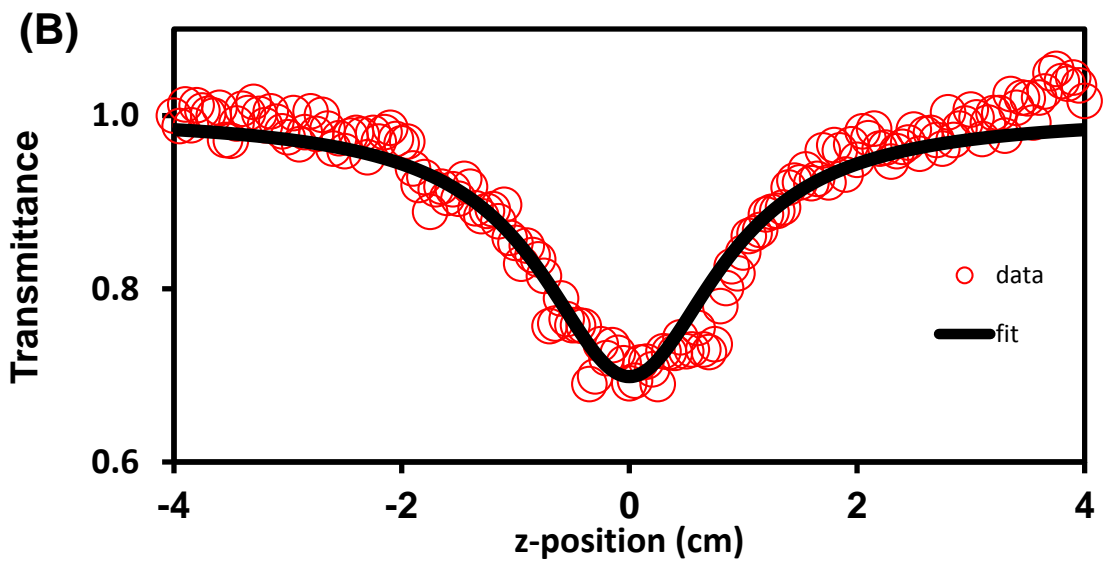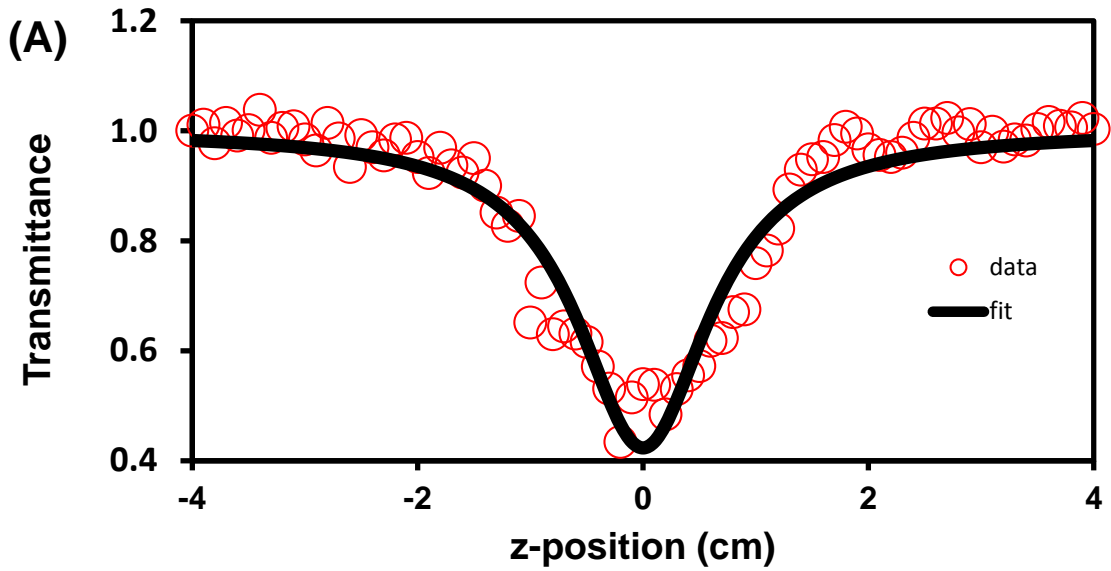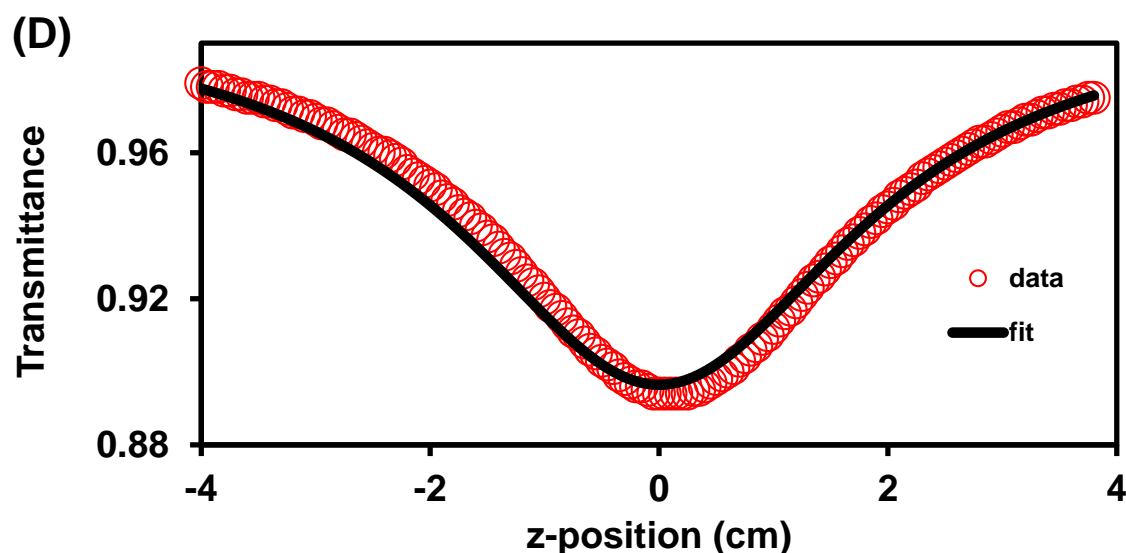
Figure 4.1: Z-scan trace of (A) PbOtBPPc, (B) CdOtBPPc, (C) 4α-POH-Pc and (D) 4β-POH-Pc showing a RSA profile (in DMSO)

The results obtained in solution suggest that both **CdOtBPPc** and **PbOtBPPc** are good optical limiters (**Table 4.1**). The contributing factors to the good I_{lim} value seen in **PbOtBPPc** are the fact that lead is a very heavy metal which does not fit into the Pc cavity affording a shuttlecock arrangement and it promotes intersystem crossing from the singlet to the triplet state. A higher intersystem crossing quantum yield means that the ϕ_T is high too, 0.88 in the case of **PbOtBPPc**. A higher ϕ_T means that the excited state absorption cross section is higher than that of the ground state. This inversion manifests itself in a physical process known as reverse saturable absorption. **Fig 4.2** shows an input intensity vs output intensity plot for **CdOtBPPc** which was used to determine the I_{lim} value. A similar curve was used for **PbOtBPPc**. We see that in solution, the response of the compound is not linear.
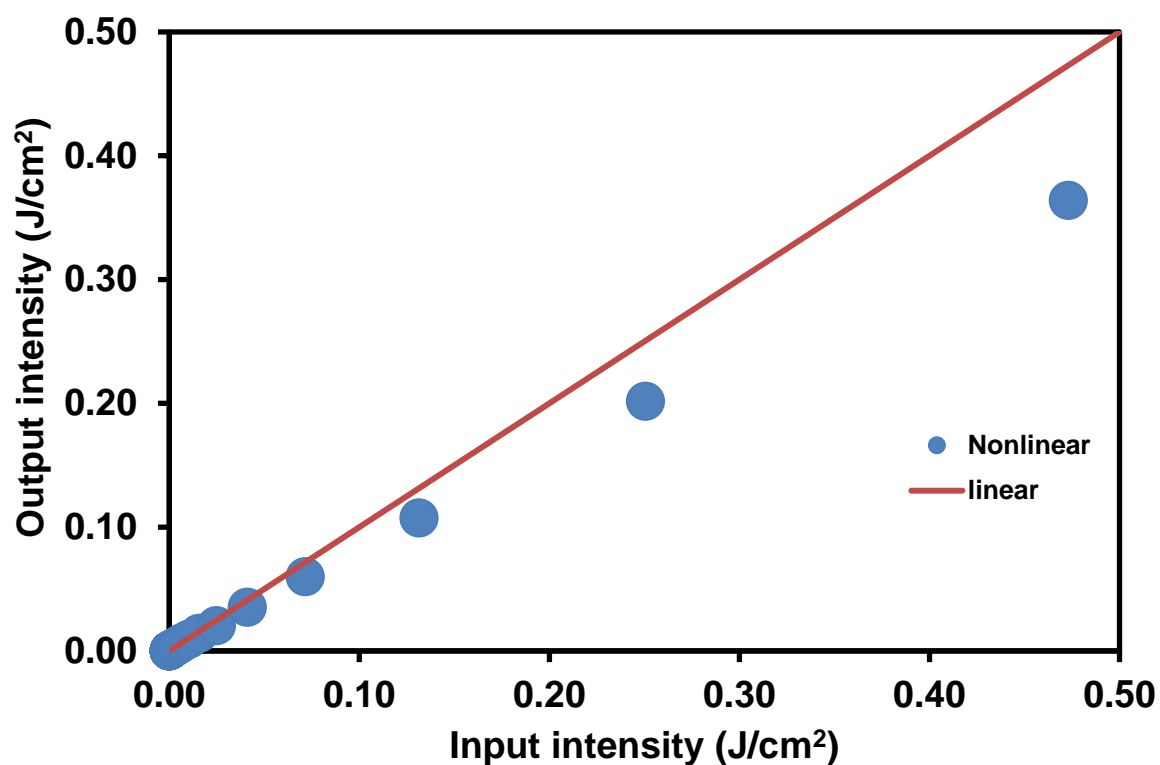
Figure 4.2: Input intensity vs output intensity plot for CdOtBPPc in DMSO

Owing to the poor photodegradation quantum yields of the P(V)Pcs, the limiting intensity value was unable to be determined. This is supported by the very low value values of γ (10^{-35}), which fall out of the range for good OL Pcs (**Table 4.1**). The signal obtained for **8β-POH-Pc** was very poor and was unable to be fitted in order to determine the parameters. **Fig 4.3** shows how **4α-POH-Pc** has almost linear dependence for output intensity as the input intensity increases. A possible reason for the very poor performance, apart from the photo instability, is the fact that the central atom is very light, thus making the compound to have a small intersystem crossing. This theory is supported by the fact that the ϕ_T of the P(V)Pcs is incalculable using methods available to us. The relatively high symmetry of the Pcs also contributes to their poorer performance as optical limiters.
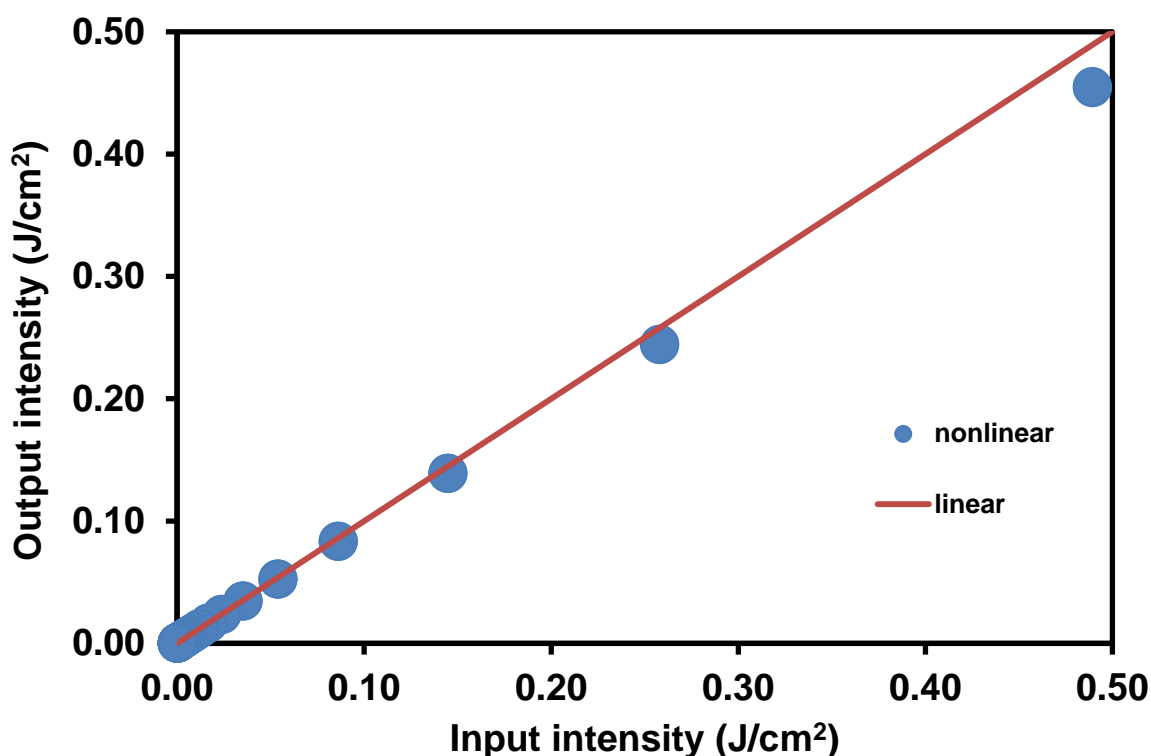
Figure 4.3: Input intensity vs output intensity plot for 4α-POH-Pc in DMSO

4.1.2 NLO in phosphorus triazatetrabenzcorroles

Owing to the permanent dipole moment associated with TBCs, it was proposed that these molecules would show enhanced NLO character. After being analysed using the Z-scan, it was found that P(V)TBCs do exhibit reverse saturable absorption in solution, but weakly (**Fig 4.4**). **Table 4.1** quantifies the results. We observe that in solution, each of the tetra substituted P(V)TBCs have I_{lim} values which are incalculable by the method demonstrated in **Fig 4.2**. The value found for **8β-POH-TBC** is 0.61 J/cm^2 and lies below the threshold value of 0.95 J/cm^2. Thus, only this TBC would be considered viable for optical limiting in solution. The enhancement of the optical limiting is due to more extensive conjugation afforded by the substituents [128]. These further increase the hyperpolarizabity of the molecule to 4.26

x 10^{-32} esu, whereas the tetra substituted P(V)TBCs have lower values, 1.68 x 10^{-34} and 8.93 x 10^{-35} esu, respectively. In other words, octa substituted compounds are more polarisable than tetra substituted variants.
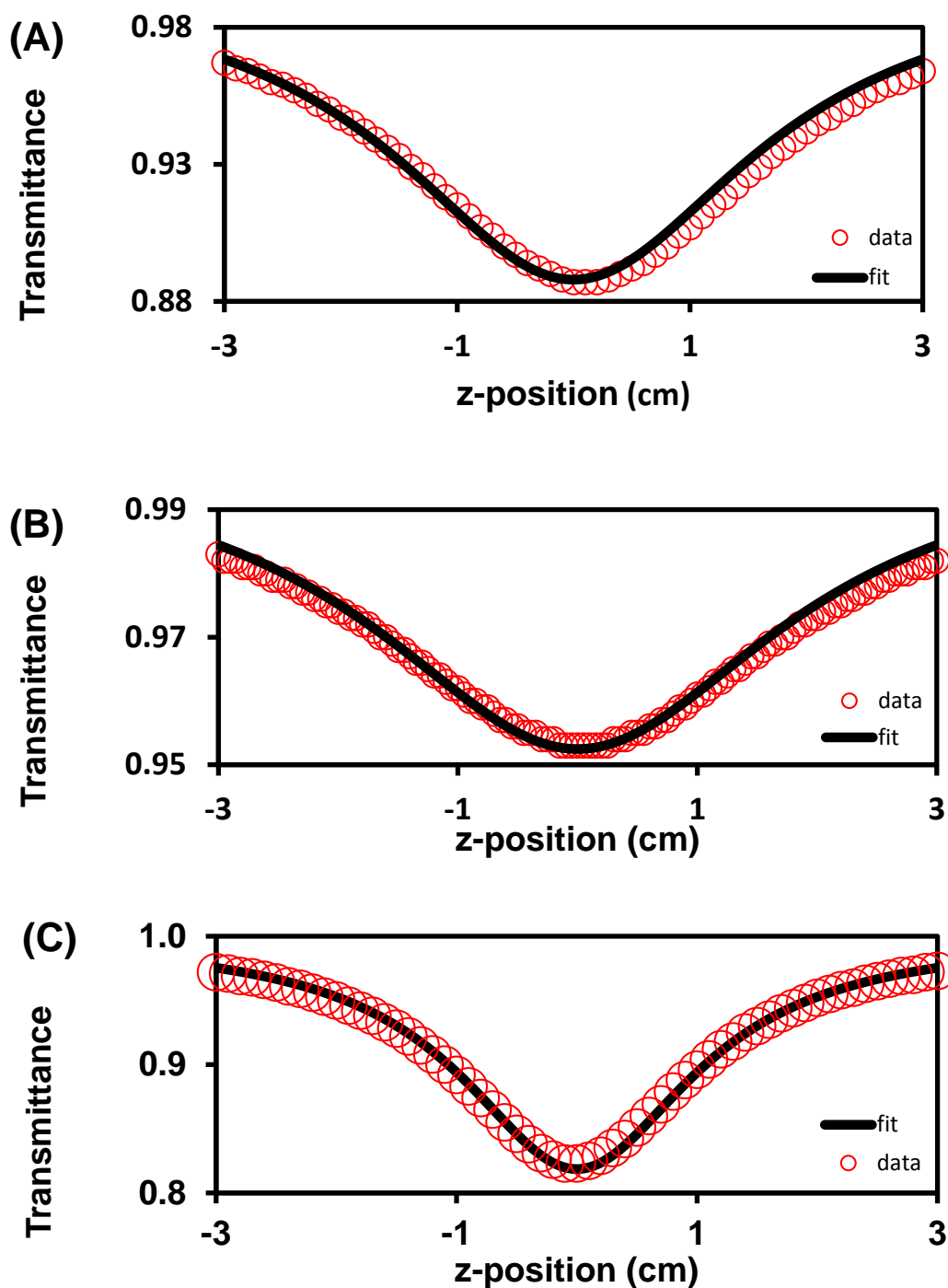
Fig 4.4: Z-scan profiles of P(V)TBCs in DMSO. (A) 4α-POH-TBC, (B) 4β-POH-TBC and (C) 8β-POH-TBC

4.2 Thin film studies

The z-scan experiments were performed at a lower energy (~25 uJ) in the films compared to the solutions owing to their thin nature. Between each run, the film was assessed for any potential thermal damage and none was observed. The results are summarised in **Table 4.2**

4.2.1 NLO in phthalocyanine films

Fig 4.5 shows Z-scan plots for Pcs in PBC or PMMA films. **Table 4.2** shows that there is a huge enhancement of the NLO parameters for the heavy metal Pcs when embedded in polymer thin films. The value of I_{lim} was determined using the plots of input vs output intensity (**Fig 4.6**). Comparing the Z-scan profiles for all the compounds in DMSO (**Figs 4.1, 4.4**) and in film (**Figs 4.5, 4.7**) it is observed that the film profiles are not as symmetric as those seen for the solution studies. The ideal Z-scan measurement should be symmetrical about z = 0 (the laser focal point), but this is difficult to achieve for films as they are not of uniform thickness. This introduces light defocusing and additional scattering which results in the signal collected to be off centre. This was taken into consideration during all the studies performed and the effects were minimised by performing multiple scans of each film at different positions and using at least three different films of each molecule and then finding the average NLO parameters.

For both **CdOtBPPc** and **PbOtBPPc**, the I_{lim} values obtained were better in PBC than in PMMA, by an order of magnitude. This is attributed to the better transmittance of light seen in PBC due to its higher refractive index. Comparing to other Pc thin films made using Ga, In and Zn Pcs [91] embedded in PMMA, the Cd and Pb Pc in this study perform better in both the PMMA and PBC films. Looking at **Fig 4.5A**, it is clear that the optical limiting is enhanced

in the PBC by assessing how far down the RSA profile reaches. It is understood that for a material to be a good limiter, the transmittance must be reduced at least 50%, preferably more. In **Fig 4.5B**, although the transmittance does not fall below the 0.5 mark, the OL property is enhanced nonetheless by virtue of being in a polymer [100]. The I_{lim} values are also much better in films than they are in solution. There is a substantial increase in the magnitude of $Im[\chi^{(3)}]/\alpha$ and γ values showing the importance of embedding Pcs in films for NLO applications. We also note that the best performing film is the PBC film embedded with the **CdOtBPPc** in terms of I_{lim}. It was expected that the **PbOtBPPc** would be the best optical limiter due to the low symmetry afforded by the shuttle-cock arrangement of the Pb ion, however this is not the case. We noted that the I_{lim} obtained here is the same (0.07 J/cm^2) as that determined by Shirk et al. for a **PbOtBPPc** in CHCl$_3$ [90]. A possible reason for this is that the cell used in their study was 30 µm thick, this allowing the solution to behave as a thin film. **CdOtBPPc** came out as a better limiter due primarily to the more pronounced aggregation of the molecule in the thin film (**Fig 3.12**). The reason for this is not yet fully understood as one would expect a more aggregated film to show a lesser NLO response, however aggregates have shown better NLO activity [106]. The thickness of the films is also a contributing factor for the NLO properties. The linear absorption coefficient is enlarged in thin films, hence the thinner the film, the better. The film thicknesses were found to average 25 µm of the PMMA and 13 µm for the PBC, therefore it was expected for the PBC to perform better. At the time of film synthesis, the control of thickness was very difficult to manage without more sophisticated methods and equipment such as spin casters and vapour deposition techniques. Due to the poor photostability of the P(V)Pc films, these were not examined for optical limiting properties.
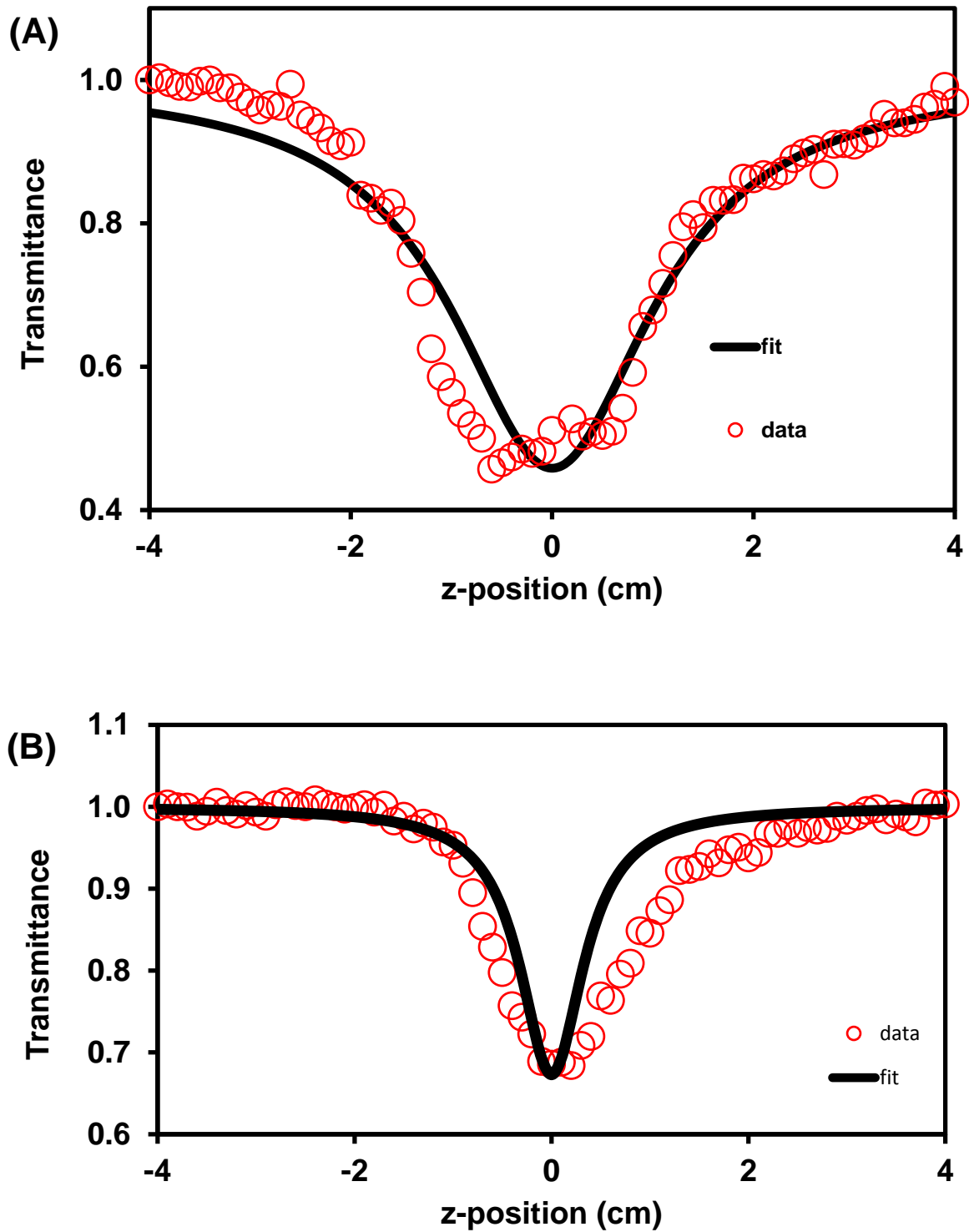
Fig 4.5: Z-scan profile of (A) PbOtBPPc in PBC and (B) CdOtBPPc in PMMA

(A)

(B)
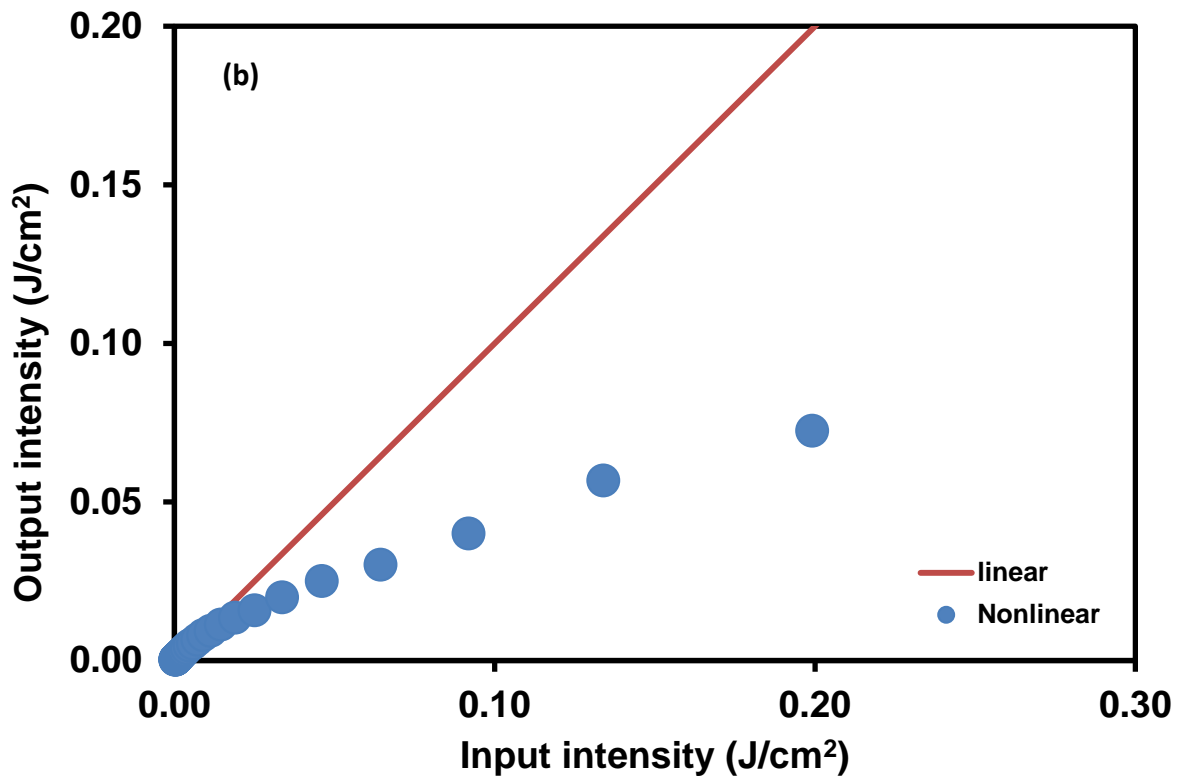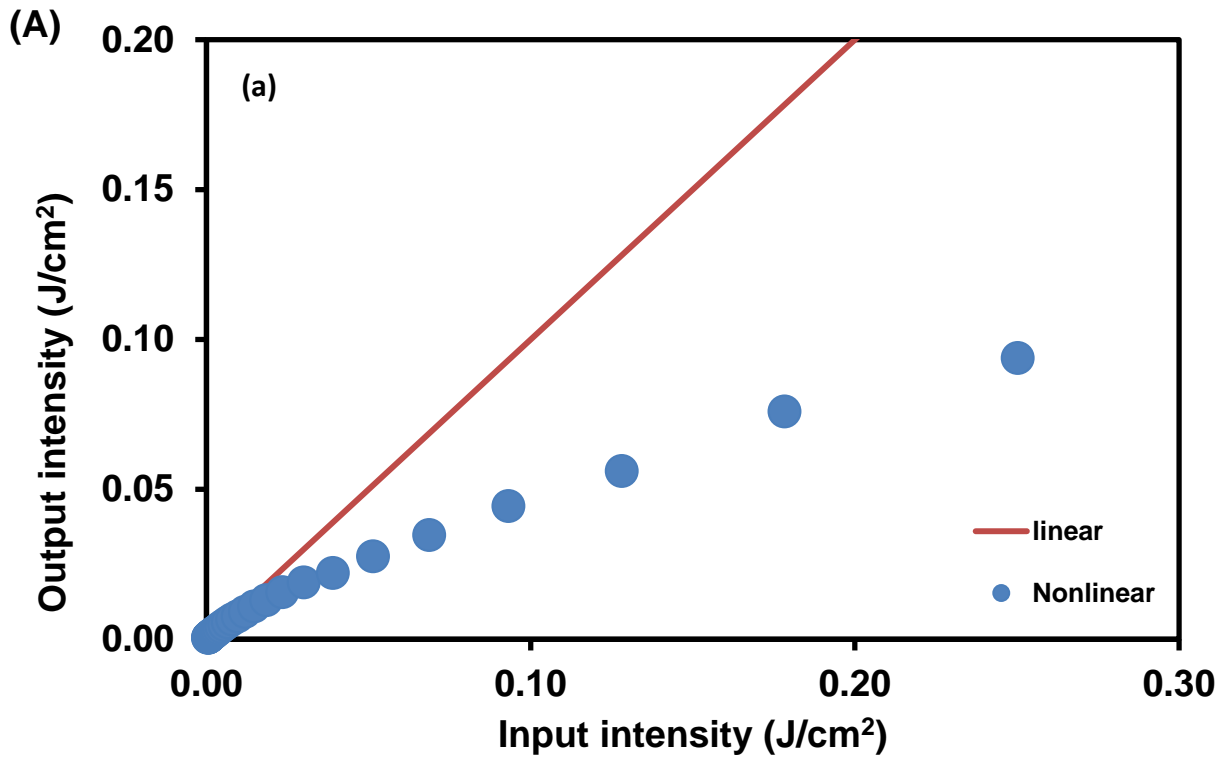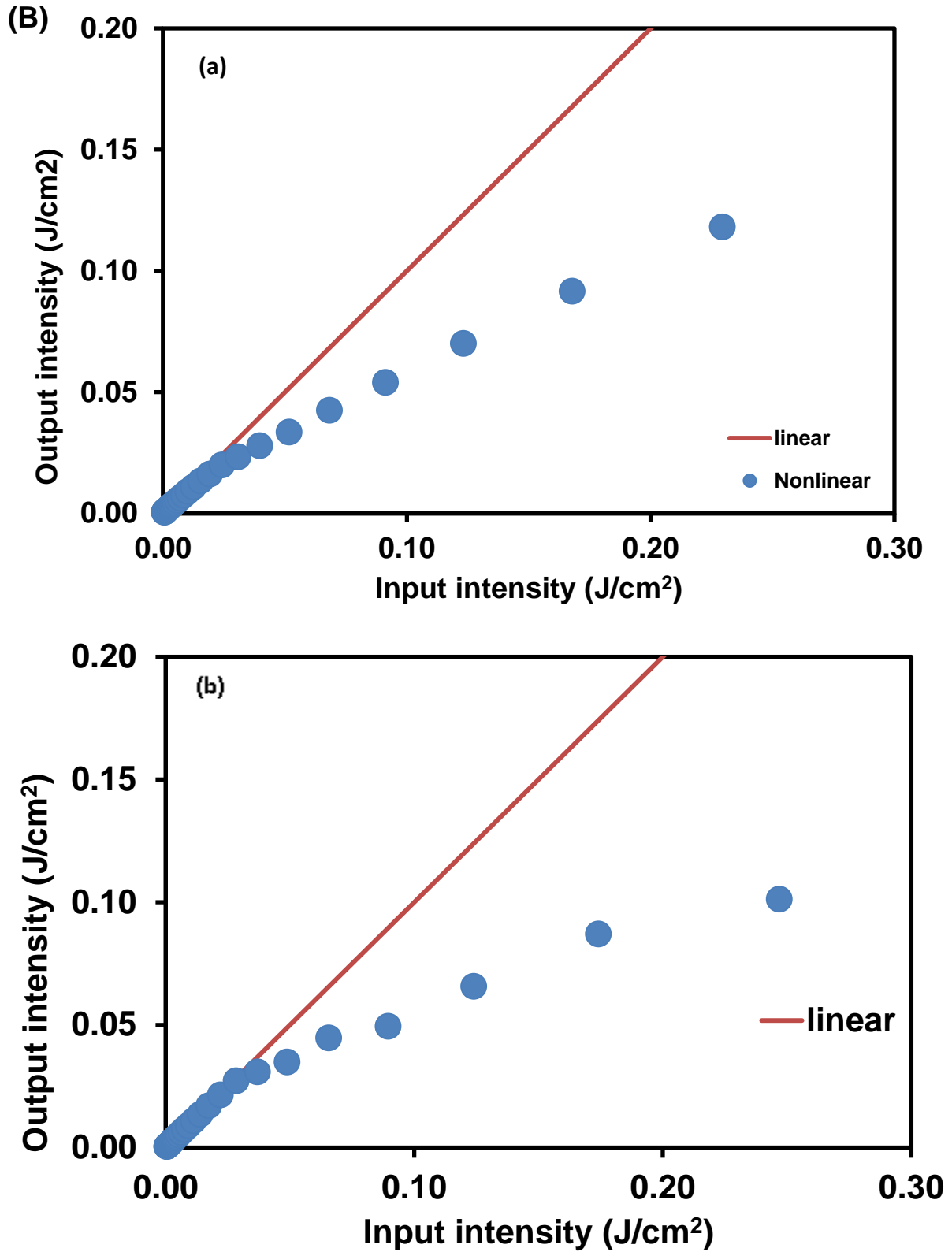
Fig 4.6: Input intensity vs output intensity plots for (A) PbOtBPPc and (B) CdOtBPPc in (a) PBC and (b) PMMA films.

Table 4.2: NLO properties of Pcs and TBCs embedded in polymer thin films

Complex (polymer)	$Im[\chi^{(3)}]/\alpha$ (esu)	γ [a] (esu)	I_{lim} (J/cm^2)
PbOtBPPc (PBC)	1.81×10^{-10}	2.70×10^{-25} (3.15×10^{-32})	0.071 (0.82)
PbOtBPPc (PMMA)	1.00×10^{-11}	6.7×10^{-26} (3.15×10^{-32})	0.25 (0.82)
CdOtBPPc (PBC)	9.56×10^{-10}	2.24×10^{-25} (1.57×10^{-32})	0.055 (1.65)
CdOtBPPc (PMMA)	7.32×10^{-10}	1.65×10^{-25} (1.57×10^{-32})	0.17 (1.65)
8β-POH-TBC (PBC)	2.87×10^{-10}	2.16×10^{-25} (4.26×10^{-32})	0.076 (0.61)
4α-POH-TBC (PBC)	2.9×10^{-10}	2.1×10^{-25} (1.68×10^{-34})	0.16 (-)
4β-POH-TBC (PBC)	1.9×10^{-11}	1.2×10^{-26} (8.93×10^{-35})	0.58 (-)

a – values in brackets are for compounds in DMSO.

4.2.2 NLO in phosphorus triazatetrabenzcorrole films

Fig 4.7 shows the Z-scan profiles for TBC films. As with the **CdOtBPPc** and **PbOtBPPc**, there was a significant increase in the optical limiting properties of the P(V)TBCs embedded in thin films (**Table 4.2**). The enhancement of the Im[$\chi^{(3)}$] in the films by four orders of magnitude is another consistency observed for all PBC films.

 The film with **4α-POH-TBC** was found to perform more than three times better than the **4β-POH-TBC** film, with limiting intensities of 0.16 and 0.58 J/cm^2 respectively. This could be attributed to the lower ground state absorption seen at 532 nm for the **4α-POH-TBC** in the solid state (figure not shown). A requirement of a good OL material is that it should have very low ground state absorption cross section in the region of interest and a very high triplet absorption cross section [98]. The best performing TBC film was **8β-POH-TBC**, with a I$_{lim}$ of 0.076 J/cm^2. This value is comparable to the values obtained for the **CdOtBPPc** and **PbOtBPPc** in PBC. From this, we can motivate that octa-substituted compounds do a better job in optical limiting.
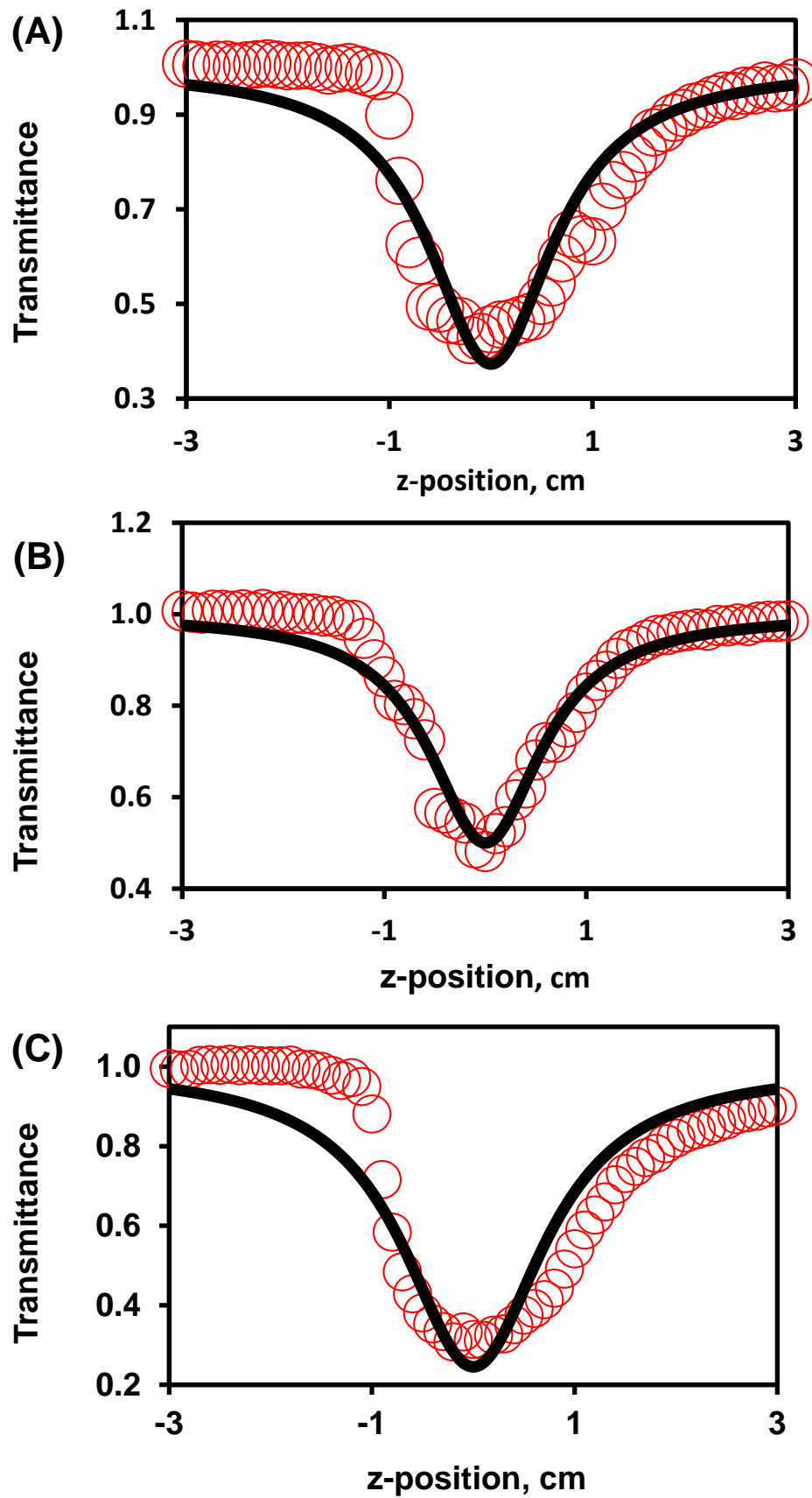
Figure 4.7: Z-scan profiles in PBC for (A) 4α-POH-TBC, (B) 4β-POH-TBC and (C) 8β-POH-TBC.

4.3 Concluding remarks

All the compounds studied exhibited RSA behaviour in solution. The Cd and Pb Pcs showed stronger NLO activity than the P(V)Pcs and P(V)TBCs as expected by virtue of the heavy atom effect. Once embedded in thin films, the PBC films of **CdOtBPPc** and **PbOtBPPc** gave better results than the PMMA films. The P(V)Pcs were unable to be studied in thin films, whilst the P(V)TBCs gave reasonable results. The best performing film was determined to be the **CdOtBPPc** in PBC, with an I_{lim} value of 0.055 J/cm^2, which is much lower than the threshold value of 0.95 J/cm^2.

5. Molecular modelling

5.1 Geometry optimization and TD-DFT calculations

The density functional theory (DFT) method was used to carry out geometry optimizations with the Becke, three-parameter, Lee-Yang-Parr (B3LYP) functional of the Gaussian09 program package [129], and 6-31G(d) basis sets at the Center for High Performance Computing in Cape Town. The B3LYP functional is a hybrid functional, meaning that it incorporates a part of exact change from Hartree-Fock theory with exchange and correlation from other sources [130]. To simplify the calculations the *t*-butyl groups on the para-positions of the phenyl rings were replaced with methyls, since replacing one alkyl group with another is unlikely to make a significant difference to the electronic structure in the context of substituents at the peripheral β-positions where there is no scope for steric interactions. This may also apply for a tetra-substituted compound at the α-positions. The Coulomb-attenuated B3LYP (CAM-B3LYP) functional was used to calculate the electronic absorption properties based on the time-dependent (TD-DFT) method, since it includes a long-range correction of the exchange potential, which incorporates an increasing fraction of Hartree-Fock (HF) exchange as the interelectronic separation increases. This makes it more suitable for studying compounds where there is significant charge transfer in the electronic excited states as is likely to be the case with TBC complexes. The P(V)TBCs were modeled and compared to their respective parent H_2Pcs. The P(V)TBCs only are reported here as these compounds are not as well understood as Pcs.

5.1.1 Molecular modeling for 8β-POH-TBC

A $C_{16}H_{16}^{2-}$ cyclic polyene corresponding to the inner ligand perimeter can be regarded as being the parent perimeter for describing and rationalizing the optical properties. The π-system contains a series of molecular orbitals (MOs) arranged in ascending energy with M_L = 0, ±1, ±2, ±3, ±4, ±5, ±6, ±7 and 8 nodal properties based on the magnetic quantum number for the cyclic perimeter, M_L. The frontier π-MOs have M_L = ±4 and ±5 nodal properties, respectively. The four spin-allowed M_L = ±4 → ±5 excitations give rise to two orbitally degenerate ^1E_u excited states, on the basis of the ΔM_L = ±9, and ΔM_L = ±1 transitions. This results in the forbidden and allowed Q and B bands of Gouterman's 4-orbital model for porphyrins [131], since an incident photon can provide only one quantum of orbital angular momentum. Michl [132–135] introduced an **a**, **s**, **-a** and **-s** terminology (**Fig. 5.1**) for the four MOs derived from the highest occupied molecular orbital (HOMO) and lowest unoccupied molecular orbital (LUMO) of the parent perimeter so that π-systems of porphyrinoids with differing molecular symmetry such as Pcs and TBCs and relative orderings of the four frontier π-MOs in energy terms can be readily compared. One MO derived from the HOMO of a $C_{16}H_{16}^{2-}$ parent hydrocarbon perimeter and another derived from the LUMO have nodal planes which coincide with the *yz*-plane and are referred to, respectively, as the **a** and **-a** MOs, while the corresponding MOs with antinodes on the *yz*-plane are referred to as the **s** and **-s** MOs (**Fig. 5.1**). Since the **a** and **s** MOs have angular nodal planes on alternating sets of atoms, the incorporation of the aza-nitrogen atoms have a much larger stabilizing effect on the energy of the **s** MO resulting in a large separation of the **a** and **s** MOs (the ΔHOMO value in the context of Michl's perimeter model [132–135]) and Q(0,0) bands that are dominated by the **a** → **-a** and **a** → **-s** one-electron transitions (**Table 5.1**) rather than having near equal

contributions from the **s → -a** and **s → -s** one-electron transitions [108]. This leads to a mixing of the allowed and forbidden properties of the Q and B bands.

The π-systems of free base Pcs and the ligands of TBC complexes have at most D_{2h} and C_{2v} symmetry, respectively, and hence lack four-fold axes of symmetry. There is therefore a minor lifting of the degeneracy of the **-a** and **-s** MOs (the ΔLUMO value in the context of Michl's perimeter model) in addition to the far larger splitting of the **a** and **s** MOs caused by the large MO coefficients on the aza-nitrogens in the context of the **s** MO (**Fig 5.2**). This results in two symmetry-split Q(0,0) bands in the electronic absorption spectra of **H₂OtBPPc** (at 703 and 669 nm) and **8β-POH-TBC** (at 664 and 637 nm) in CHCl₃ (**Figs. 5.3 and 5.4**), with coupled pairs of Faraday $\mathcal{B}_0$ terms replacing the positive Faraday $\mathcal{A}_1$ terms that dominate the MCD of most D_{4h} symmetry metal porphyrin and phthalocyanine complexes [136,137]. Michl [132–135] has demonstrated that when ΔLUMO < ΔHOMO, as is the case with most tetraazaporphyrinoids, a –ve / +ve sequence is anticipated in $\mathcal{B}_0$ term intensity in ascending energy terms, while a +ve / –ve sequence is anticipated when ΔLUMO > ΔHOMO. In the B band region there is a broad B1/B2 band envelope with a maximum at 344 nm, while the B bands of **8β-POH-TBC** are markedly red shifted to 443 and 450 nm relative to the B1/B2 band of **H₂OtBPPc**. The Stillman group [138–142] used the simultaneous spectral band deconvolution of the electronic absorption and MCD spectra of phthalocyanines to identify the presence of a second intense absorption band close in the B band region, so the band nomenclature for phthalocyanines was modified to, in ascending energy, the Q (ca. 670 nm), B1 (ca. 370 nm), B2 (ca. 330 nm), N (ca. 275 nm), L (ca. 245 nm) and C (ca. 210 nm) bands [131,139]. The trends observed in the spectra of **8β-POH-TBC**, such as the blue-shift of the Q(0,0) bands and a red-shift of the B(0,0) bands relative to the Pc precursor, are similar to the those reported previously for other TBC complexes [68,136,137]. As has been reported

previously [136], the alignment of the nodal planes in the frontier π-MOs of the TBC complex are broadly similar to those of the parent Pc. The loss of one of the aza-nitrogens results in a marked destabilization of **s** MO but has a much smaller impact on the **a** MO (**Fig. 5.2**), which has nodal planes on or near the bridging atoms. The resulting decrease in the ΔHOMO value leads to a mixing of the allowed and forbidden properties of the Q and B bands (**Table 5.1**). The spectrum of **8β-POH-TBC** is somewhat similar to that of a porphyrin, therefore, since there is a weakening of the Q(0,0) bands relative to the B band and a relatively narrow and well-resolved B band is observed beyond 400 nm. The loss of an aza-nitrogen atom also destabilizes the **-a** and **-s** MOs of **8β-POH-TBC** to a greater extent than the **a** MO relative to the electronic structure of **H₂OtBPPc** (**Fig. 5.2**) and this leads to an increase in the HOMO-LUMO gap and hence in a significant blue-shift of the Q(0,0) bands (**Figs. 5.3 and 5.4**). The Q(0,0) bands still lie within the therapeutic window, however, so **8β-POH-TBC** is potentially useful for biomedical applications.

The TD-DFT calculations for **H₂OtBPPc** and **8β-POH-TBC** that were carried out with the CAM-B3LYP functional are consistent with the experimental data in this regard, since no ππ* bands are predicted to lie between the Q and B bands of **8β-POH-TBC**. The loss of an aza-nitrogen atom markedly destabilizes the **-a**, **-s** and **s** MOs of **8β-POH-TBC** (**Fig. 5.2**), which have large MO coefficients on the inner perimeter of the ligand, so there are no π-MOs associated primarily with the ligand π-system with energies that lie between those of the **a** and **s** MOs. In contrast in the electronic structure of **H₂OtBPPc**, six MOs are predicted to lie between the **a** and **s** MOs (**Fig. 5.2**).
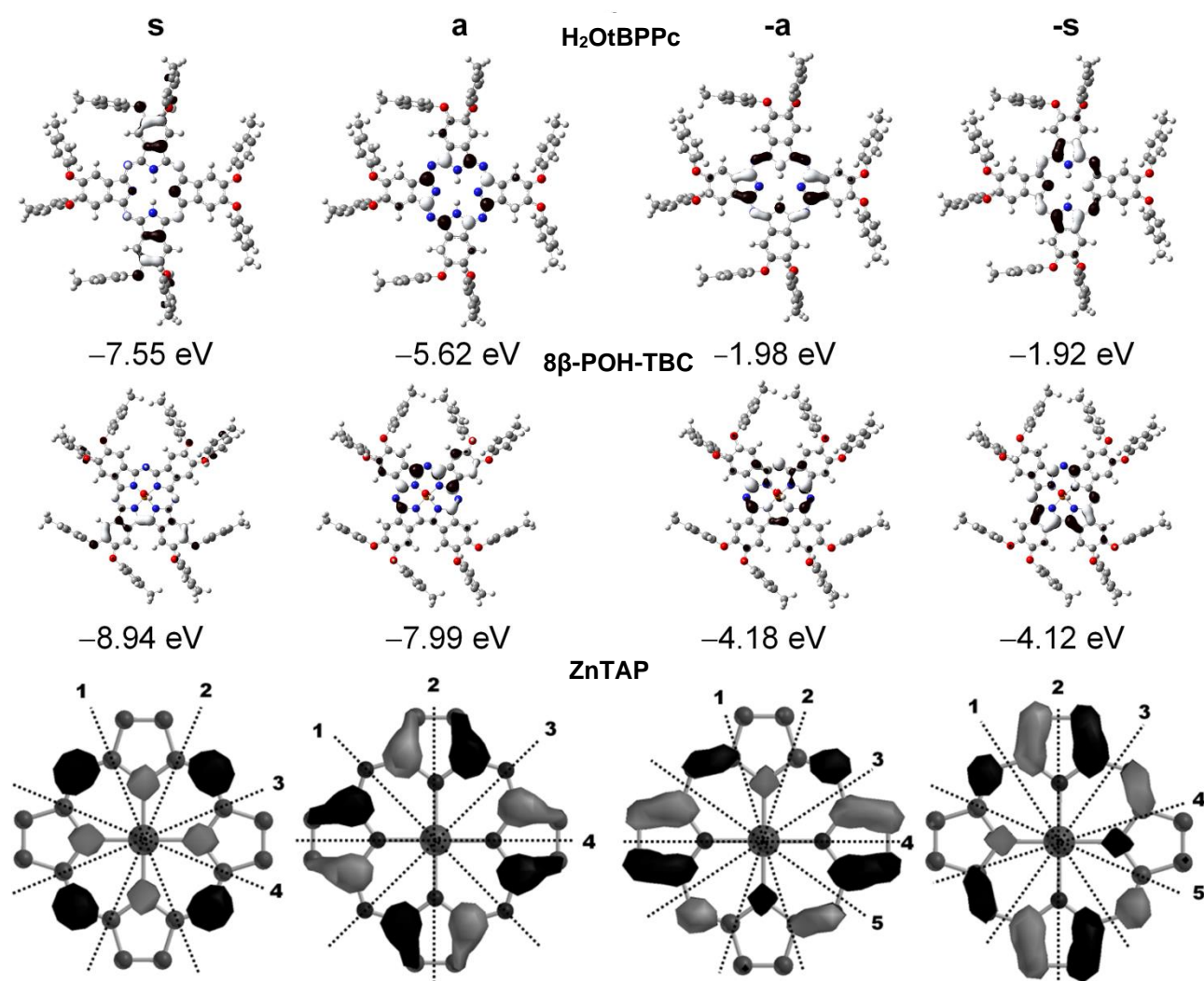
Fig. 5.1: Nodal patterns of the four frontier π–MOs of zinc tetraazaporphyrin (ZnTAP) with the angular nodal planes highlighted to describe the $M_L = \pm 4$ and ± 5 nodal patterns, and the nodal patterns and MO energies of H$_2$OtBPPc and 8β-POH-TBC at an isosurface value of 0.04 a.u. Michl [132–135] introduced a, s, -a and -s nomenclature to describe the four frontier π-MOs based on whether there is a nodal plane (a and -a) or an antinode (s and -s) on the *y*-axis. Once the alignment of the angular nodal planes has been clearly defined the effect of different structural perturbations can be readily conceptualized on a qualitative basis through a consideration of the relative size of the MO coefficients on each atom on the perimeter

Fig. 5.2: The MO energies of H₂OtBPPc and 8β-POH-TBC relative to the energy of the LUMOs. The a, s, -a and -s MOs of Michl's perimeter model [132–135] **are highlighted in gray. MOs associated primarily with the peripheral *t*-butylphenoxy substituents are offset to the right. Occupied MOs are denoted with small black diamonds and a gray dashed line is used to highlight the HOMO–LUMO gap.**
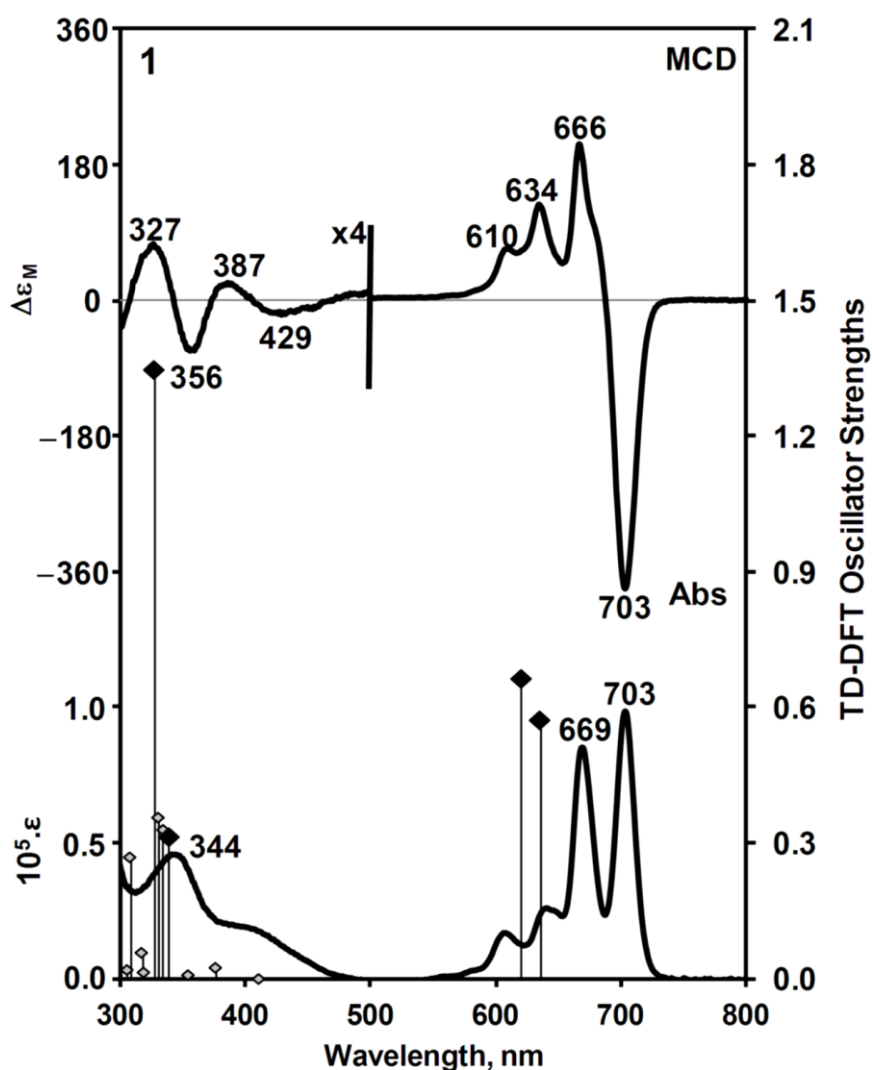
Fig. 5.3: Magnetic circular dichroism (top) and electronic absorption (bottom) spectra of H$_2$OtBPPc in CHCl$_3$. The calculated TD-DFT spectrum (Table 5.1) is plotted against a secondary axis. The transitions associated with the Q and B bands of Gouterman's 4-orbital model [131] are highlighted with black diamonds.
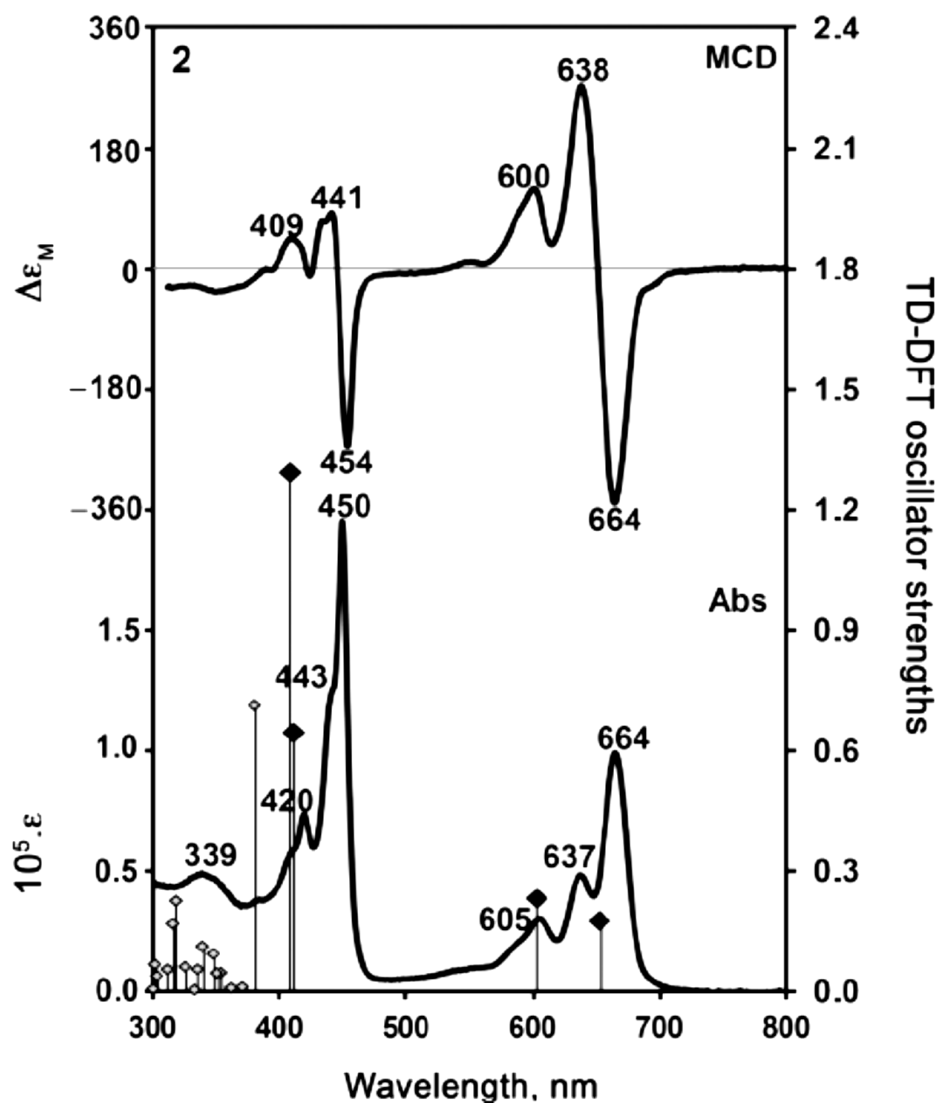
Fig. 5.4: Magnetic circular dichroism (top) and electronic absorption (bottom) spectra of 8β-POH-TBC in CHCl₃. The calculated TD-DFT spectrum (Table 5.1) is plotted against a secondary axis. The transitions associated with the Q and B bands of Gouterman's 4-orbital model [131] are highlighted with black diamonds.

Table 5.1: TD-DFT spectra of the B3LYP optimized geometries of H₂OtBPPc and 8β-POH-TBC calculated with the CAM-B3LYP functional and 6-31G(d) basis sets.

						H₂OtBPPc
Band[a]	#[b]	Calc[c]			Exp[d]	Wave Function[e] =
----	**1**	---- ---- ----		----	----	Ground State
Q	**2**	15.8635	(0.57)	14.2	703	**91% a → -a; 4% s → -s;** …
Q	**3**	16.1620	(0.66)	15.0	666	**94% a → -s; 3% s → -a;** …
--	**4**	24.4410	(0.00)	---	---	76% H−1 → -s; 11% H−4^{Ph} → -s; …
--	**5**	26.6376	(0.03)	---	---	48% H−2 → -s; 18% H−10 → -s; 17% H−5 → -s; …
--	**6**	28.2354	(0.01)	---	---	82% H−1 → -a; …
B	**7**	29.5339	(0.31)	28.1	356	**30% s → -a;** 28% H−3 → -a; 15% H−2 → -a; …
--	**8**	29.9334	(0.33)	---	---	40% H−8 → -a; 24% H−4^{Ph} → -a; **10% s → -s;** …
--	**9**	30.3330	(0.36)	---	---	38% H−2 → -a; 12% H−5 → -a; …
B	**10**	30.6327	(1.35)	30.6	327	**31% s → -s;** 25% H−3 → -a; …

|						8β-POH-TBC
Band[a]	#[b]	Calc[c]			Exp[d]	Wave Function[e] =
----	**1**	---- ---- ----		----	----	Ground State
Q	**2**	15.3652	(0.18)	15.1	664	**88% a → -s; 7% s → -a;** …
Q	**3**	16.6603	(0.23)	15.7	638	**83% a → -a; 10% s → -s;** …
B	**4**	24.3411	(0.65)	22.0	454	**32% s → -a;** 31% a → L+1; 15% H−1^{Ph} → -a; …
B	**5**	24.5408	(1.29)	22.7	441	**43% s → -s;** 30% H−1^{Ph} → -a; **15% a → -a;** …
--	**6**	26.3380	(0.71)	----	----	50% a → L+1; **17% s → -a;** 12% H−1^{Ph} → -a; …

a – Band assignment described in the text. b – The number of the state assigned in terms of ascending energy within the TD-DFT calculation. c – Calculated band energies (10^3.cm^{-1}), wavelengths (nm) and oscillator strengths in parentheses (f). d – Observed energies (10^3.cm^{-1}) and wavelengths (nm) in Figs. 5.3 and 5.4. e – The wave functions based on the eigenvectors predicted by TD-DFT. One-electron transitions associated with the four frontier π-MOs of Gouterman's 4-orbital model [131] are highlighted in bold. H and L refer to the HOMO and LUMO, respectively. MOs associated primarily with the peripheral *t*-butylphenoxy substituents are denoted with a superscript Ph.

5.1.2 Molecular modeling for 4α-POH-TBC and 4β-POH-TBC

The loss of an aza-nitrogen atom also destabilizes the **-a** and **-s** MOs of **4β-POH-TBC** and **4α-POH-TBC** to a greater extent than the **a** MO relative to the electronic structures of **4β-H₂Pc** and **4α-H₂Pc** (**Fig 5.5**) and this leads to an increase in the HOMO−LUMO gap and hence in a significant blue-shift of the Q(0,0) bands relative to those of the analogous Pcs [136,137], as was seen for **8β-POH-TBC**. The −/+/−/+ sign sequence observed for the Q and B bands in the MCD spectra (**Figs 5.6 - 5.7**) is consistent with what would be anticipated based on the predicted ΔHOMO and ΔLUMO values (**Fig 5.8, Table 5.2**) [132,133]. The spectra of **4β-POH-TBC** and **4α-POH-TBC** are somewhat similar to that of a porphyrin complex, therefore, since there is a weakening of the Q(0,0) bands relative to the well-resolved B band observed beyond 400 nm. and a relatively narrow and well-resolved B band is observed beyond 400 nm. This is more pronounced in the spectrum of **4α-POH-TBC**, due to the smaller ΔHOMO value (**Figs 5.8 − 5.9**). Relatively narrow band widths are observed in the Q band regions of the optical spectra of **4β-POH-TBC** and **4α-POH-TBC**, while a range of ca. 20 nm is predicted for the Q(0,0) bands of the nine possible positional isomers of **4α-POH-TBC** (**Fig 5.7**) in TD-DFT calculations with the CAM-B3LYP functional for B3LYP optimized geometries. This is seen in all the isomers of **4α-POH-TBC (Fig 5.10)**. It seems probable therefore that the more sterically hindered isomers α-tetrasubstituted isomers are formed in significantly lower yields. TBCs are heteroatomic π-systems, and like Pcs, are rigid planar structures. Due to this, their geometry is easy to optimize accurately thus making the study of their optical and redox properties possible and reliable [58,108].
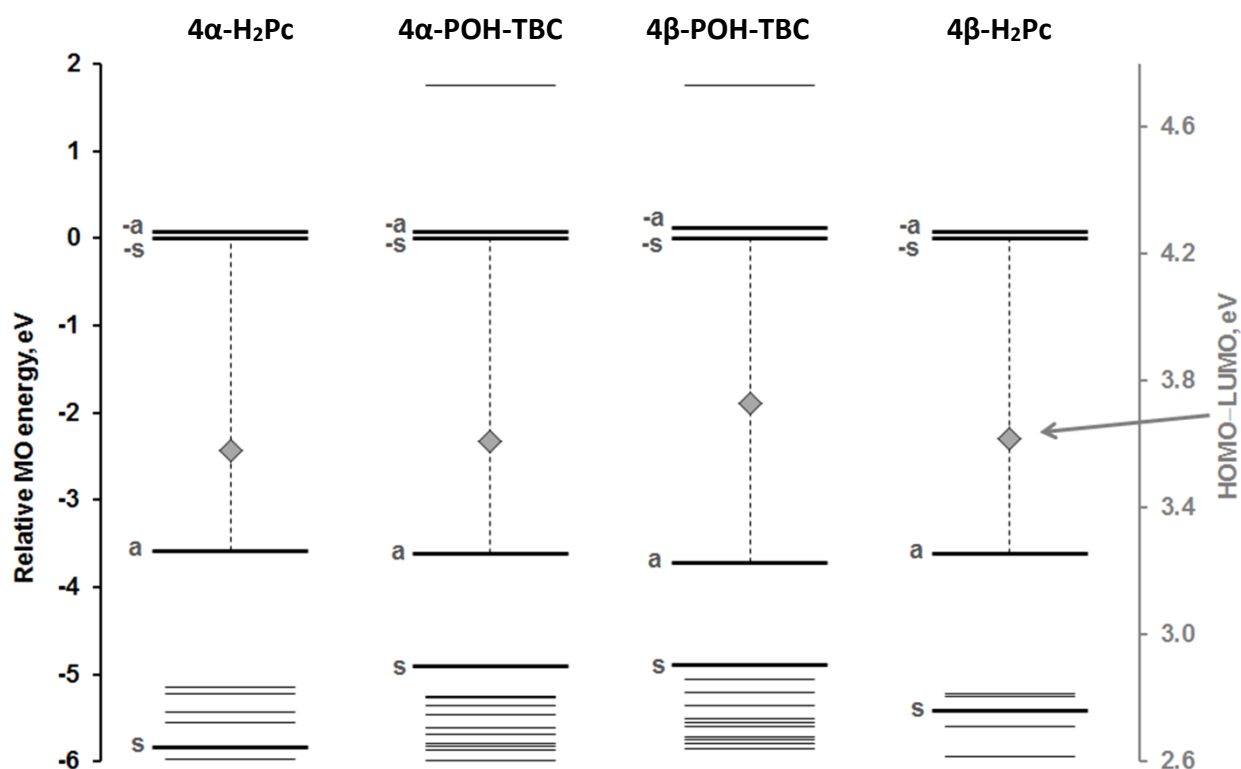
Fig 5.5. Relative MO energies of the C$_4$ symmetry 4α-H$_2$Pc and 4β-H$_2$Pc and the analogous positional isomers (Fig 5.8) for 4α-POH-TBC and 4β-POH-TBC in TD-DFT calculations (Table 5.2) with the CAM-B3LYP functional with the energy of the LUMO set to zero in each case. The a, s, -a and -s of Michl's [132–135] perimeter model are highlighted in bold black. The diamonds represent the HOMO-LUMO energy difference and the gray dashed lines highlight the HOMO-LUMO gap
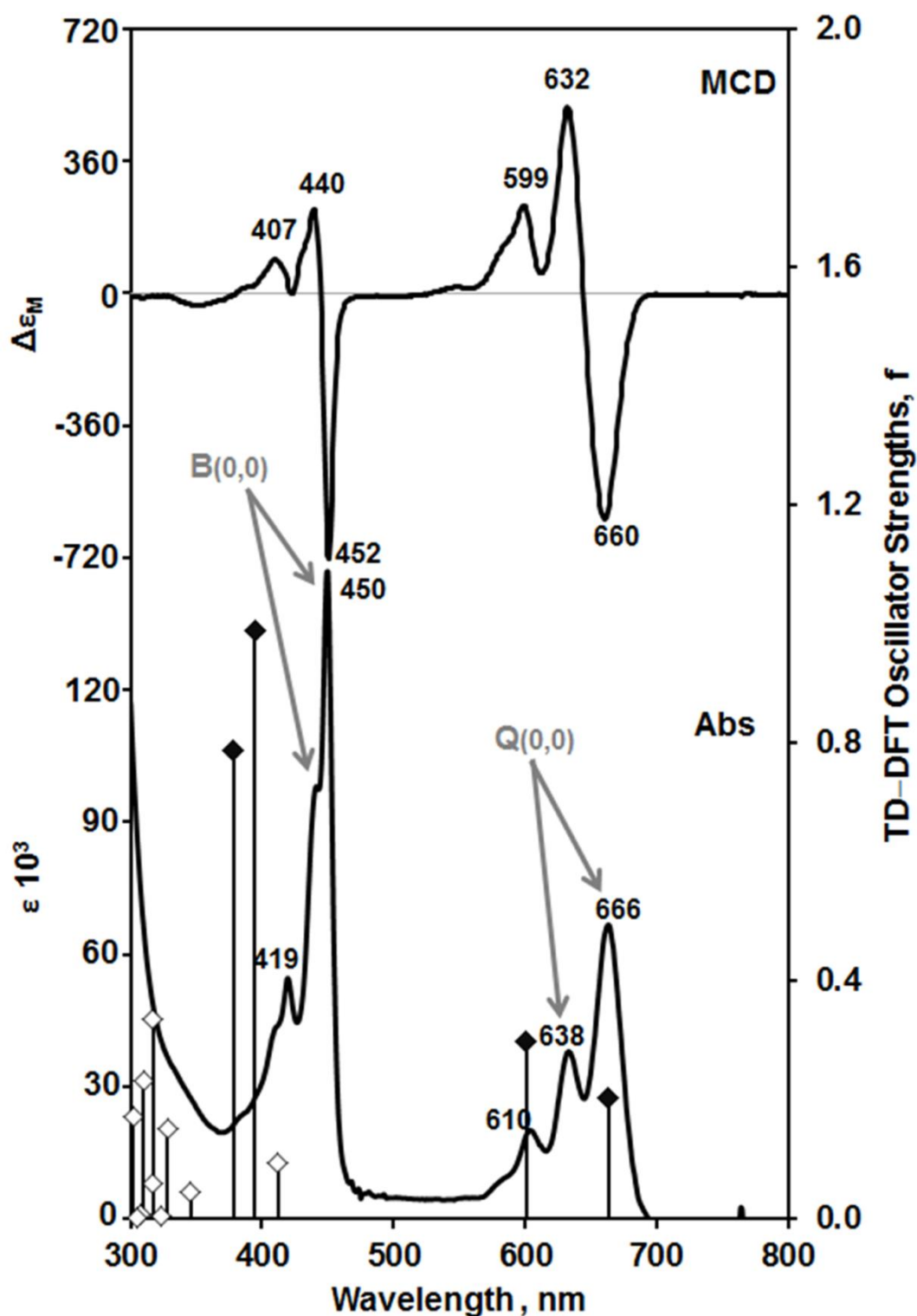
Fig. 5.6: MCD (top) and electronic absorption spectra (bottom) of 4β-POH-TBC in DMSO. The TD-DFT oscillator strengths (Table 5.2) are plotted against a secondary axis. The Q and B band transitions which are described by Gouterman's [131] 4-orbital model are highlighted with black diamonds.
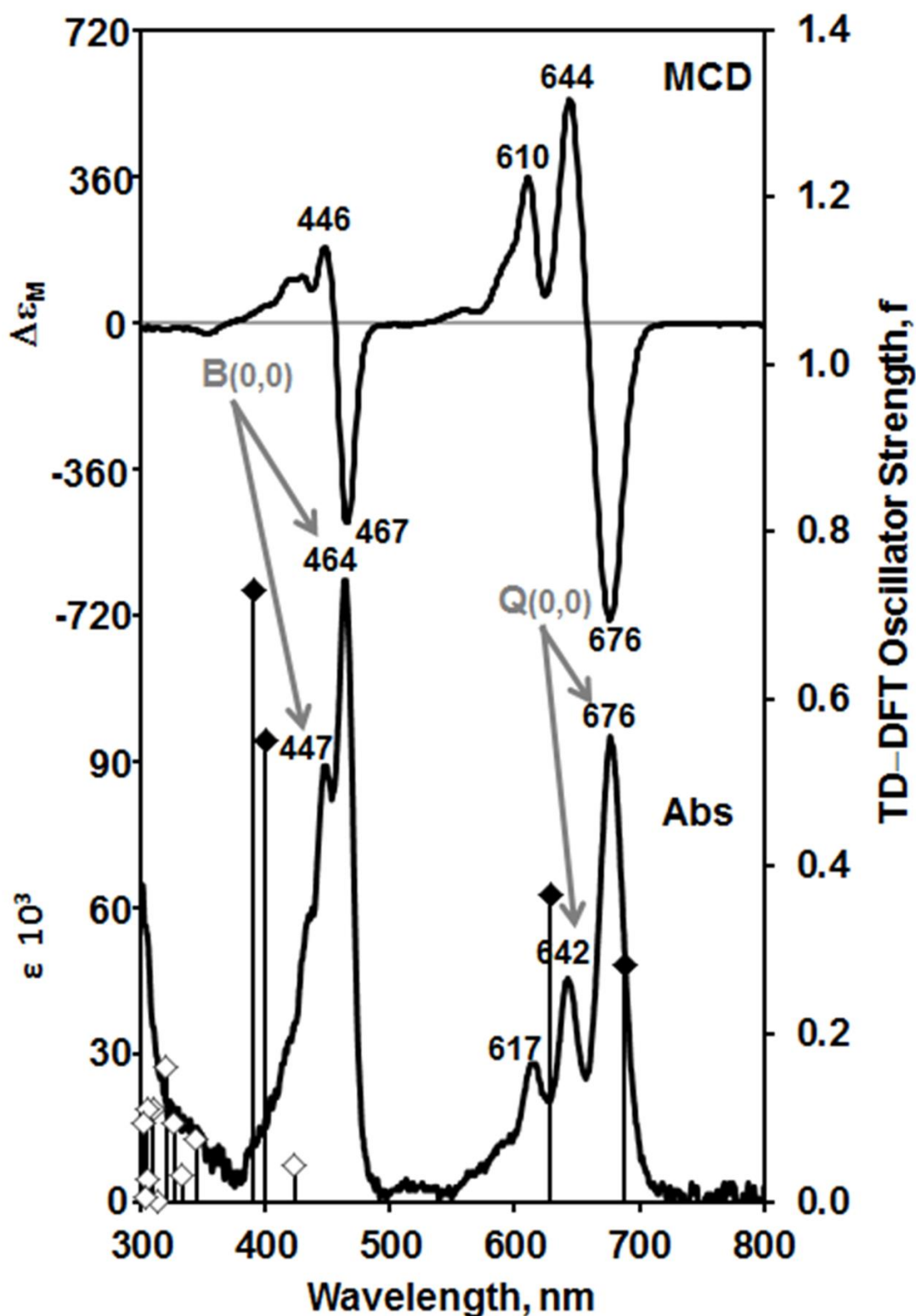
Fig. 5.7: MCD spectrum (top) and ground state electronic absorption spectrum (bottom) of the 4α-POH-TBC in DMSO. The TD-DFT oscillator strengths (Table 5.2) are plotted on the secondary axis. The Q and B band transitions which are described by Gouterman's 4-orbital model [131] **are highlighted with black diamonds.**
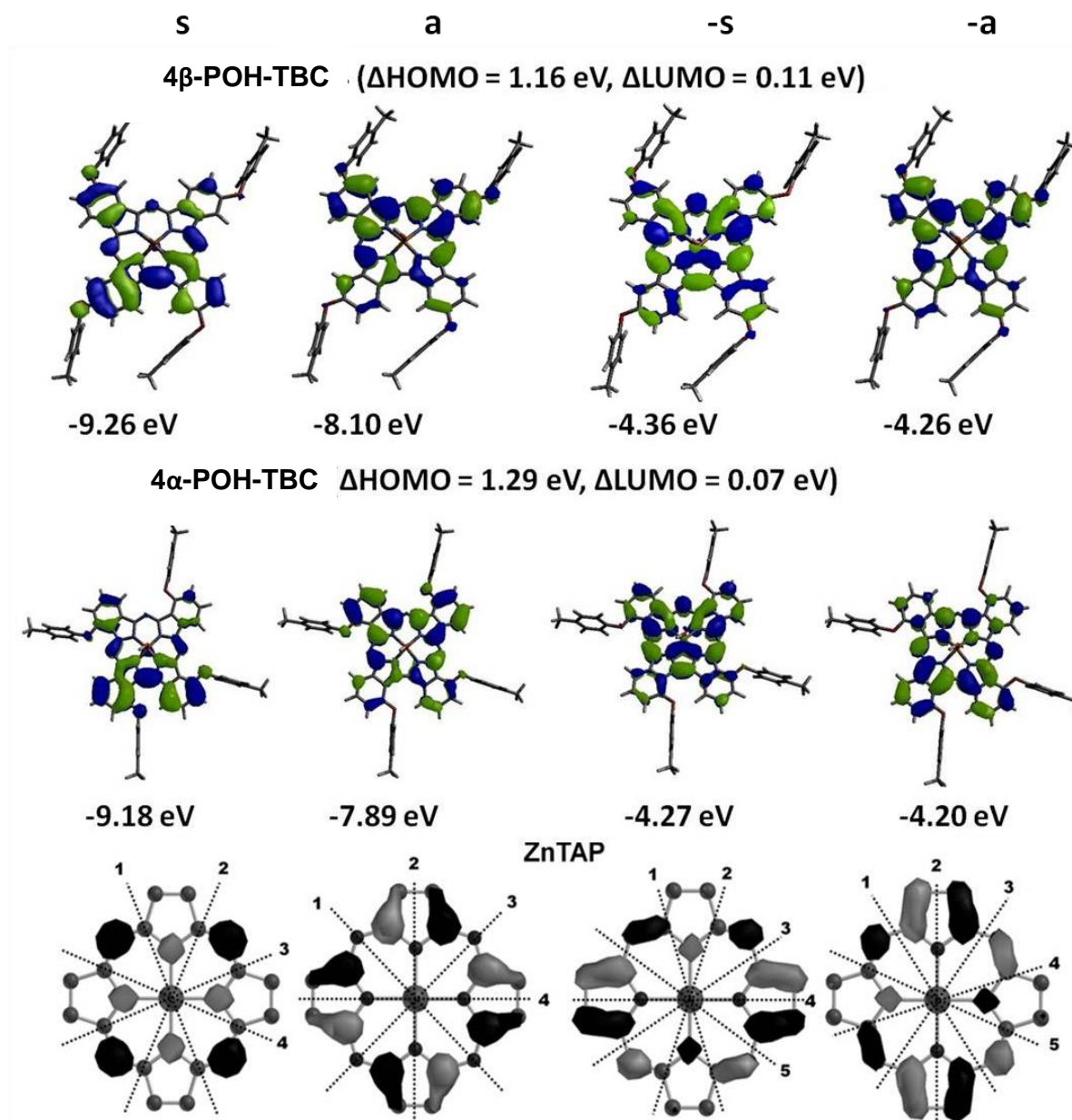
Fig 5.8: Nodal patterns of the four frontier π-MOs of zinc tetraazaporphyrin (ZnTAP) with the angular nodal planes highlighted to describe the $M_L = \pm4$ and ±5 nodal patterns, and the nodal patterns and MO energies for one of the positional isomers of 4β-POH-TBC and 4α-POH-TBC at an isosurface value of 0.04 a.u. Michl [132–135] introduced a, s, -a and -s nomenclature to describe the four frontier π-MOs based on whether there is a nodal plane (a and -a) or an antinode (s and -s) on the *y*-axis. Once the alignment of the angular nodal planes has been clearly defined the effect of different structural perturbations can be readily conceptualized on a qualitative basis through a consideration of the relative size of the MO coefficients on each atom on the perimeter.

1 ($\lambda_Q = 684.4$ nm, $\lambda_B = 421.1$ nm)   2 ($\lambda_Q = 685.3$ nm, $\lambda_B = 419.8$ nm)   3 ($\lambda_Q = 685.8$ nm, $\lambda_B = 420.0$ nm)

4 ($\lambda_Q = 696.9$ nm, $\lambda_B = 424.7$ nm)   5 ($\lambda_Q = 690.4$ nm, $\lambda_B = 422.0$ nm)   6 ($\lambda_Q = 674.5$ nm, $\lambda_B = 417.4$ nm)

7 ($\lambda_Q = 684.7$ nm, $\lambda_B = 419.7$ nm)   8 ($\lambda_Q = 688.3$ nm, $\lambda_B = 423.3$ nm)   9 ($\lambda_Q = 683.8$ nm, $\lambda_B = 417.1$ nm)
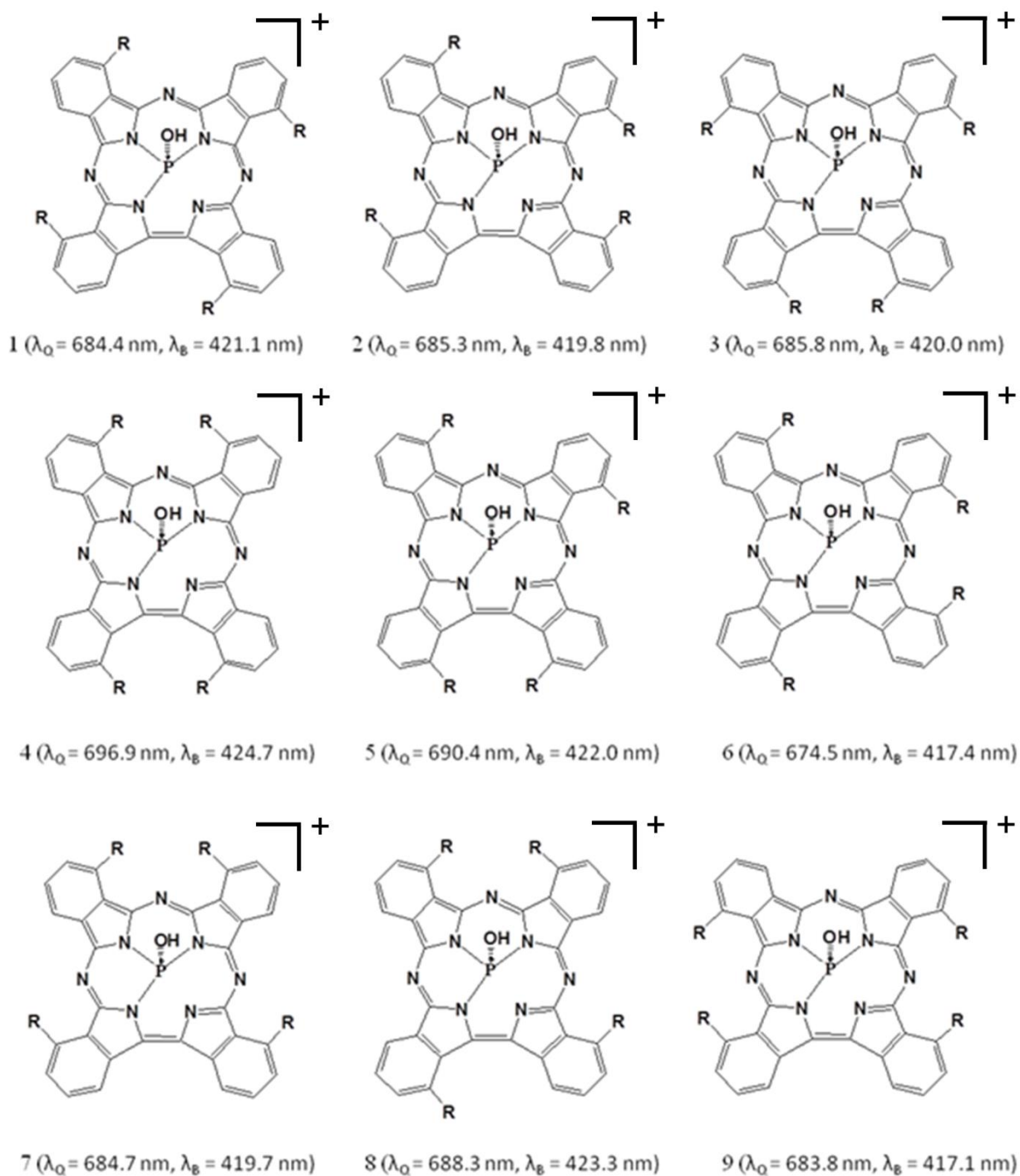
Fig 5.9. Structures of the nine positional isomers of the 4α-POH-TBC with the calculated values for the more intense Q and B band components.
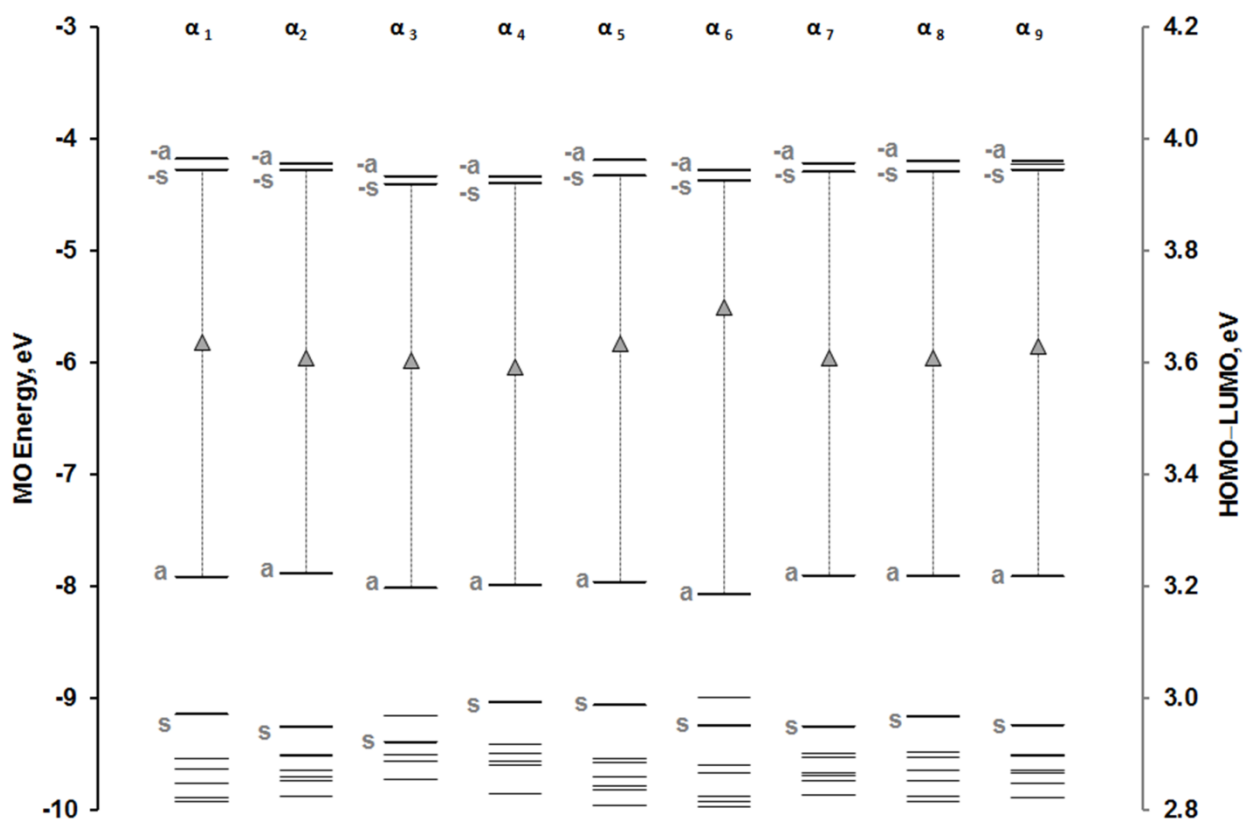
Fig 5.10: MO energies of the nine α-tetrasubstituted TBC isomers (Fig 5.7). The a, s, -a, and -s MOs of Michl's perimeter model [132–135] **MOs are shown with thick black lines. The diamonds represent the HOMO–LUMO gap difference and the gray dashed lines represent the HOMO–LUMO gap.**

Table 5.2: TD-DFT spectra of the B3LYP optimized geometries of 4β-POH-TBC and 4α-POH-TBC calculated with the CAM-B3LYP functional and 6-31G(d) basis sets.

|			4α-POH-TBC				
Band[a]	**#[b]**		**Calc[c]**		**Exp[d]**		**Wavefunction=[e]**
--	1	---	---	---	---	---	Ground state
Q	2	14.6	684.5	(0.28)	14.8	676	**91% a→-s; 5% s → -a;** …
Q	3	16.2	618.1	(0.34)	15.5	644	**85% a→-a; 12% s → -s;** …
--	4	23.7	421.1	(0.08)	---	---	67% a→L+2; **18% s → -a;** …
B	5	24.8	402.7	(0.56)	21.4	467	**86% s→-s; 9% a → -a;** …
B	6	25.5	392.5	(0.72)	22.2	450	**64% s→-a;** 20% s → L+2; **5% a→-s;**
			4β-POH-TBC				
Band	**#**		**Calc**		**Exp**		**Wavefunction=**
--	1	---	---	---	---	---	Ground state
Q	2	15.1	664	(0.20)	15.2	660	**90% a→-s; 7% s → -a;** …
Q	3	16.6	401	(0.30)	15.8	633	**88% a→-a; 8% s → -s;** …
--	4	24.3	412	(0.09)	---	---	66% a→L+2; **23% s → -a;** …
B	5	25.3	395	(0.99)	22.2	451	**86% s→-s; 9% a → -a;** …
B	6	26.4	378	(0.79)	22.7	440	**64% s→-a;** 20% s → L+2; **5% a→-s;** …

a − Band assignment described in the text. b − The number of the state assigned in terms of ascending energy within the TD-DFT calculation. c − Calculated band energies ($10^3.cm^{-1}$), wavelengths (nm) and oscillator strengths in parentheses (f). d − Observed energies ($10^3.cm^{-1}$) and wavelengths (nm) in Figs. 5.6 and 5.7. e − The wave functions based on the eigenvectors predicted by TD-DFT. One-electron transitions associated with the four frontier π-MOs of Gouterman's 4-orbital model [131] are highlighted in bold. H and L refer to the HOMO and LUMO, respectively.

5.2 Concluding remarks

The TD-DFT calculations, along with the MCD spectra reveal more information about the electronic transitions seen in the P(V)TBCs. The results are consistent with Gouterman's 4-orbital model. The predicted spectra for the P(V)TBCs match the experimental results well, but not exactly. The reason for this is that the model used for prediction is not robust enough to find the exact electronic position. This would require much more time.

The removal of an aza-nitrogen destabilizes the **-a** and **-s** orbitals of the P(V)TBCS compared to the respective H_2Pcs which is why a huge blue shift of the Q and B bands is observed. Understanding these trends helps us to be able to rationally design molecules which will be able to be used for applications such as NLO and PDT.

6. Conclusions

A novel cadmium Pc, three phosphorus Pcs and three novel P(V)TBCs were successfully synthesised and fully characterized using various techniques. These compounds were investigated for their photophysical and, where applicable, photochemical properties. The fluorescence of the **CdOtBPPc** and previously reported **PbOtBPPc** was much less than for the phosphorus compounds due to the high intersystem crossing induced by the heavy atom effect. The phosphorus Pcs showed unusually high instability in the presence of light. The P(V)TBCs were successfully modelled using TD-DFT calculations, and these results predicted quite accurately the observed trends. The P(V)TBCs showed very significant singlet oxygen and triplet quantum yields which are good for singlet oxygen applications, but their high photodegradation quantum yields limit their use. Nonlinear optical studies were carried out successfully in DMSO, with the cadmium and lead Pcs performing better than the P(V)TBCs due to the heavy atom effect. It was observed that the octa substituted TBC gave a better limiting intensity than the two tetra substituted TBCs, implying that more extended conjugation leads to better optical limiting.

The **CdOtBPPc**, **PbOtBPPc** and P(V)TBCs were successfully embedded into polymer thin films, with poly(bisphenol A carbonate) films yielding better optical limiting results than the polymethyl methacrylate which was used as comparison. The optical limiting intensities obtained for the materials were all much less than the safety threshold of 0.95 J/cm^2, with the cadmium PBC film giving the best results.

7.References

[1]   T. Maiman, Nature 187 (1960) 493.

[2]   M. Beesley, Lasers and Their Applications, Taylor & Franics LTD, London, 1971.

[3]   F. Fankhauser, H. Lortscher, E. Van Der Zypen, Int. Opthalmology 5 (1982) 15.

[4]   Y. Barkana, M. Belkin, Surv. Ophthalmol. 44 (2000) 459.

[5]   K. Blau, G. Buono, (2011) (presentation offered by Association of European Airlines)

[6]   R.S. Umar, K. Pillay, C. Dolley, Daily News (2012),
        http://www.iol.co.za/dailynews/news/lasers-threaten-sa-air-safety-
        1.1266401#.VASssfmSySo, Accessed: 6 July 2014

[7]   N. Masilela, T. Nyokong, Dye. Pigment. 84 (2010) 242.

[8]   S. Shi, W. Ji, J.P. Lang, X.Q. Xin, J. Phys. Chem. 98 (1994) 3570.

[9]   Y. Sun, J.E. Riggs, Int. Rev. Phys. Chem. 18 (1999) 43.

[10]   A. Persoons, J. Bredas, C. Adant, P. Tackx, B.M. Pierce, Chem. Rev. 94 (1994) 243.

[11]   S.J. Mathews, S. Chaitanya Kumar, L. Giribabu, S. Venugopal Rao, Opt. Commun. 280 (2007)
        206.

[12]   J.S. Shirk, R.G.S. Pong, S.R. Flom, H. Heckmann, M. Hanack, O. Sciences, V. Di, V. Na, J. Phys.
        Chem. 104 (2000) 1438.

[13]   T. Nyokong, Coord. Chem. Rev. 251 (2007) 1707.

[14]   A. von Braum, J. Tcherniak, Berichte Der Dtsch. Chem. Gesellschaft 40 (1907) 2709.

[15]   H. de Diesbach, E. von de Weid, Helv. Chim. Acta 10 (1927) 886.

[16]   R.P. Linstead, J. Chem. Soc. (1933) 1933.

[17]   G.T. Byrne, R.P. Linstead, A.R. Lowe, J. Chem. Soc. (1934) 1017.

[18]   R.P. Linstead, J. Chem. Soc. (1933) 1016.

[19]   J.M. Robertson, J. Chem. Soc. (1934) 615.

[20]   M.A. Dahlen, Ind. Eng. Chem. 31 (1939) 839.

[21]   T. Nyokong, Pure Appl. Chem. 83 (2011) 1763.

[22] T.C. Tempesti, E.N. Durantini, in:, 11th Int. Electron. Conf. Synth. Org. Chem., 2007.

[23] T. Nyokong, in:, J.H. Zagal, F. Bedioui, J.-P. Dodelet (Eds.), N4-Macrocyclic Metal Complexes Electrocatalysis, Electrophotochemistry and Biomimetic Electrocatalysis., Springer, 2006, pp. 315–361.

[24] C.G. Claessens, W.J. Blau, M. Cook, M. Hanack, Â.Y.Ã. Torres, D. Wo, Monatshefte Fur Chemie 132 (2001) 3.

[25] J.J. Doyle, J. Wang, S.M. O'Flaherty, Y. Chen, A. Slodek, T. Hegarty, L.E. Carpenter II, D. Wöhrle, M. Hanack, W.J. Blau, J. Opt. A Pure Appl. Opt. 10 (2008) 075101.

[26] B.L. Justus, A.L. Huston, Appl. Phys. Lett. 63 (2001) 1483.

[27] G. de la Torre, C.G. Claessens, T. Torres, European J. Org. Chem. 2000 (2000) 2821.

[28] Y. Liu, Y. Chen, L. Cai, J. Wang, Y. Lin, J.J. Doyle, W.J. Blau, Mater. Chem. Phys. 107 (2008) 189.

[29] E.M. Antunes, T. Nyokong, J. Porphyr. Phthalocyanines 13 (2009) 153.

[30] D.K. Modibane, T. Nyokong, Polyhedron 28 (2009) 479.

[31] J.S. Shirk, R.G.S. Pong, S.R. Flom, F.J. Bartoli, M.E. Boyle, A.W. Snow, Pure Appl. Opt. J. Eur. Opt. Soc. Part A 5 (1996) 701.

[32] E.M. Maya, A.W. Snow, J.S. Shirk, R.G.S. Pong, S.R. Flom, G.L. Roberts, J. Mater. Chem. 13 (2003) 1603.

[33] R.C. Hollins, Curr. Opin. Solid State Mater. Sci. 4 (1999) 189.

[34] N.B. McKeown, in:, K.M. Kadish, K.S. Smith, R. Guilard (Eds.), The Porphyrin Handbook. Vol. 15, Academic Press, San Diego, 2003, pp. 61–124.

[35] K.-W. Poon, X. Li, D.K.P. Ng, Organometallics 18 (1999) 3528.

[36] H. Tomoda, S. Saito, S. Sharaishi, Chem. Lett. (1983) 313.

[37] A. Kempa, J. Dobrowolski, Can. J. Chem. 66 (1988) 2553.

[38] A. Shaabani, J. Chem. Res. (S) (1998) 672.

[39] H. Uchida, P.Y. Reddy, S. Nakamura, T. Toru, J. Org. Chem. 68 (2003) 8736.

[40] L. Jin, W. Chen, D. Chen, J. Serbian Chem. Soc. 77 (2012) 1223.

[41] K. Sakamoto, E. Ohno-Okumura, Materials (Basel). 2 (2009) 1127.

[42] W. Eberhardt, M. Hanack, Synthesis (Stuttg). 1997 (1997) 95.

[43] A. Ogunsipe, D. Maree, T. Nyokong, J. Mol. Struct. 650 (2003) 131.

[44]   Z. Chen, L. Niu, Y. Cheng, X. Zhou, C. Zhong, F. Zhang, Dalton Trans. 40 (2011) 393.

[45]   E.. Emerson, M.A. Conlin, A.E. Rosenoff, K.S. Norland, D. Chin, H. Rodriguez, G.R. Bird, J. Phys. Chem. 71 (1967) 2396.

[46]   S. Khene, A. Ogunsipe, E. Antunes, T. Nyokong, J. Porphyr. Phthalocyanines 11 (2007) 109.

[47]   X.-F. Zhang, Coord. Chem. Rev. 285 (2015) 52.

[48]   E.M. Antunes, T. Nyokong, Met. Based. Drugs 2008 (2008) 498916.

[49]   N. Kobayashi, F. Furuya, G. Yug, H. Wakita, Chem. A Eur. J. 8 (2002) 1474.

[50]   R.L. Stover, C.L. Thrall, R.D. Joyner, Inorg. Chem. 10 (1971) 2335.

[51]   M.O. Breusova, V.E. Pushkarev, L.G. Tomilova, Russ. Chem. Bull. Int. Ed. 56 (2007) 1456.

[52]   M.J. Chen, R.J. Klingler, J.W. Rathke, J. Porphyr. Phthalocyanines 05 (2001) 442.

[53]   M. Fujiki, H. Tabei, K. Isas, J. Am. Chem. Soc. 108 (1986) 1532.

[54]   M. Gouterman, P. Sayer, E. Shankland, J.P. Smith, Inorg. Chem. 20 (1981) 87.

[55]   J. Liu, F. Zhang, F. Zhao, Y. Tang, X. Song, G. Yao, J. Photochem. Photobiol. A Chem. 91 (1995) 99.

[56]   J. Li, L. R. Subramanian, M. Hanack, Chem. Commun. (1997) 679.

[57]   K. Kasuga, L. Lin, M. Handa, T. Sugimori, K. Isa, K. Matsuura, Y. Takinami, Inorg. Chem. 38 (1999) 4174.

[58]   N. Kobayashi, M. Yokoyama, A. Muranaka, A. Ceulemans, Tetrahedron Lett. 45 (2004) 1755.

[59]   V.N. Myakov, Y. a. Kurskii, V.N. Sedel'nikova, T. V. Makhrova, M. a. Lopatin, Russ. J. Coord. Chem. 34 (2008) 522.

[60]   Ł. Łapok, G. Schnurpfeil, R. Gerdes, S.M. Gorun, O. Suvorova, G. Kudryavtseva, D. Wohrle, J. Porphyr. Phthalocyanines 13 (2009) 346.

[61]   J. Choi, W. Lee, J.W. Namgoong, T.-M. Kim, J.P. Kim, Dye. Pigment. 99 (2013) 357.

[62]   J. Li, L.R. Subramanian, M. Hanack, European J. Org. Chem. 1998 (1998) 2759.

[63]   Z. Song, F. Zhang, X. Li, S.-K. Chan, F. Zhao, Y. Tang, J. Porphyr. Phthalocyanines 06 (2002) 484.

[64]   X. Zhang, Y. Chang, Y. Peng, F. Zhang, Aust. J. Chem. 62 (2009) 434.

[65]   Y. Zhou, M. Deng, Y. Du, S. Yan, R. Huang, X. Weng, C. Yang, X. Zhang, X. Zhou, Analyst 136 (2011) 955.

[66] X.-F. Zhang, J. Huang, H. Zhao, X. Zheng, Z. Junzhong, J. Photochem. Photobiol. A Chem. 215 (2010) 96.

[67] L. Huang, P. Zhao, Z. Li, F. Zhang, C.-H. Tung, J. Phys. Chem. A 112 (2008) 4165.

[68] J.P. Fox, D.P. Goldberg, Inorg. Chem. 42 (2003) 8181.

[69] X.-F. Zhang, Y. Rong, J. Photochem. Photobiol. A Chem. 222 (2011) 141.

[70] J. Li, L.R. Subramanian, M. Hanack, Chem. Commun. (1997) 679.

[71] L. Huang, Z. Li, F. Zhang, C.-H. Tung, K. Kasatani, Opt. Commun. 281 (2008) 1275.

[72] A.M. Brouwer, Pure Appl. Chem. 83 (2011) 2213.

[73] S. Fery-Forgues, D. Lavabre, J. Chem. Educ. 76 (1999) 1260.

[74] J. Britton, E. Antunes, T. Nyokong, J. Photochem. Photobiol. A Chem. 210 (2010) 1.

[75] T.H. Tran Thi, C. Desforge, C. Thiec, S. Gaspard, J. Phys. Chem. 93 (1989) 1226.

[76] C.S. Foote, in:, C.J. Gomer (Ed.), Future Directions and Applications in Photodynamic Therarpy, SPIE Optical Engineering Press, San Diego, 1990, pp. 115–126.

[77] F. Wilkinson, W.P. Helman, A.B. Ross, J. Chem. Phys. Ref. Data 22 (1993) 113.

[78] C.S. Foote, in:, H.H. Wasserman, R.W. Murray (Eds.), Singlet Oxgen, Academic Press, New York, 1979, pp. 139–171.

[79] M.S. Patterson, S.J. Madsen, B.C. Wilson, J. Photochem. Photobiol. B Biol. 5 (1990) 69.

[80] N.A. Kuznetsova, N.S. Gretsova, E. Kalmykova, E. Makarova, S. Dashkevich, V. Negrimovskii, O. Kaliya, E. Luk'yanets, Russ. J. Gen. Chem. 70 (2000) 133.

[81] S. Hackbarth, B. Roder, W. Spiller, H. Kliesch, D. Wohrle, G. Schnurpfeil, J. Porphyr. Phthalocyanines 2 (1998) 145.

[82] J. Wang, W.J. Blau, Chem. Phys. Lett. 465 (2008) 265.

[83] G. de la Torre, P. Vázquez, F. Agulló-López, T. Torres, Chem. Rev. 104 (2004) 3723.

[84] M. Calvete, G.Y. Yang, M. Hanack, Synth. Met. 141 (2004) 231.

[85] H.S. Nalwa, M. Hanack, G. Pawlowski, M.K. Engel, Chem. Phys. 245 (1999) 17.

[86] D. Dini, M. Hanack, in:, K.M. Kadish, K. Smith, R. Guilard (Eds.), The Porphyrin Handbook., Academic Press, 1999, pp. 22–31.

[87] H.S. Nalwa, Appl. Organomet. Chem. 5 (1991) 349.

[88] F.. Henari, W.J. Blau, J. Callaghan, P. Haisch, M. Hanack, Pure Appl. Opt. J. Eur. Opt. Soc. Part A 6 (1997) 741.

[89] D. Dini, M. Barthel, M. Hanack, European J. Org. Chem. 2001 (2001) 3759.

[90] J.S. Shirk, R.G.S. Pang, F.J. Bartoli, A.W. Snow, Appl. Phys. Lett. 63 (1993) 1880.

[91] J. Britton, C. Litwinski, M. Durmuş, V. Chauke, T. Nyokong, J. Porphyr. Phthalocyanines 15 (2011) 1239.

[92] S.G. Raptis, M.G. Papadopoulos, A.J. Sadlej, J. Chem. Phys. 111 (2001) 7904.

[93] D.K. Modibane, T. Nyokong, Polyhedron 27 (2008) 1102.

[94] M. Sheik-Bahae, a a Said, E.W. Van Stryland, Opt. Lett. 14 (1989) 955.

[95] M. Sheik-Bahae, a. a. Said, T.-H. Wei, D.J. Hagan, E.W. Van Stryland, IEEE J. Quantum Electron. 26 (1990) 760.

[96] E.W. Van Stryland, M. Sheik-bahae, in:, M.G. Kuzyk, C.W. Dirk (Eds.), Characterization Techniqes and Tabulations for Organic Nonlinear Materials, Marcel Dekker, Inc., 1998, pp. 655–692.

[97] R.L. Sutherland, D.G. Mclean, S. Kirkpatrick, eds., Handbook of Nonlinear Optics, 2nd ed., Marcel Dekker, Inc., 2003.

[98] L.E.E.W. Tutt, T.F. Boggess, Prog. Quantum Electron. 17 (1993) 299.

[99] M. Sheik-Bahae, Opt. Eng. 30 (1991) 1228.

[100] Y. Chen, N. He, J.J. Doyle, Y. Liu, X. Zhuang, W.J. Blau, J. Photochem. Photobiol. A Chem. 189 (2007) 414.

[101] M.D. Hecimovich, Sport. Chiropr. Rehabil. 55912 (2000) 24.

[102] T. Kololuoma, J.A.I. Oksanen, P. Raerinne, J.T. Rantala, J. Mater. Res. 16 (2011) 2186.

[103] A. Sarkar, P.R. Dvornic, J.P. Godschalx, Polymeric Dye for Optical Power Limiting, 2012.

[104] A. Slodek, Optical Limiting Effect of New Synthesised Phthalocyanines in Solution and in Solid State (Thesis), Bremen University, 2010.

[105] F. Kajzar, J. Messier, C. Rosilio, J. Appl. Phys. 60 (1986) 3040.

[106] J. Britton, C. Litwinski, E. Antunes, M. Durmuş, V. Chaukea, T. Nyokong, J. Macromol. Sci. Part A 50 (2013) 110.

[107] S.V. Rao, Mater. Sci. Appl. 02 (2011) 299.

[108] J. Mack, Y. Asano, N. Kobayashi, M.J. Stillman, J. Am. Chem. Soc. (2005) 59.

[109] P. Tau, T. Nyokong, Electrochim. Acta 52 (2007) 3641.

[110] M. Durmuş, T. Nyokong, Tetrahedron 63 (2007) 1385.

[111] J. Mack, J. Stone, T. Nyokong, J. Porphyr. Phthalocyanines 18 (2014) 630.

[112] Z. Cai, M.J. Crossley, J.R. Reimers, R. Kobayashi, R.D. Amos, J. Phys. Chem. 110 (2006) 15624.

[113] D.K. Modibane, T. Nyokong, Polyhedron 28 (2009) 1475.

[114] J. Rusanova, M. Pilkington, S. Decurtins, Chem. Commun. 2002 (2002) 2236.

[115] G. Mbambisa, P. Tau, E. Antunes, T. Nyokong, Polyhedron 26 (2007) 5355.

[116] T. Fukuda, K. Ono, S. Homma, N. Kobayashi, Chem. Lett. 32 (2003) 736.

[117] M.V. Martínez-Díaz, M. Ince, T. Torres, Monatshefte Für Chemie - Chem. Mon. 142 (2011) 699.

[118] S.P. McGlynn, T. Azumi, M. Kasha, J. Chem. Phys. 2 (1964) 507.

[119] M. Durmuş, T. Nyokong, Spectrochim. Acta. A. Mol. Biomol. Spectrosc. 69 (2008) 1170.

[120] M.-R. Ke, J.-D. Huang, S.-M. Weng, J. Photochem. Photobiol. A Chem. 201 (2009) 23.

[121] D. Magde, R. Wong, P.G. Seybold, Photochem. Photobiol. 75 (2002) 327.

[122] W. Chidawanyika, A. Ogunsipe, T. Nyokong, New J. Chem. 31 (2007) 377.

[123] M.G. Debacker, O. Deleplanque, B. Van Vlierberg, F.X. Sauvage, Laser Chem. 8 (1988) 1.

[124] T. Nyokong, E. Antunes, in:, K.M. Kadish, K. Smith, R. Guilard (Eds.), The Handbook of Porphyrin Science Vol. 7, Academic Press, Singapore, 2010, pp. 247–349.

[125] N.A. Kuznetsova, N.S. Gretsova, V.M. Derkacheva, O.L. Kaliya, E. a. Lukyanets, J. Porphyr. Phthalocyanines, 7 (2003) 147.

[126] J.W. Perry, K. Mansour, S.R. Marder, K.J. Perry, D. Alvarez, I. Choong, Opt. Lett. 19 (1994) 625.

[127] K. Sanusi, E. Antunes, T. Nyokong, Dalton Trans. 43 (2014) 999.

[128] C.W. Spangler, J. Mater. Chem. 9 (1999) 2013.

[129] M.J. Frisch, G.W. Trucks, H.B. Schlegel, G.E. Scuseria, M.A. Robb, J.R. Cheeseman, G. Scalmani, V. Barone, B. Mennucci, G.A. Petersson, H. Nakatsuji, M. Caricato, X. Li, H.P. Hratchian, A.F. Izmaylov, J. Bloino, G. Zheng, J.L. Sonnenberg, M. Hada, M. Ehara, K. Toyota, R. Fukuda, J. Hasegawa, M. Ishida, T. Nakajima, Y. Honda, O. Kitao, H. Nakai, T. Vreven, J.A. Montgomery, J.E. Jr, Peralta, F. Ogliaro, M. Bearpark, J.J. Heyd, E. Brothers, K.N. Kudin, R. Staroverov, V. N. Kobayashi, K. Normand, J. Raghavachari, A. Rendell, J.C. Burant, S.S. Iyengar, J. Tomasi, M. Cossi, N. Rega, M.J. Millam, M. Klene, J.E. Knox, J.B. Cross, V. Bakken, C. Adamo, J. Jaramillo, R. Gomperts, R.E. Stratmann, O. Yazyev, A.J. Austin, R. Cammi, C. Pomelli, J.W. Ochterski, R.L.

Martin, K. Morokuma, V.G. Zakrzewski, G.A. Voth, P. Salvador, J.J. Dannenberg, S. Dapprich, A.D. Daniels, Ö. Farkas, J.B. Foresman, J. V. Ortiz, J. Cioslowski, D.J. Fox, (2009).

[130]   A.D. Becke, J. Chem. Phys. 98 (1993) 5648.

[131]   M. Gouterman, in:, D. Dolphin (Ed.), The Porphyrins, Vol. III, Academic Press, New York, 1978, pp. 1–165.

[132]   J. Michl, J. Am. Chem. Soc. 100 (1978) 6801.

[133]   J. Michl, J. Am. Chem. Soc. 2 (1978) 6812.

[134]   J. Michl, Pure Appl. Chem. 52 (1980) 1549.

[135]   J. Michl, Tetrahedron 40 (1984) 3845.

[136]   J. Mack, M. Bunya, D. Lansky, D.P. Goldberg, N. Kobayashi, Heterocycles 76 (2008) 1369.

[137]   J. Mack, N. Kobayashi, Chem. Rev. 111 (2011) 281.

[138]   T. Nyokong, Z. Gasyn, M.J. Stillman, Inorg. Chem. 26 (1987) 548.

[139]   T. Nyokong, Z. Gasyna, M. Stillman, Inorg. Chem. 26 (1987) 1087.

[140]   E. Ough, T. Nyokong, K. Creber, M.J. Stillman, Inorg. Chem. 27 (1988) 2724.

[141]   J. Mack, M. Stillman, J. Phys. Chem. 95 (1995) 7935.

[142]   J. Mack, M. Stillman, Inorg. Chem. 36 (1997) 413.